Cyclotriveratrylene-tethered trinuclear palladium(II)-NHC complexes; reversal of site selectivity in Suzuki-Miyaura reactions

Jonathan M. Fowler, Edward Britton, Christopher M. Pask, Charlotte E. Willans and Michaele J. Hardie

School of Chemistry, University of Leeds, Woodhouse Lane, Leeds LS2 9JT, UK

Supplementary Information

Contents

1.1 NMR Spectra

1.2 Mass spectra

1.3 Infrared Spectra

2. Crystallography

3. Additional Catalytic Studies

1. Synthesis

(±)-*Tris*-(1-methylbenzimidazolyl)cyclotriguaiacylene [1] and 1-(2-methoxyphenoxymethyl)benzimidazole [2] were synthesized according to literature methods. All other chemicals were obtained from commercial sources and were used without further purification. Reactions performed under a nitrogen atmosphere were carried out using standard Schlenk procedures. NMR spectra were recorded by automated procedures on a Bruker DPX 300 MHz NMR spectrometer. Electrospray mass spectra (ESI-MS) were measured on a Bruker Maxis Impact instrument in positive ion mode. Infra-red spectra were recorded as solid phase samples on a Bruker ALPHA Platinum ATR. Elemental analyses were performed by London Metropolitan University or University of Leeds

microanalytical services on material that had been washed with diethyl ether, subsequently dried at 80-90℃ under vacuum and then exposed to the atmosphere.

1.1 NMR spectra

$H_3L1{\cdot}3I$

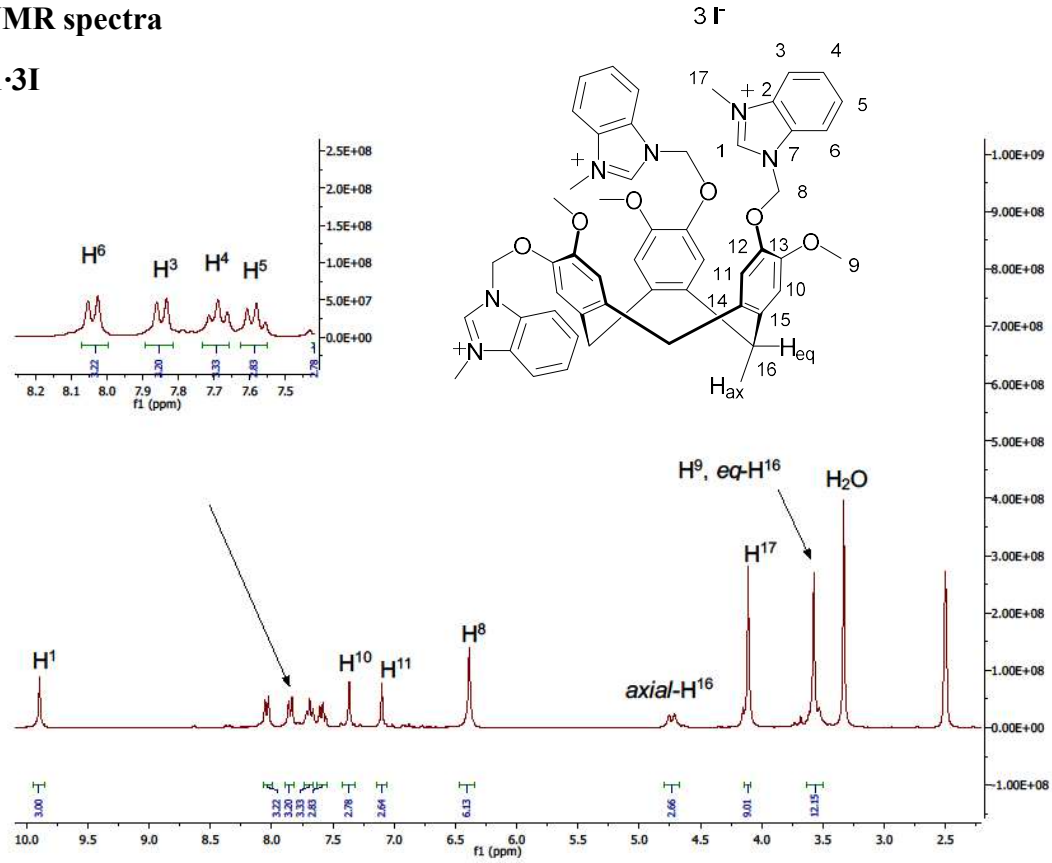

Figure S1: ^{1}H NMR spectrum (300 MHz, DMSO-d_6) of **H_3L1·3I**. δ (ppm) 9.86 (s, 3H, H^1), 8.04 (d, 3H, J = 8.3 Hz, H^6), 7.84 (d, 3H, J = 8.3 Hz, H^3), 7.69 (t, 3H, J = 7.4 Hz, H^4), 7.58 (t, 3H, J = 7.5 Hz, H^5), 7.33 (s, 3H, H^{10}), 7.08 (s, 3H, H^{11}), 6.37 (s, 6H, H^8), 4.73 (d, 3H, J = 13.5 Hz, *ax*-H^{16}), 4.10 (s, 9H, H^{17}), 3.56 (s, 9H, H^9), 3.55 (d, 3H, J = 23.1 Hz, *eq*-H^{16}).

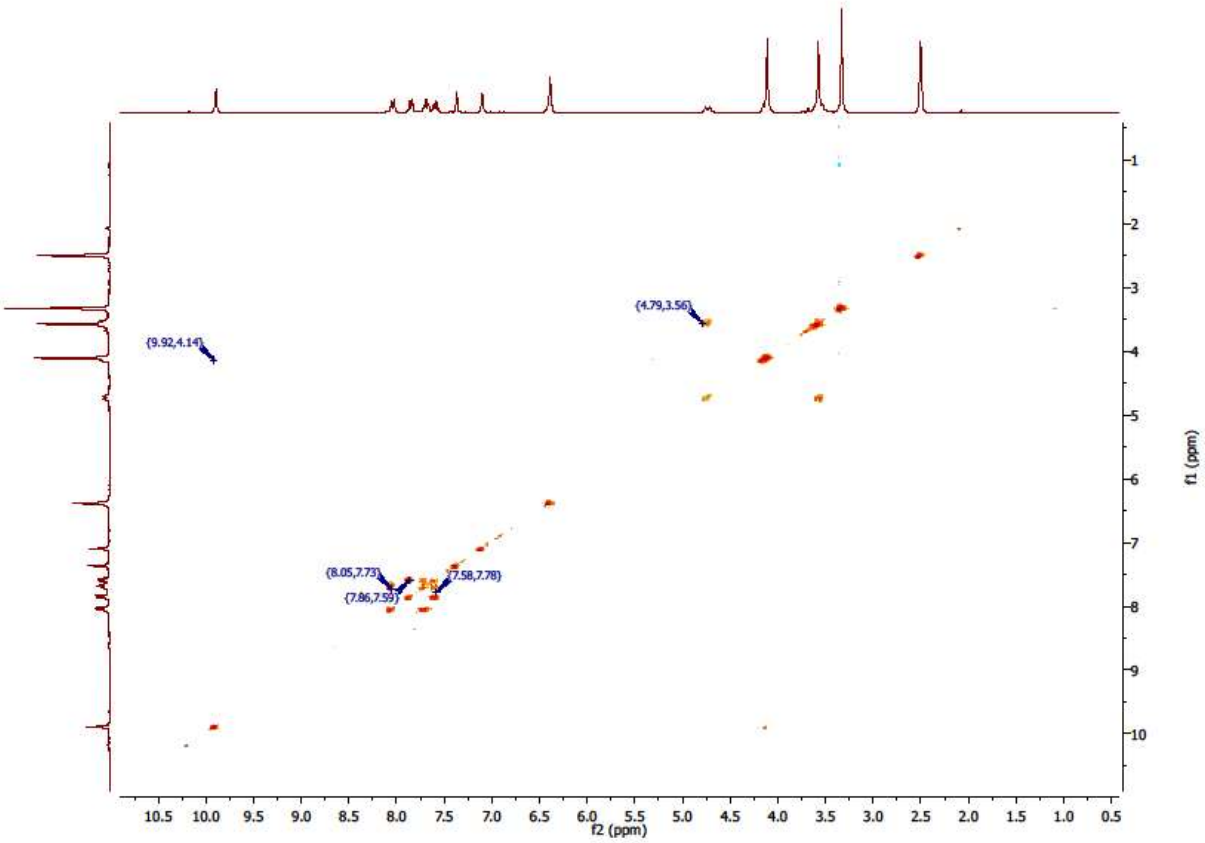

Figure S2. ^{1}H-^{1}H COSY (300 MHz, DMSO-d_6) NMR spectrum of **H_3L1·3I**

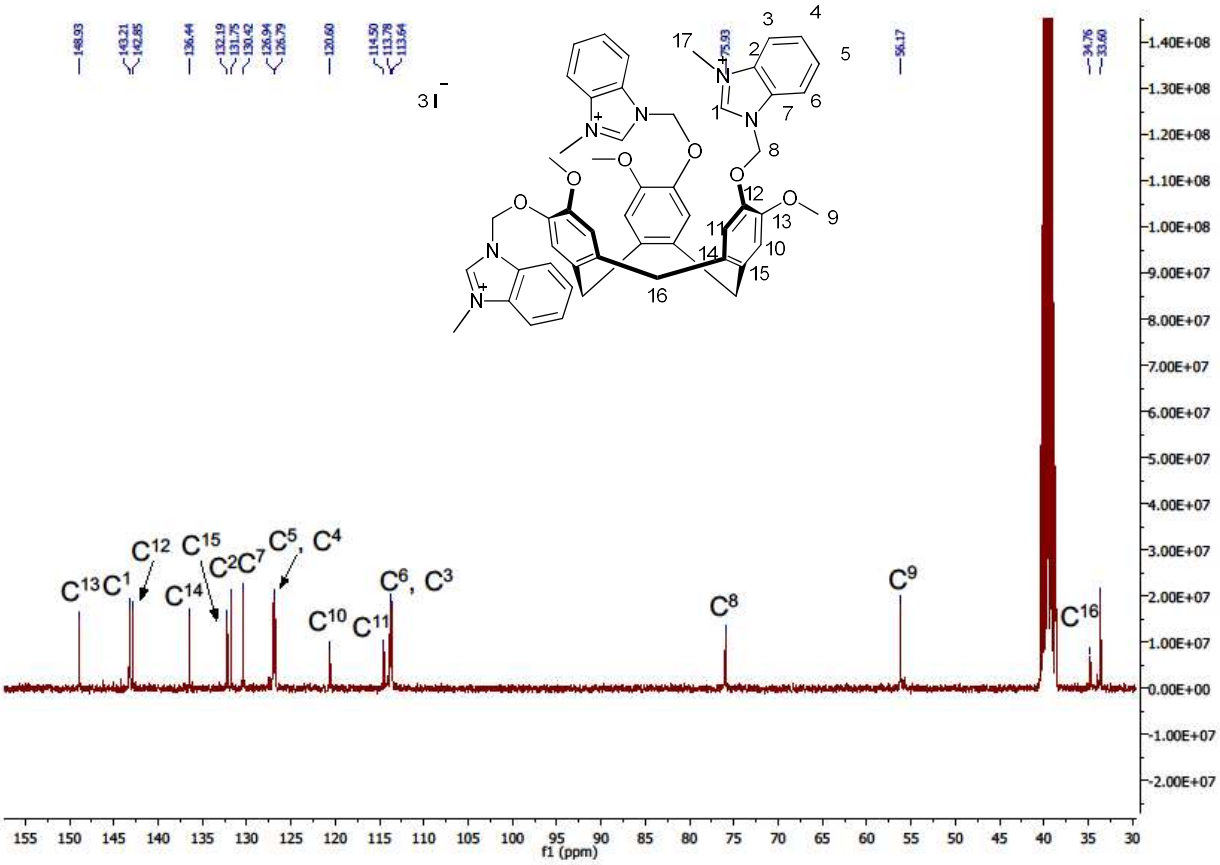

Figure S3. $^{13}C\{^{1}H\}$ NMR spectrum (75 MHz, DMSO-d_6) of **H_3L1·3I**. δ 148.95 (C^{13}), 143.24 (C^{1}), 142.90 (C^{12}), 136.43 (C^{14}), 132.19 (C^{15}), 131.78 (C^{2}), 130.43 (C^{7}), 126.96 (C^{5}), 126.81 (C^{4}), 120.59 (C^{10}), 114.49 (C^{11}), 113.79 (C^{6}), 113.64 (C^{3}), 75.92 (C^{8}), 56.10 (C^{9}), 34.79 (C^{16}), 33.56 (C^{17}).

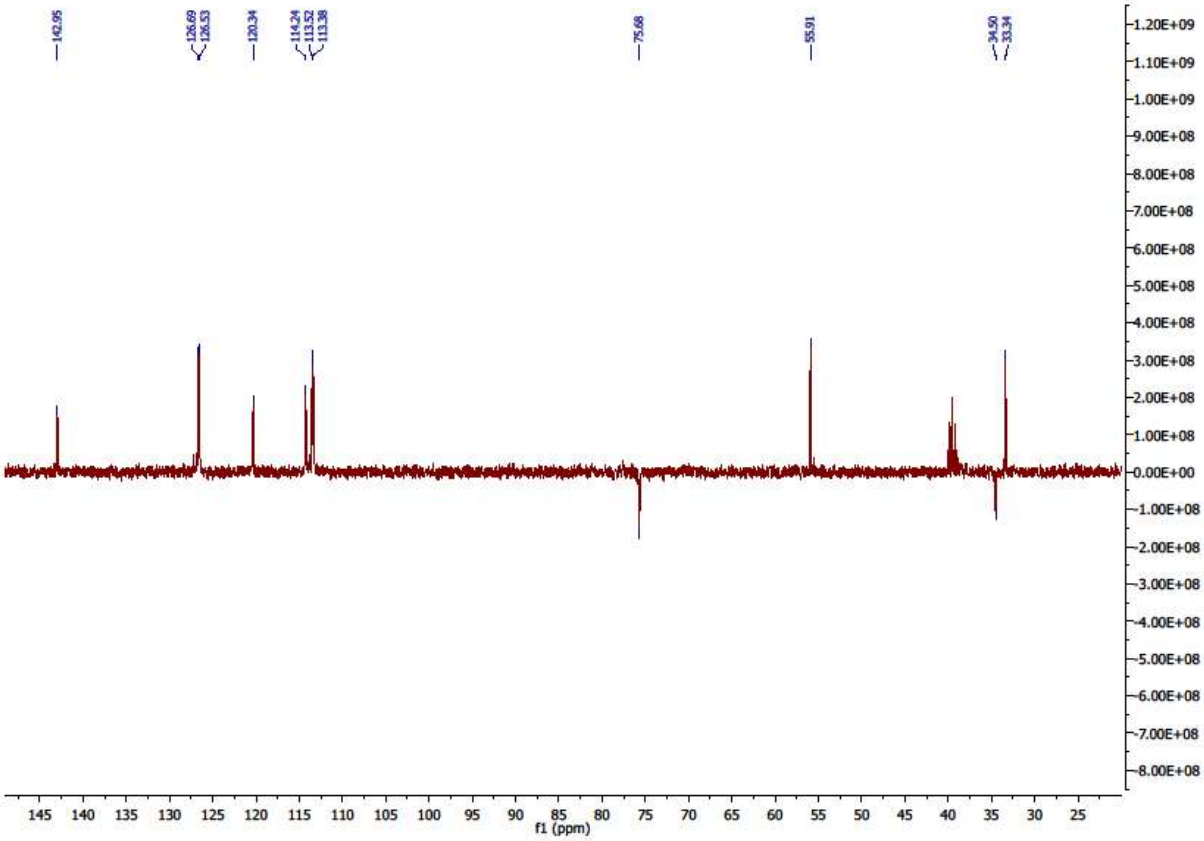

Figure S4. DEPT-135 NMR spectrum of **H_3L1·3I**.

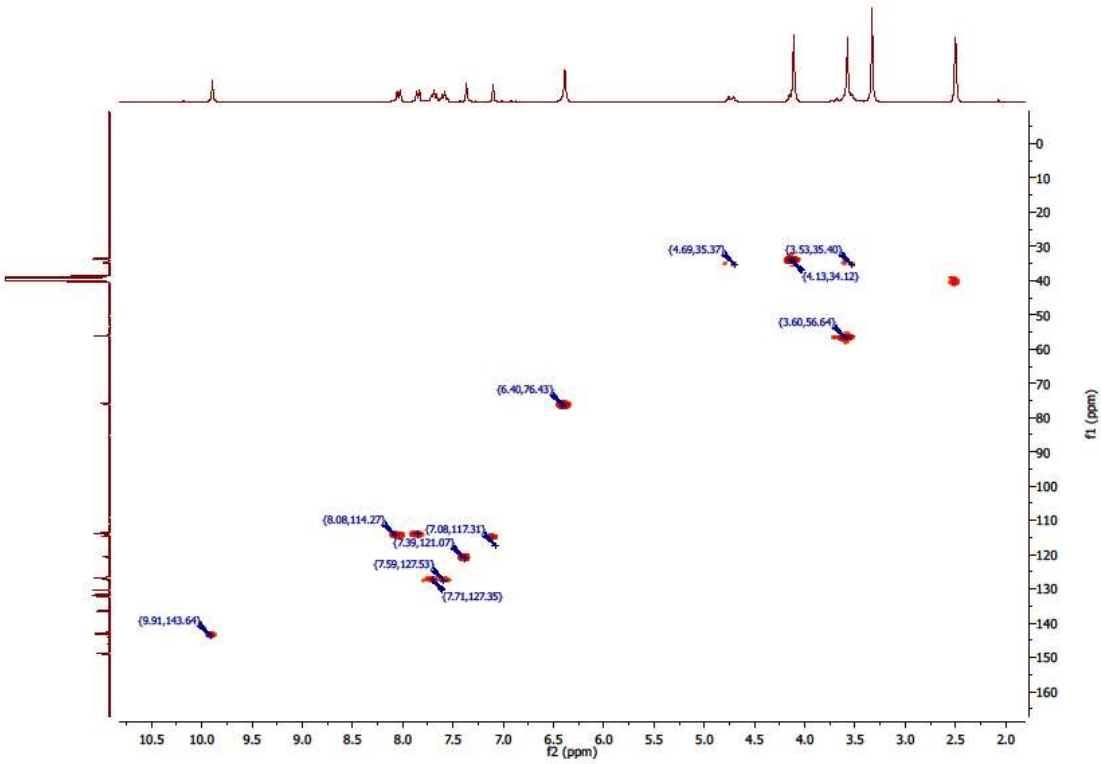

Figure S5. ^{1}H-^{13}C HSQC NMR spectrum of **H_3L1·3I**.

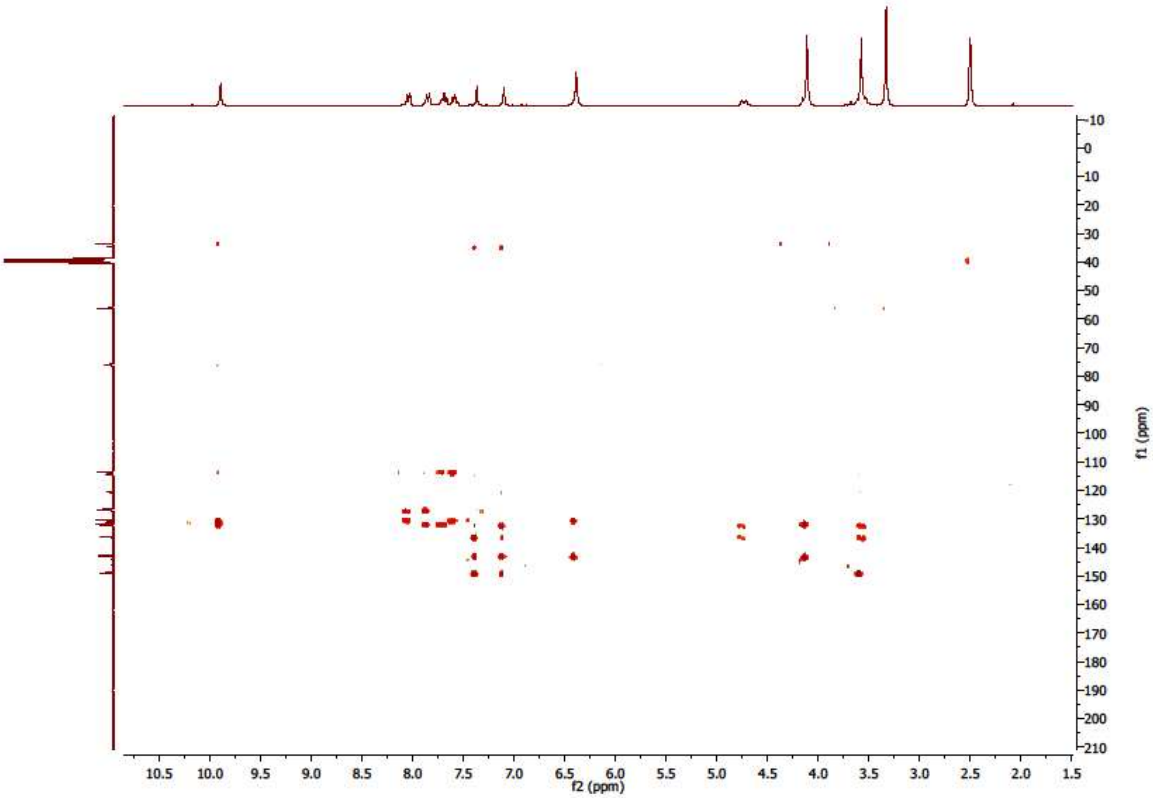

Figure S6. ^{1}H-^{13}C HMBC NMR spectrum of **H_3L1·3I**.

$H_3L2{\cdot}3Br$

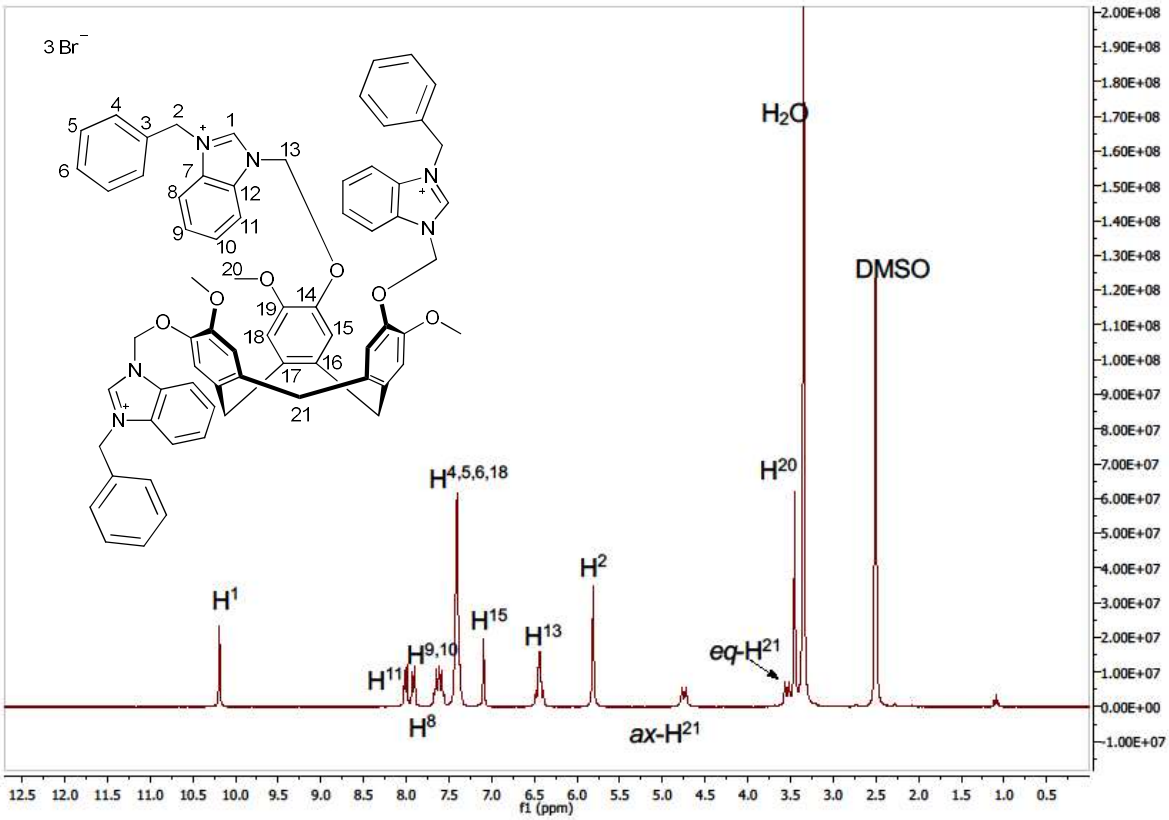

Figure S7. ^{1}H NMR spectrum (300 MHz, DMSO-d_6) of **$H_3L2{\cdot}3Br$**. δ (ppm) 10.18 (s, 3H, H^1), 8.00 (d, 3H, J = 8.1 Hz, H^{11}), 7.91 (d, 3H, J = 8.1 Hz, H^8), 7.61 (m, 6H, H^9, H^{10}), 7.40 (bs, 6H, H^4, H^5, H^6, H^{18}), 7.09 (s, 3H, H^{15}), 6.43 (m, 6H, H^{13}), 5.81 (s, 6H, H^2), 4.74 (d, 3H, J= 13.6 Hz, *ax*-H^{21}), 3.54 (d, 3H, J = 13.4 Hz, *eq*-H^{21}), 3.45 (s, 9H, H^{20}).

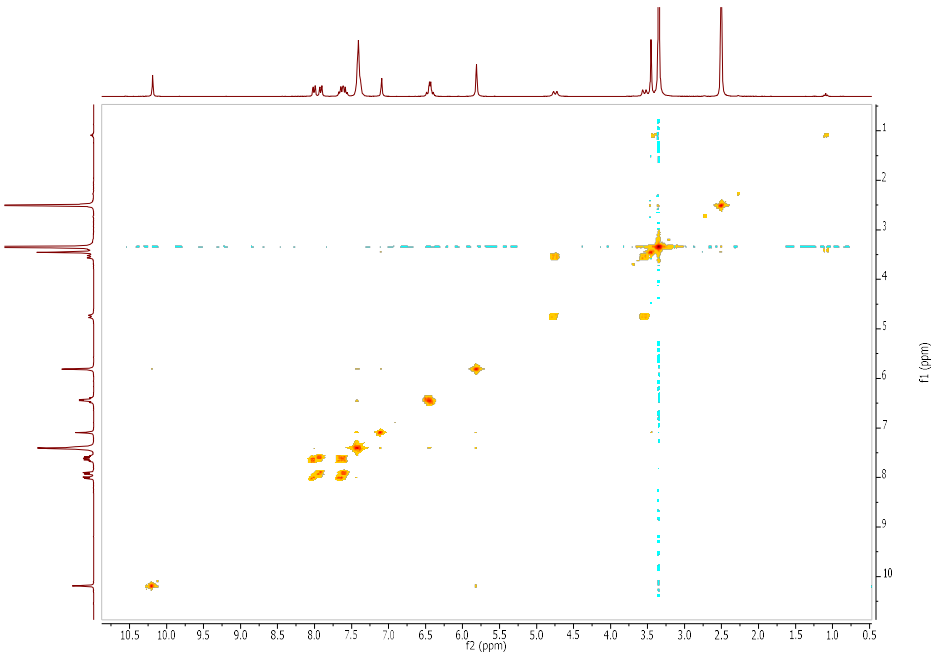

Figure S8. ^{1}H-^{1}H COSY NMR spectrum (300 MHz, DMSO-d_6) of **$H_3L2{\cdot}3Br$**.

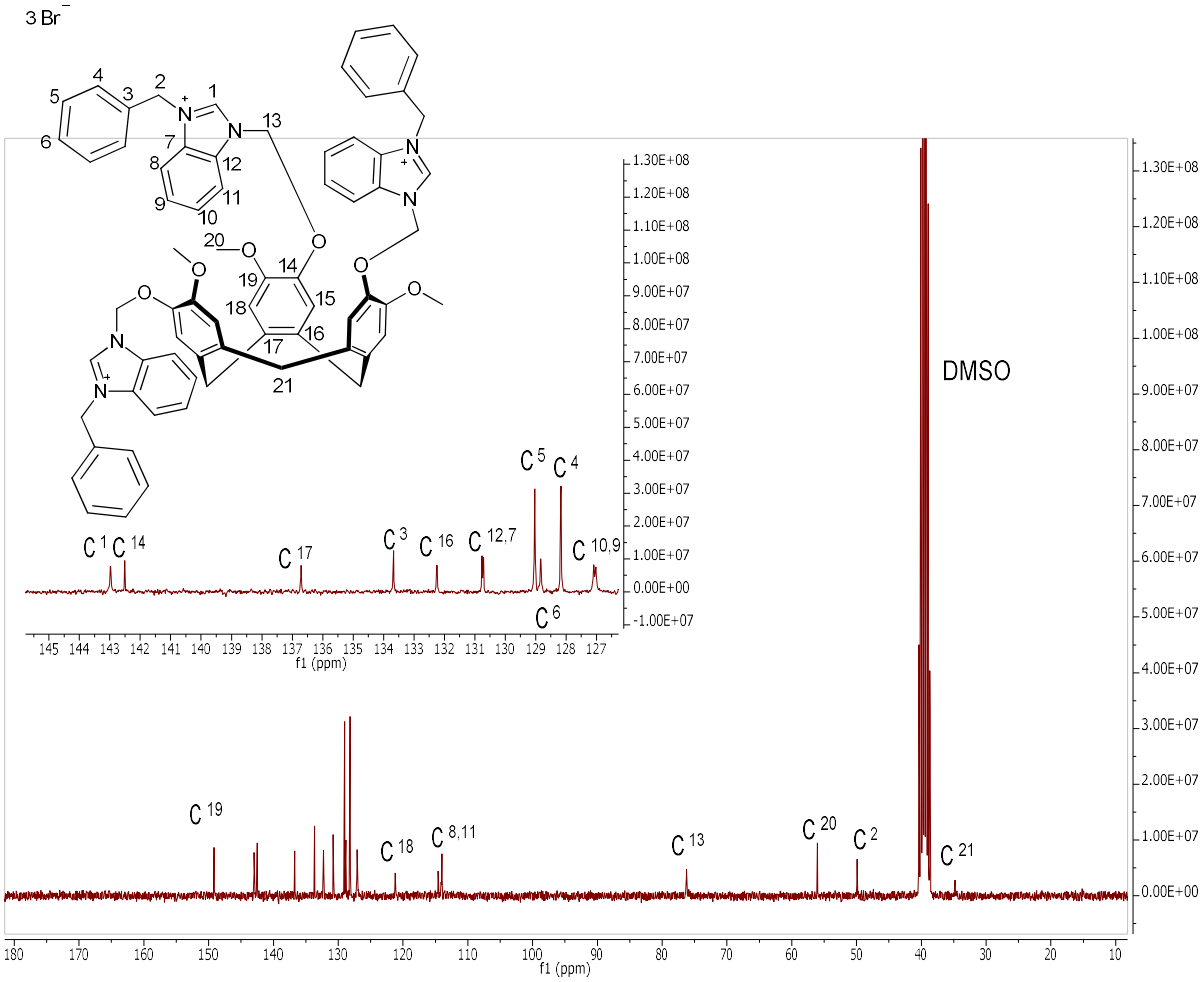

Figure S9. $^{13}C\{^{1}H\}$ NMR spectrum (75 MHz, DMSO-d_6) of **H_3L2·3Br**. δ (ppm) 149.17 (C19), 142.98 (C1), 142.51 (C14), 136.71 (C17), 133.68 (C3), 132.25 (C16), 130.76 (C12), 130.72 (C7), 129.03 (C5), 128.83 (C6), 128.17 (C4), 127.09 (C10), 127.02 (C9), 121.18 (C18), 114.57 (C15), 114.11 (C8), 114.00 (C11), 76.24 (C13), 56.02 (C20), 49.92 (C2), 34.80 (C21).

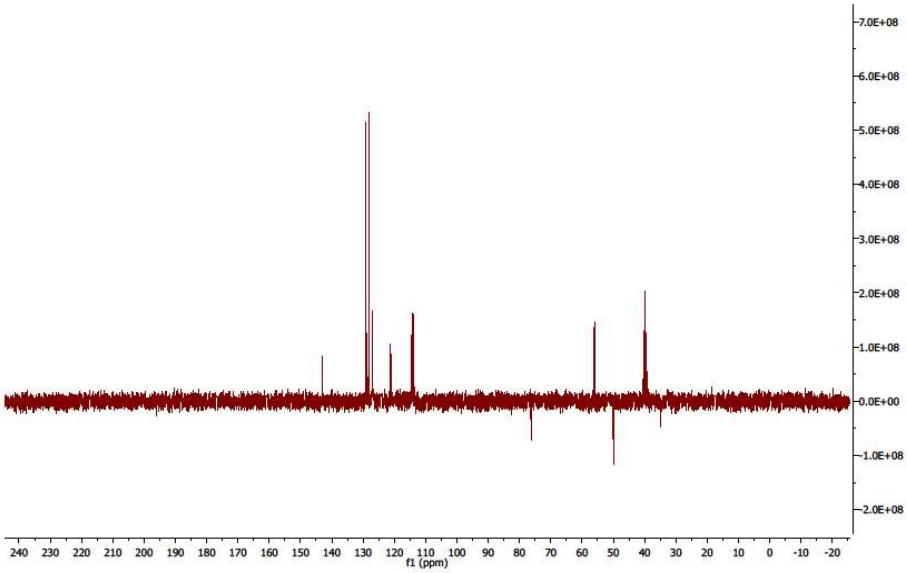

Figure S10. DEPT-135 NMR spectrum of **H_3L2·3Br**.

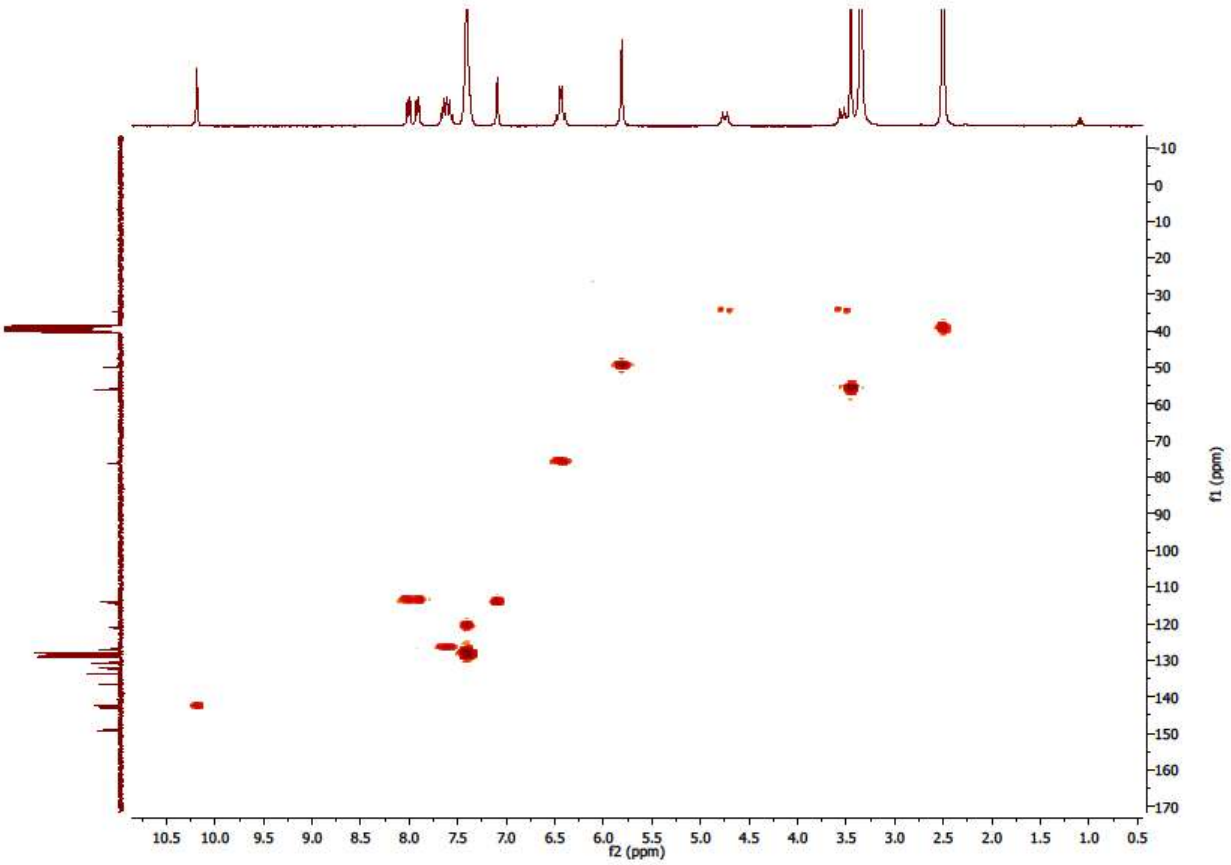

Figure S11. ^{1}H-^{13}C HSQC NMR spectrum of **H_3L2·3Br**

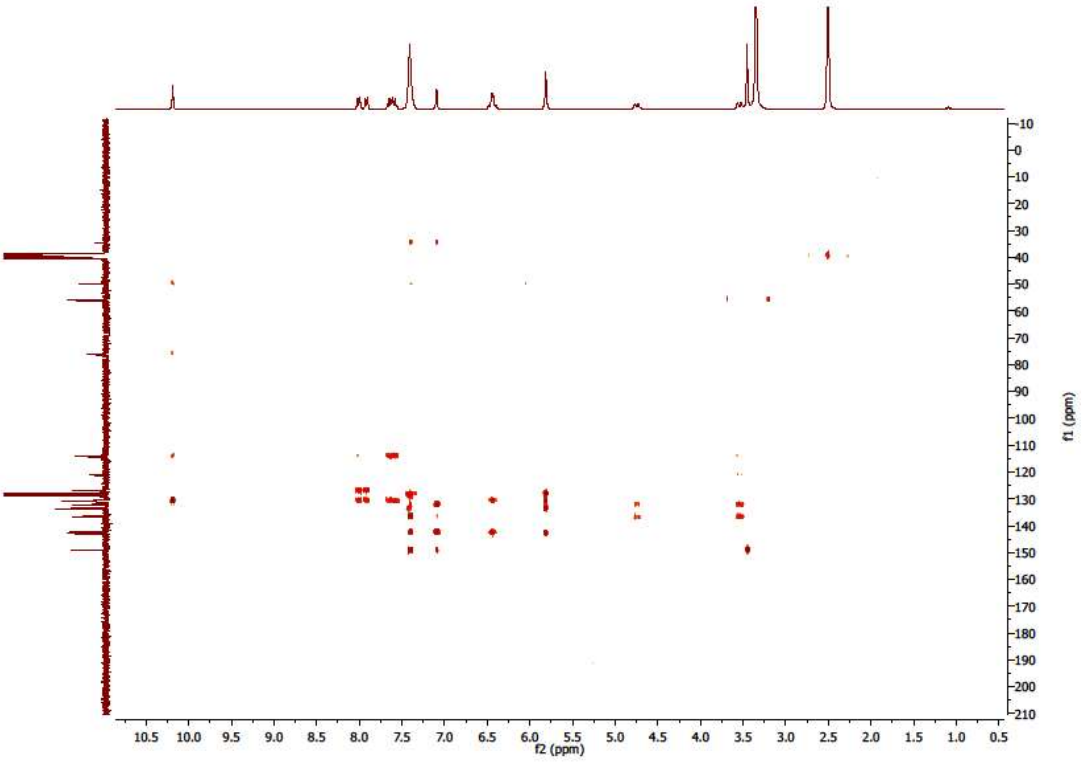

Figure S12. ^{1}H-^{13}C HMBC NMR spectrum of **H_3L2·3Br**

HL3·I

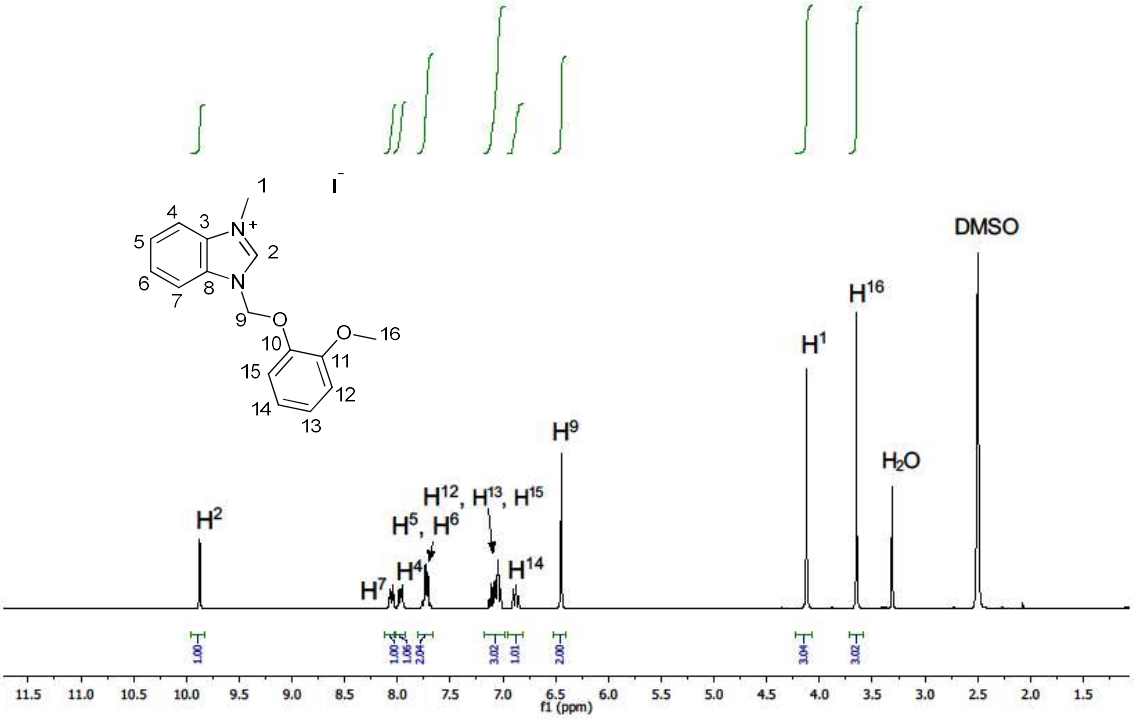

Figure S13. ^{1}H NMR spectrum (300 MHz, DMSO-d_6) of **HL3·I.** δ (ppm) 9.87 (s, 1H, H^2), 8.11 – 8.01 (m, 1H, H^7), 8.00 – 7.92 (m, 1H, H^4), 7.77 – 7.67 (m, 2H, H^5, H^6), 7.16 – 7.00 (m, 3H, H^{12}, H^{13}, H^{15}), 6.88 (ddd, 1H, J= 8.3, 7.2, 1.7 Hz, H^{14}), 6.45 (s, 2H, H^9), 4.12 (s, 3H, H^1), 3.65 (s, 3H, H^{16}).

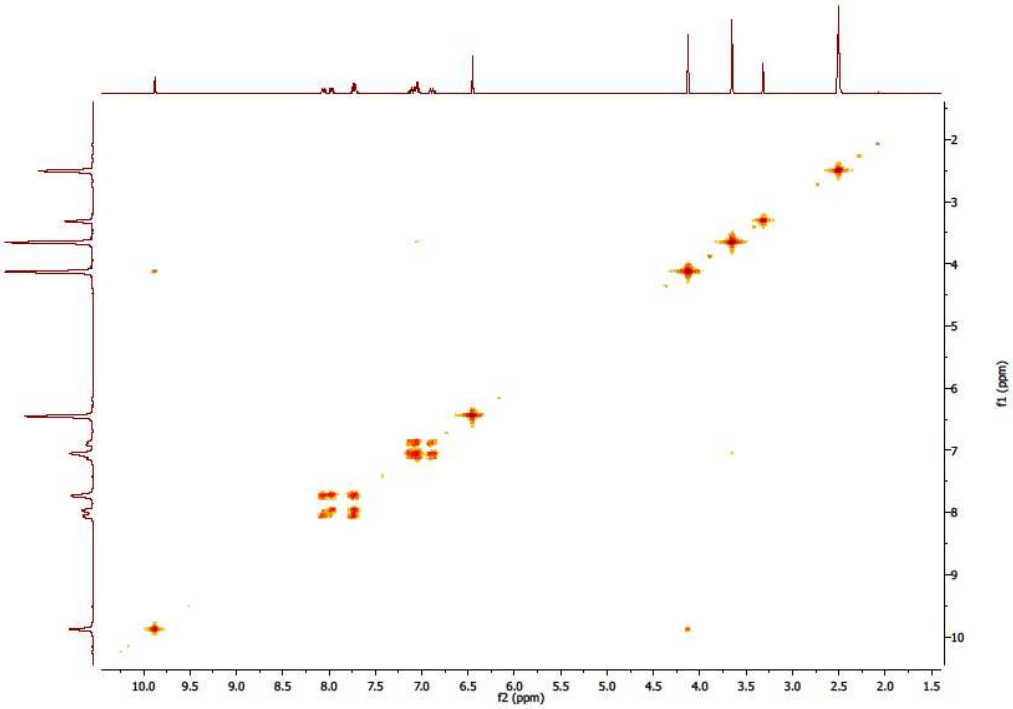

Figure S14. ^{1}H-^{1}H COSY (300 MHz, DMSO-d_6) NMR spectrum of **HL3·I**.

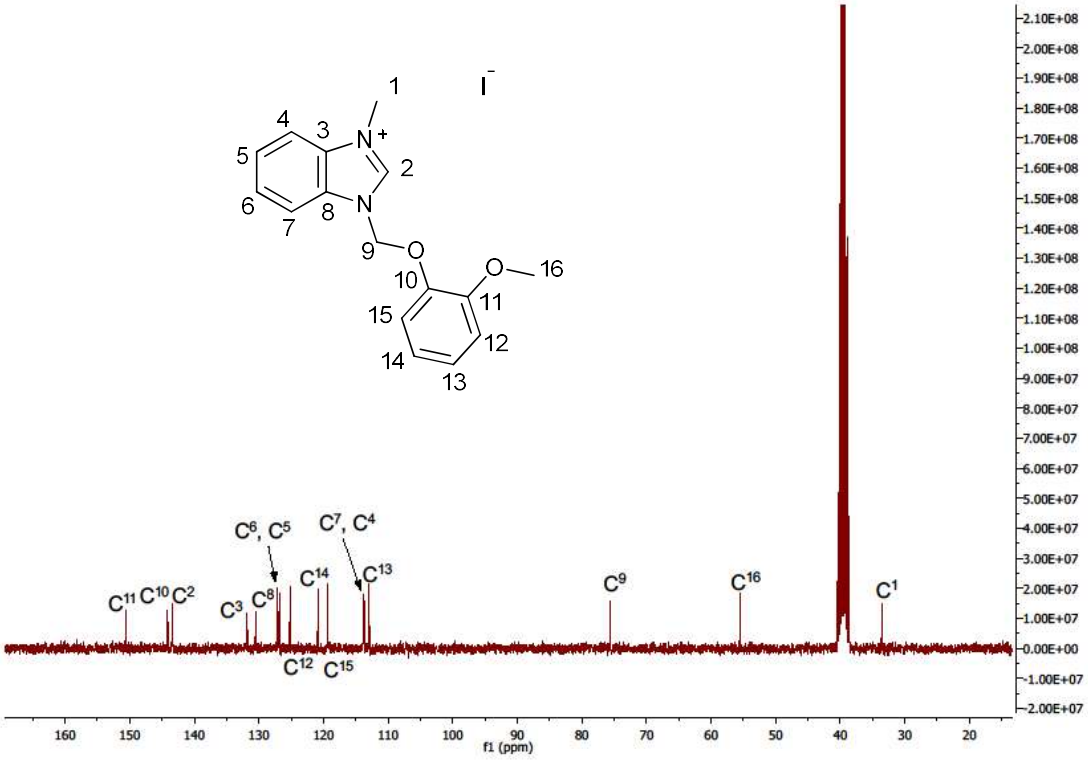

Figure S15: $^{13}C\{^{1}H\}$ NMR spectrum (75 MHz, DMSO-d_6) of **HL3·I**. δ (ppm) 150.60 (C^{11}), 144.13 (C^{10}), 143.36 (C^{2}), 131.82 (C^{3}), 130.48 (C^{8}), 127.10 (C^{6}), 126.83 (C^{5}), 125.17 (C^{12}), 120.84 (C^{14}), 119.36 (C^{15}), 113.82 (C^{7}), 113.72 (C^{4}), 112.98 (C^{13}), 75.66 (C^{9}), 55.53 (C^{16}), 33.57 (C^{1}).

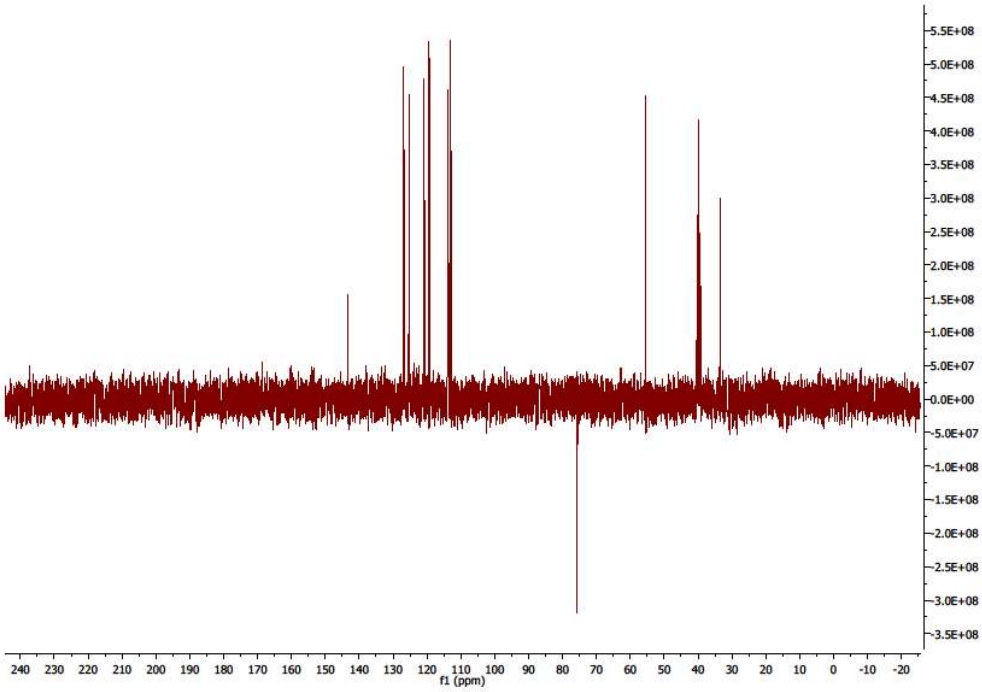

Figure S16. DEPT-135 NMR spectrum of **HL3·I**.

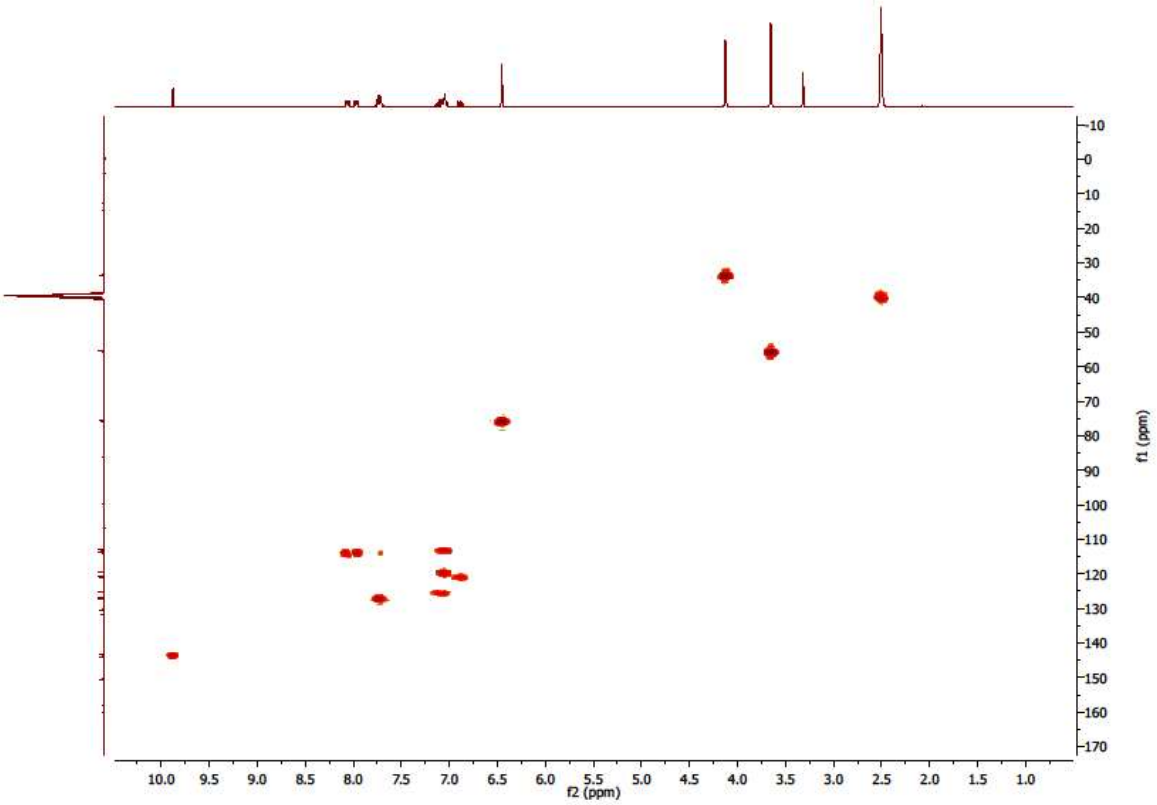

Figure S17. ^{1}H-^{13}C HSQC NMR spectrum of **HL3·I**.

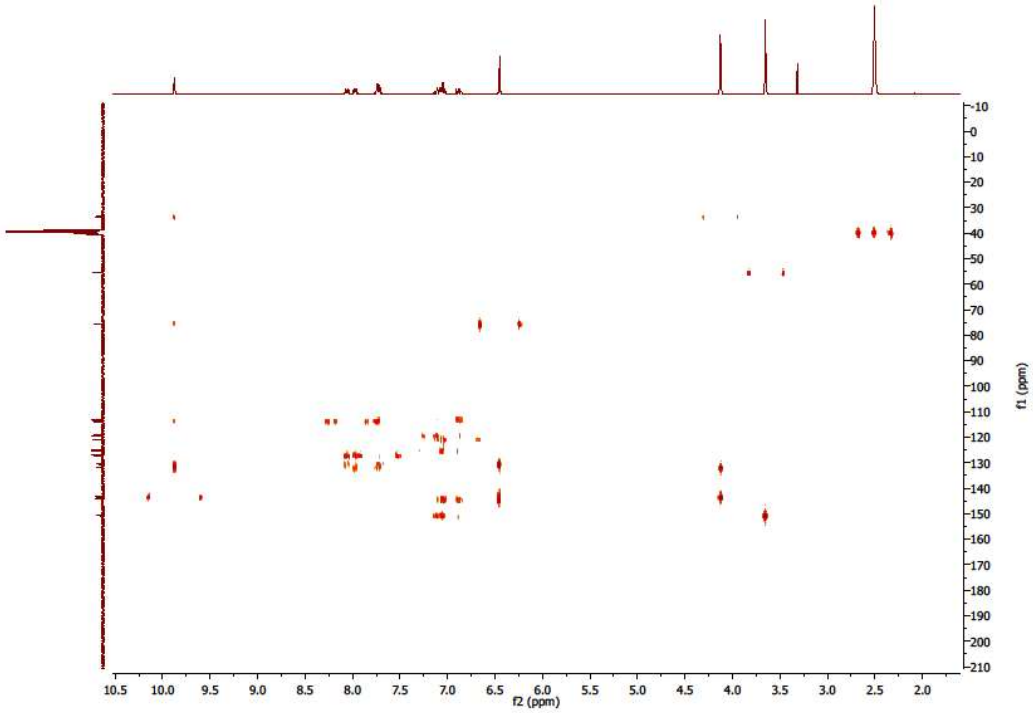

Figure S18. ^{1}H-^{13}C HMBC NMR spectrum of **HL3·I**.

HL4·Br

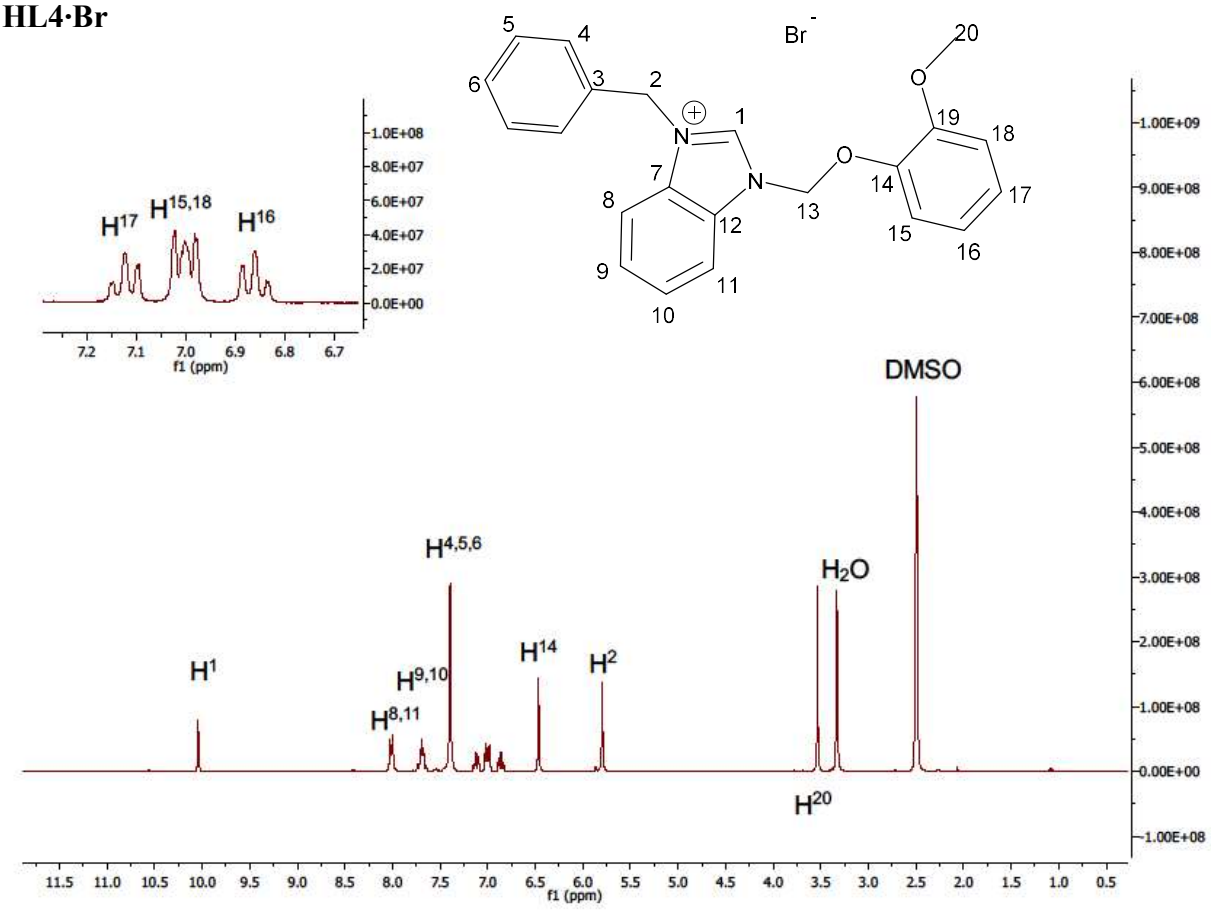

Figure S19: ^{1}H NMR spectrum (300 MHz, DMSO-d_6) of **HL4·Br**. δ (ppm) 10.04 (s, 1H, H^{1}) , 8.06-7.95 (m, 2H. H^{8}, H^{11}), 7.77 – 7.60 (m, 2H, H^{9}, H^{10}), 7.39 (s, 5H, H^{4}, H^{5}, H^{6}), 7.12 (t, 1H, J= 7.0 Hz, H^{17}), 7.06 – 6.94 (m, 2H, H^{15}, H^{18}), 6.86 (t, 1H, J= 7.0 Hz, H^{16}), 6.47 (s, 2H, H^{14}), 5.80 (s, 2H, H^{2}), 3.54 (s, 3H, H^{20}).

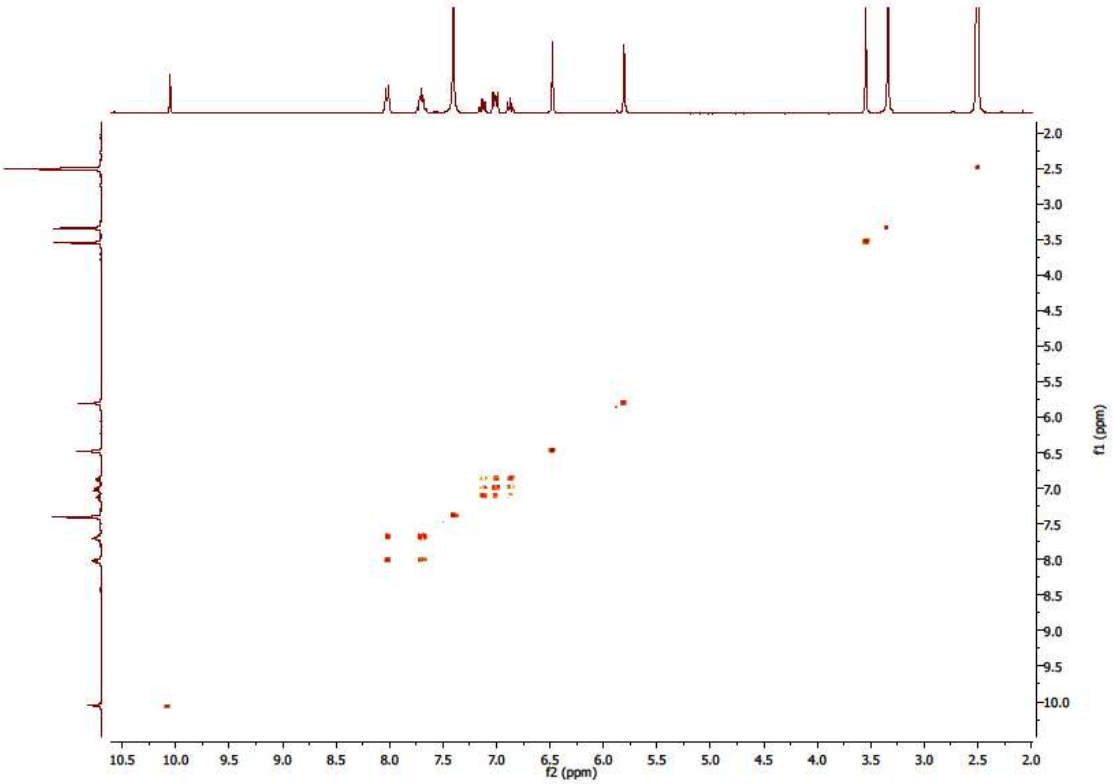

Figure S20. ^{1}H-^{1}H COSY (300 MHz, DMSO-d_6) NMR spectrum of **HL4·Br**.

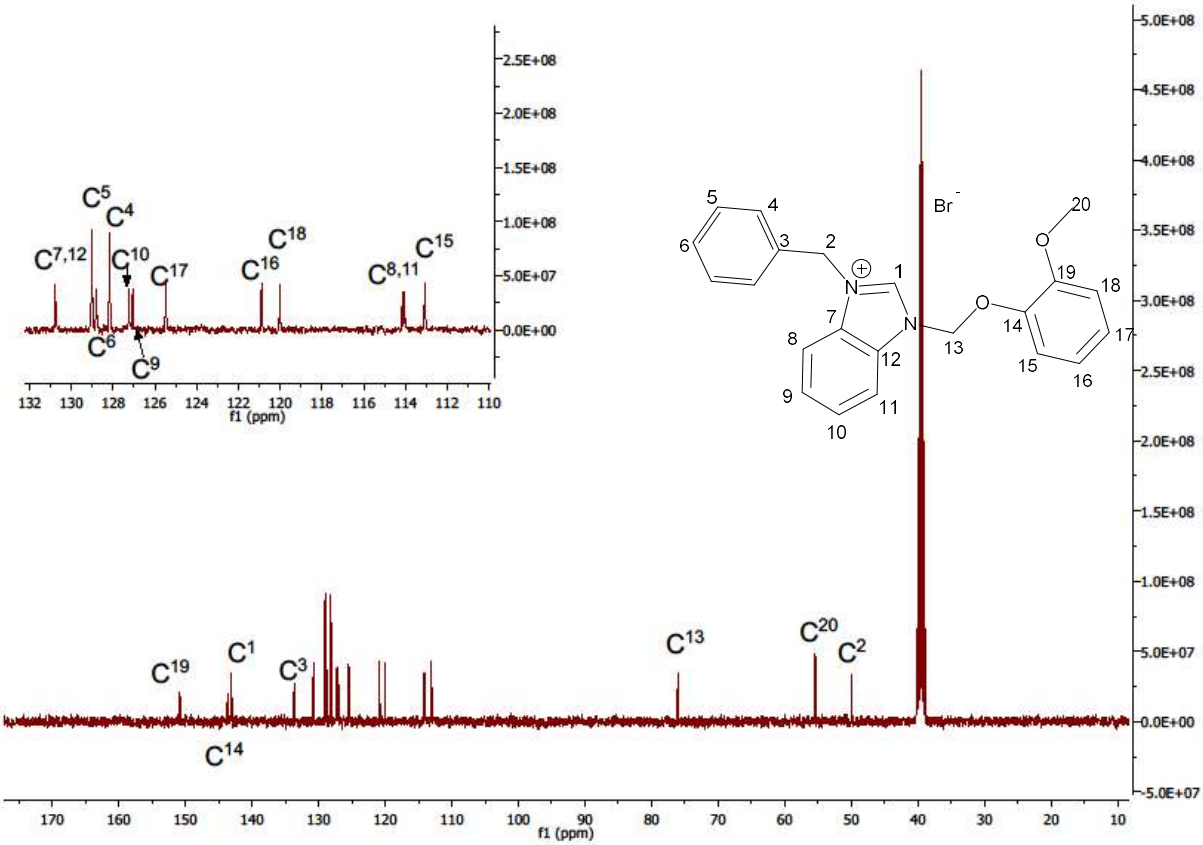

Figure S21. $^{13}C\{^{1}H\}$ NMR spectrum (101 MHz, DMSO-d_6) of **HL4·Br**. δ (ppm) 150.84 (C^{19}), 143.67 (C^{14}), 143.08 (C^{1}), 133.66 (C^{3}), 130.77 (C^{7}, C^{12}), 129.02 (C^{5}), 128.80 (C^{6}), 128.17 (C^{4}), 127.25 (C^{10}), 127.06 (C^{9}), 125.47 (C^{17}), 120.89 (C^{16}), 120.02 (C^{18}), 114.14 (C^{8}), 114.04 (C^{11}), 113.06 (C^{15}), 76.06 (C^{13}), 55.42 (C^{20}), 49.95 (C^{2}).

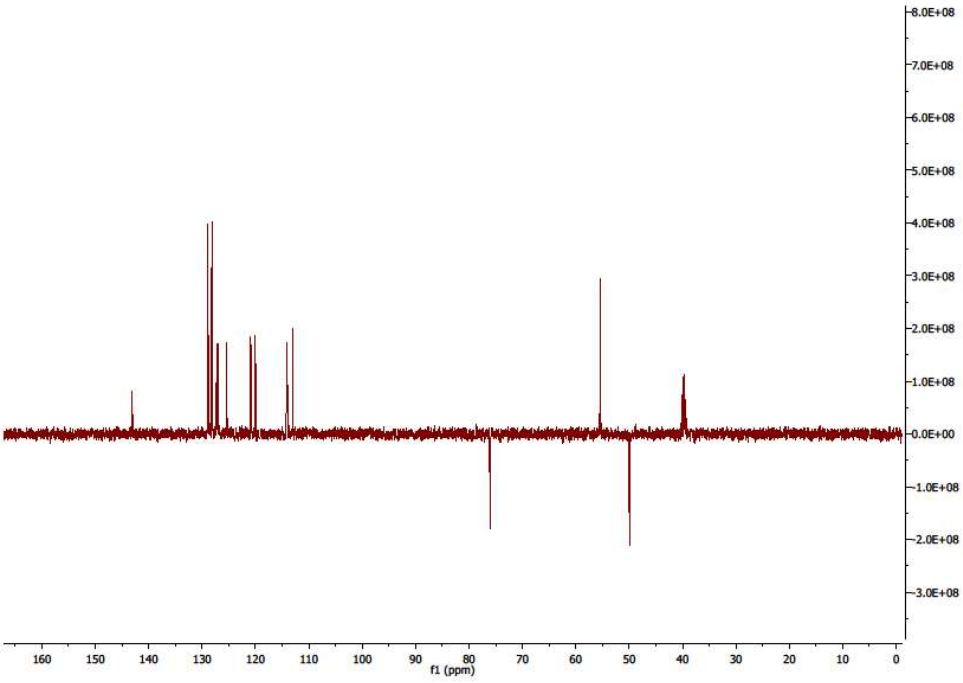

Figure S22. DEPT-135 NMR spectrum of **HL4·Br**.

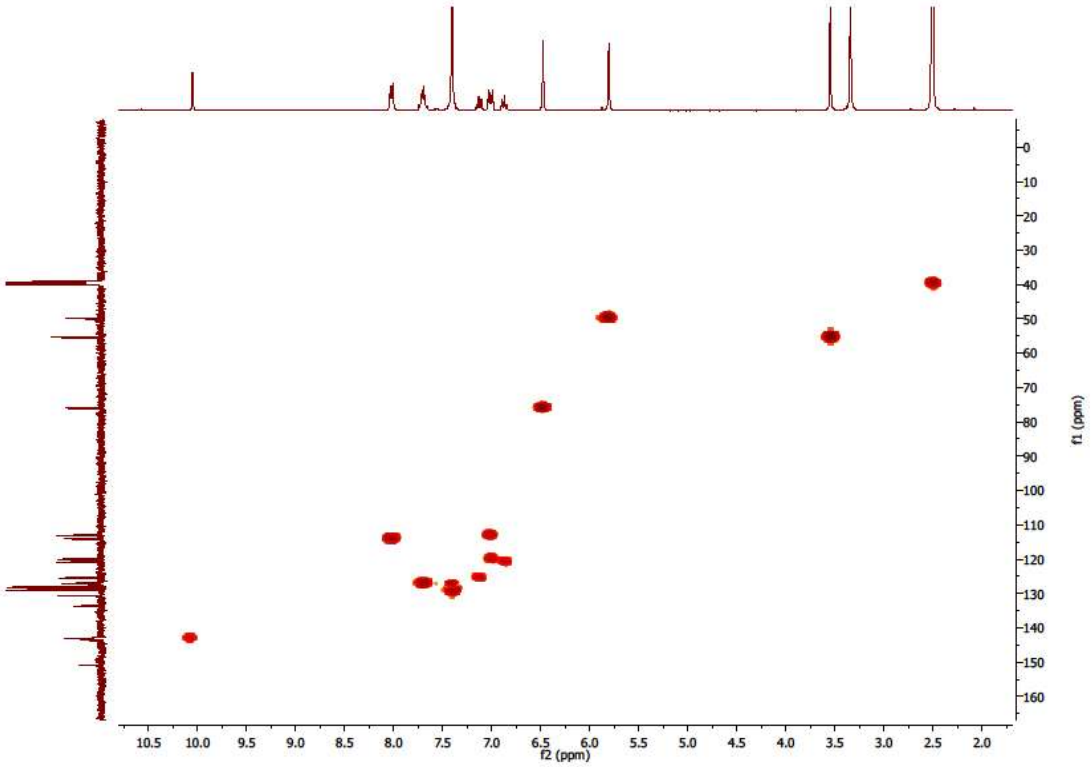

Figure S23. ^{1}H-^{13}C HSQC NMR spectrum of **HL4·Br**.

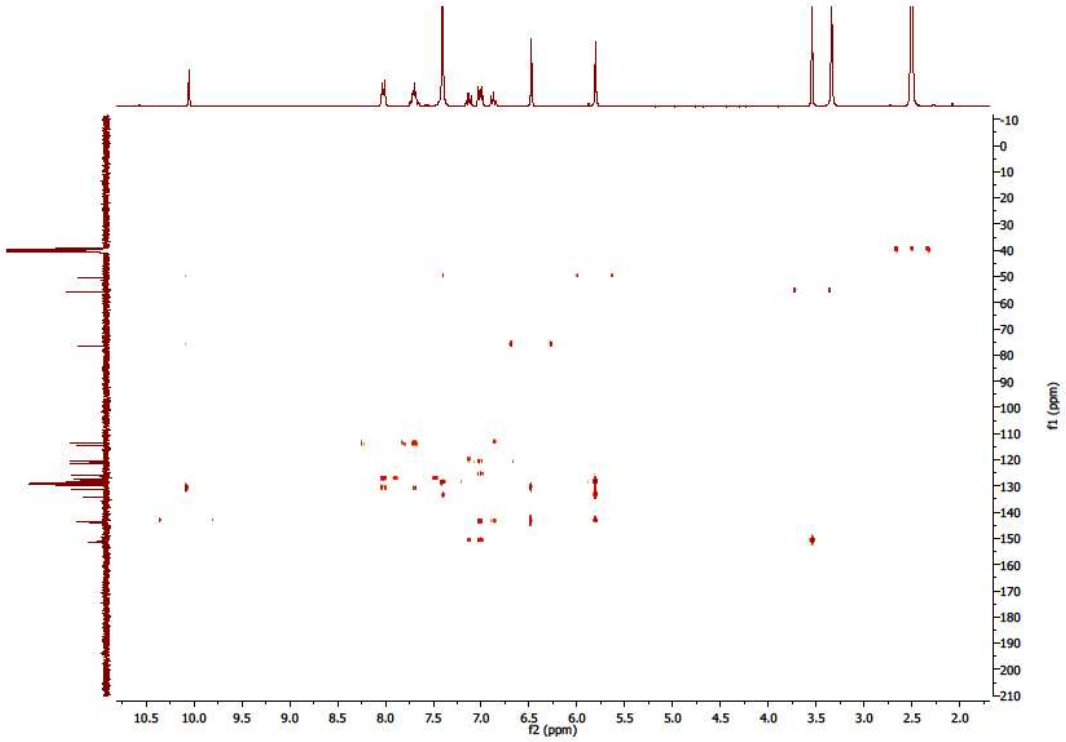

Figure S24. ^{1}H-^{13}C HMBC NMR spectrum of **HL4·Br**.

[{PdI2(pyCl)}3(L1)] C1

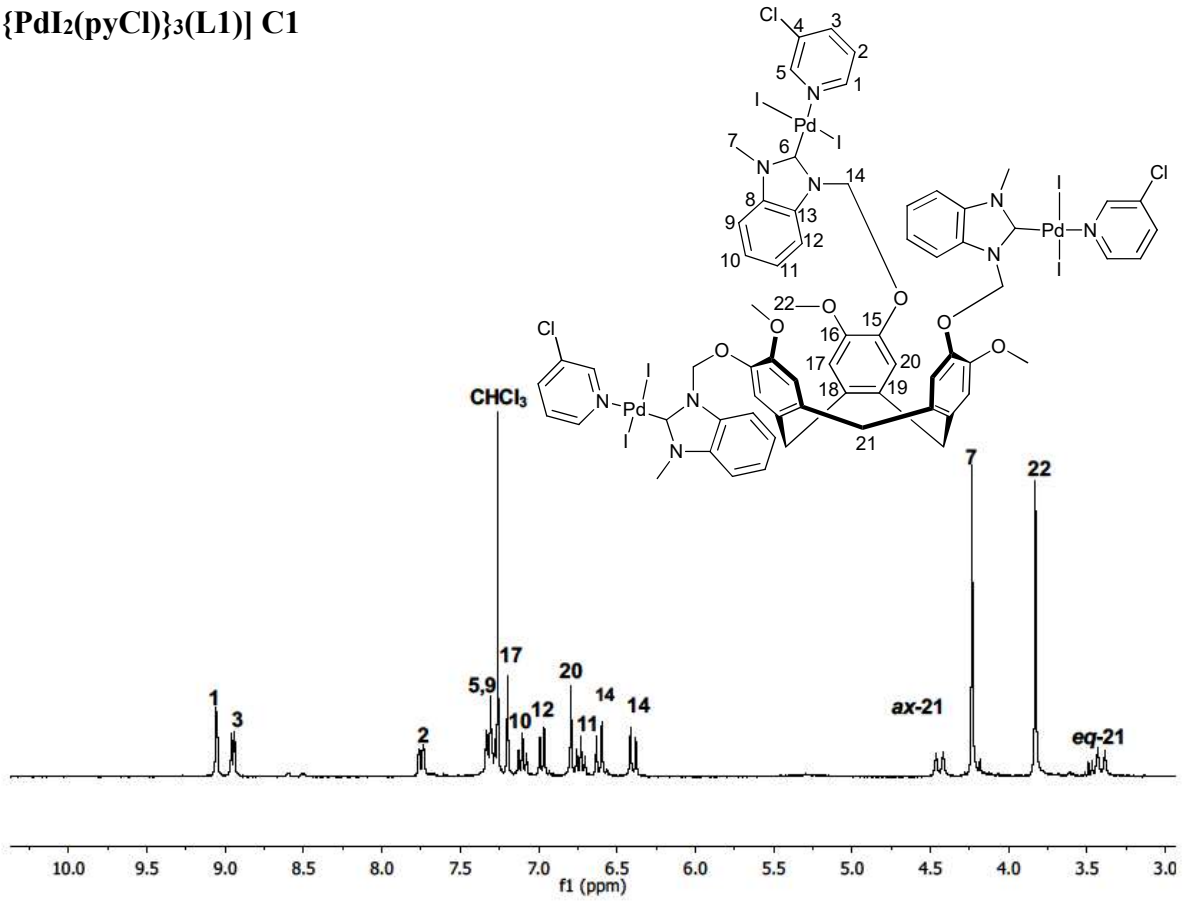

Figure S25. ^{1}H NMR spectrum (300 MHz, DMSO-d_6) of [{PdI_2(pyCl)}$_3$(L1)] **C1**. δ (ppm) 9.05 (d, 3H, J= 2.2 Hz, H^1), 8.95 (dd, 3H, J= 5.4, 1.1 Hz, H^3), 7.77-7.72 (m, 3H, H^2), 7.34-7.27 (m, 6H, H^5, H^9), 7.20 (s, 3H, H^{17}), 7.10 (t, 3H, J= 7.7 Hz, H^{10}), 6.98 (d, 3H, J= 8.2 Hz, H^{12}), 6.79 (s, 3H, H^{20}), 6.73 (t, 3H, J= 7.8 Hz, H^{11}), 6.61 (d, 3H, J= 10.2 Hz, H^{14}), 6.40 (d, 3H, J= 10.2 Hz, H^{14}), 4.44 (d, 3H, J= 13.8 Hz, *ax*-H^{21}), 4.23 (s, 9H, H^7), 3.83 (s, 9H, H^{22}), 3.41 (d, 3H, J= 13.8 Hz, *eq*-H^{21}).

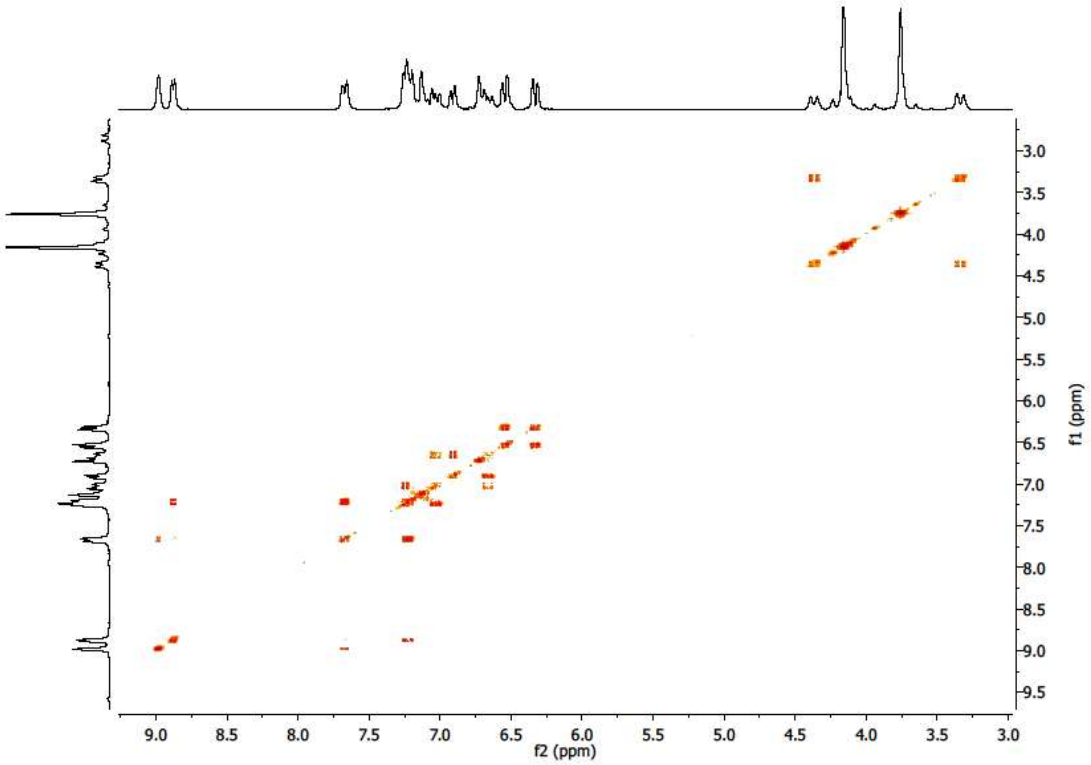

Figure S26. ^{1}H-^{1}H COSY (300 MHz, DMSO-d_6) NMR spectrum of **C1**.

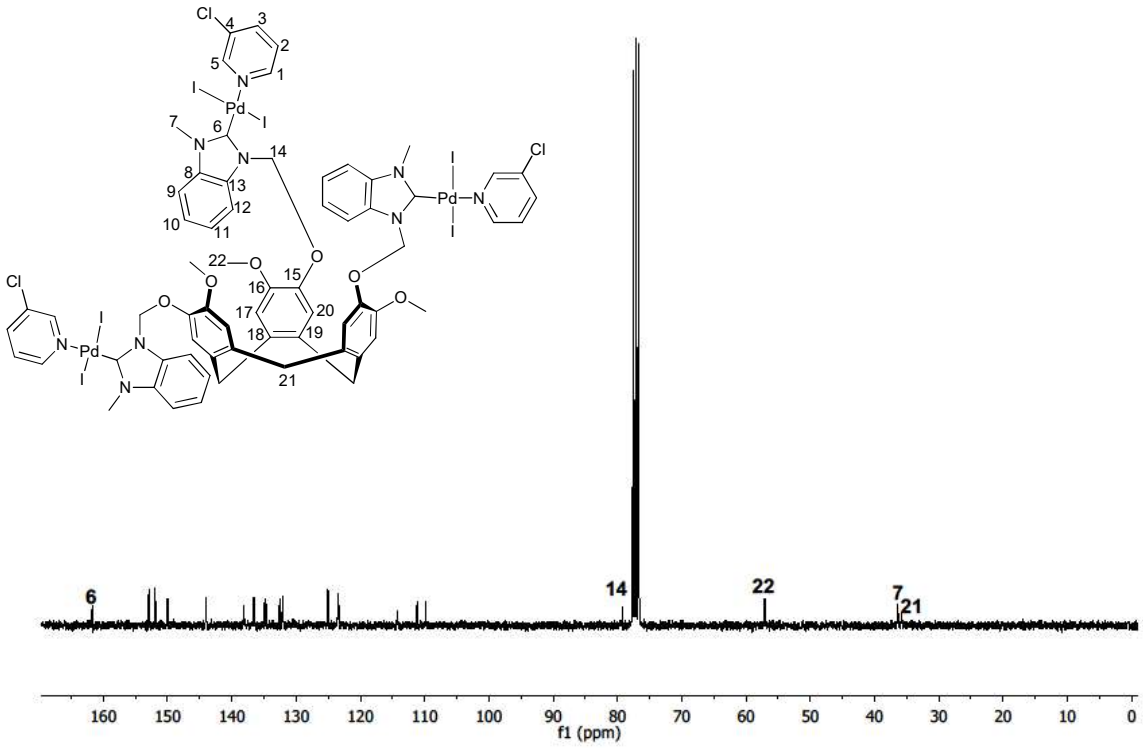

Figure S27. ^{13}C{^{1}H} NMR spectrum (75 MHz, DMSO-d_6) of **C1**. δ (ppm) 161.69 (C^{6}), 152.88 (C^{1}), 151.92 (C^{13}), 149.97 (C^{16}), 143.99 (C^{15}), 138.10 (C^{2}), 136.55 (C^{18}), 134.96 (C^{8}), 134.68 (C^{13}), 132.54 (C^{4}), 132.07 (C^{19}), 125.04 (C^{5}), 123.54 (C^{10}), 123.41 (C^{11}), 123.36 (C^{17}), 114.19 (C^{20}), 111.15 (C^{12}), 109.78 (C^{9}), 79.20 (C^{14}), 57.07 (C^{22}), 36.36 (C^{7}), 35.76 (C^{21}).

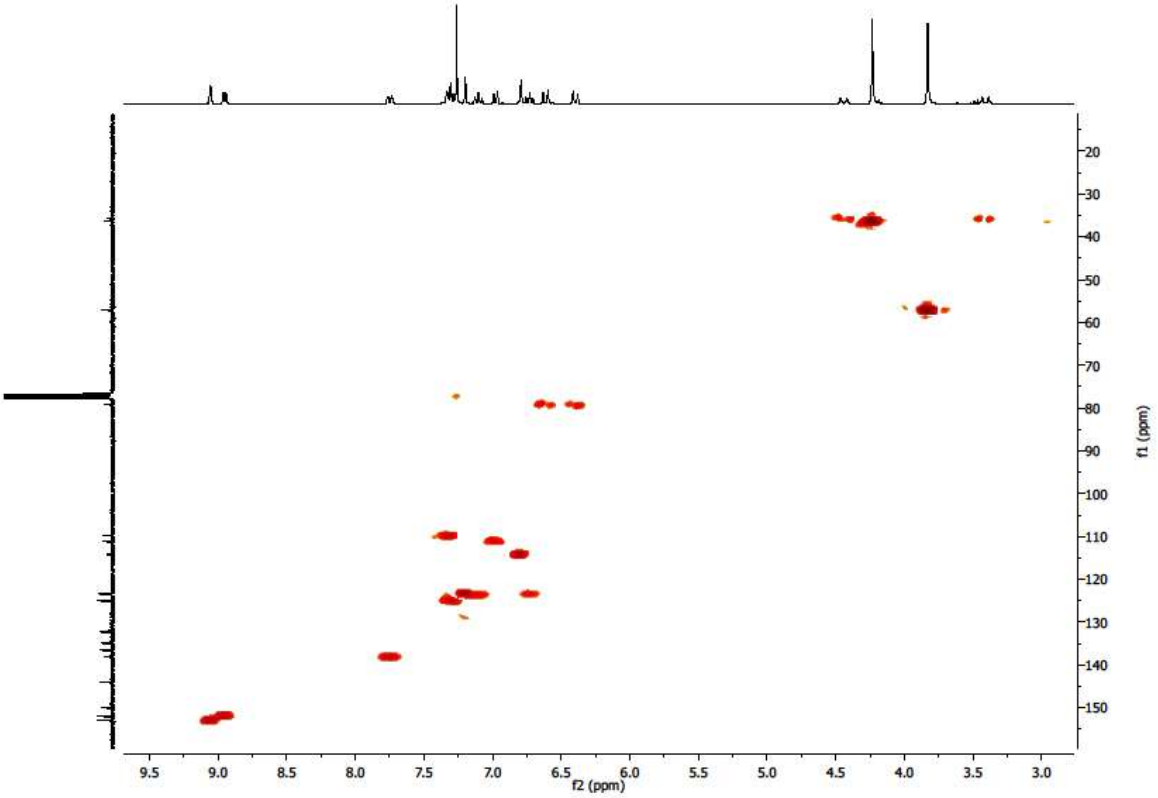

Figure S28. ^{1}H-^{13}C HSQC NMR spectrum of **C1**.

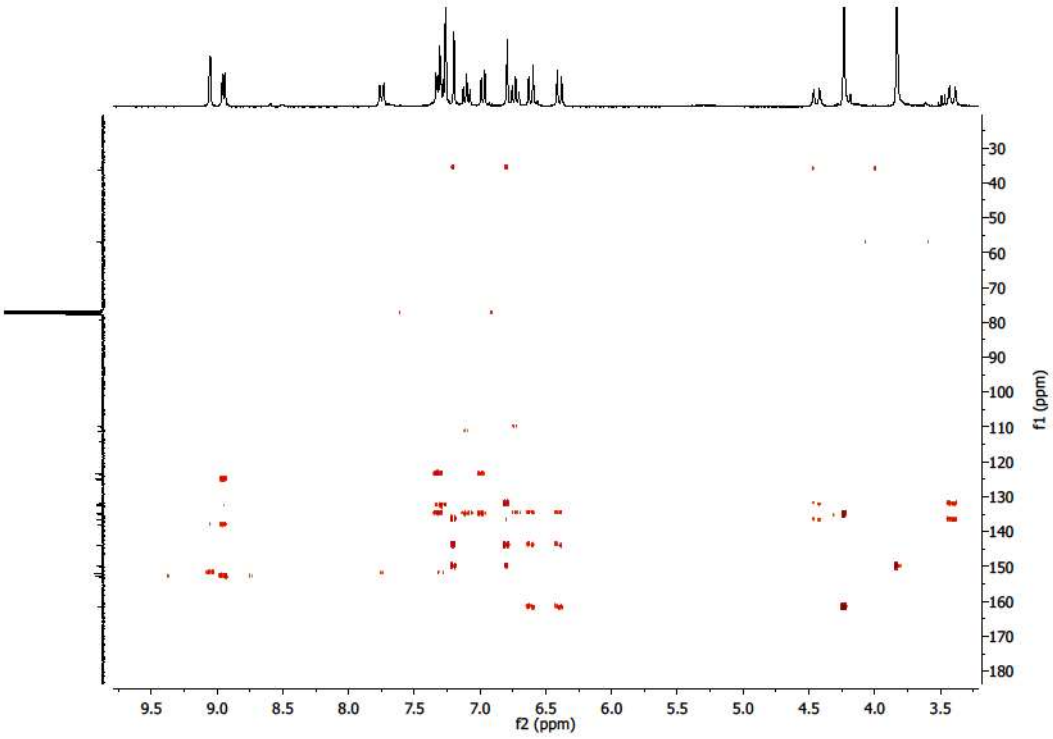

Figure S29. ^{1}H-^{13}C HMBC NMR spectrum of **C1**.

[{PdI$_2$(pyCl)}$_3$(L2)] C2

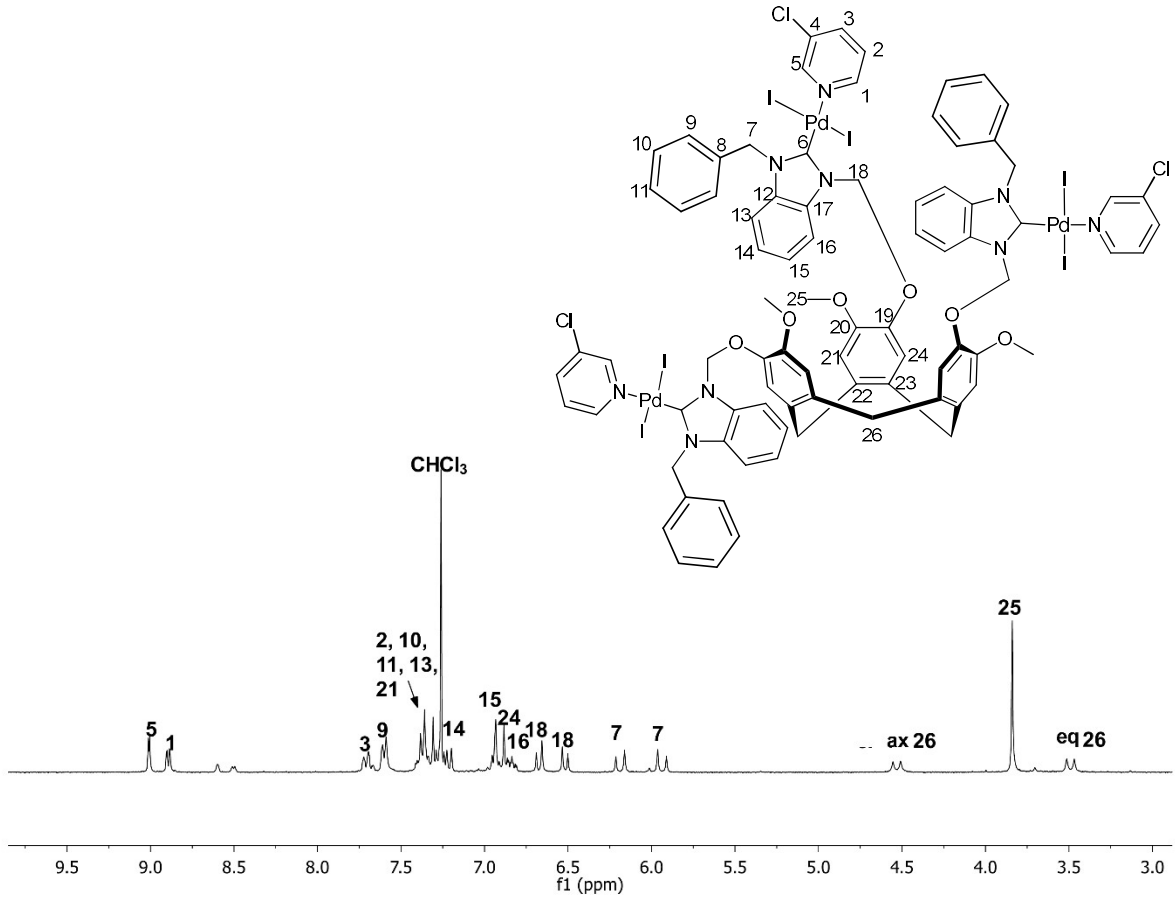

Figure S30: ^{1}H NMR spectrum (300 MHz, DMSO-d_6) of **C2**. δ (ppm) 9.01, (d, 3H, J= 2.3 Hz H^5), 8.89 (dd, 3H, J= 5.5, 1.4 Hz, H^1), 7.70 (tdd, 3H, J= 8.5, 2.4, 1.3 Hz, H^3), 7.63 – 7.57 (m, 6H, H^9), 7.42 – 7.28 (m, 18H, H^2, H^{10}, H^{11}, H^{13}, H^{21}), 7.21 (d, 6H, J = 8.2 Hz, H^{14}), 6.94 (d, 3H, J = 6.3 Hz H^{15}), 6.91 (s, 3H, H^{24}), 6.84 (ddd, 3H, J= 8.3, 6.1, 2.3 Hz, H^{16}), 6.67 (d, 3H, J= 10.0 Hz, H^{18}), 6.52 (d, 3H, J= 9.9 Hz, H^{18}), 6.19 (d, 3H, J= 15.7 Hz, H^7), 5.94 (d, 3H, J= 15.8 Hz, H^7) 4.53 (d, 3H J = 13.8 Hz, ax-H^{26}), 3.84 (s, 9H, H^{25}), 3.49 (d, 3H, J = 13.5 Hz, eq-H^{26}).

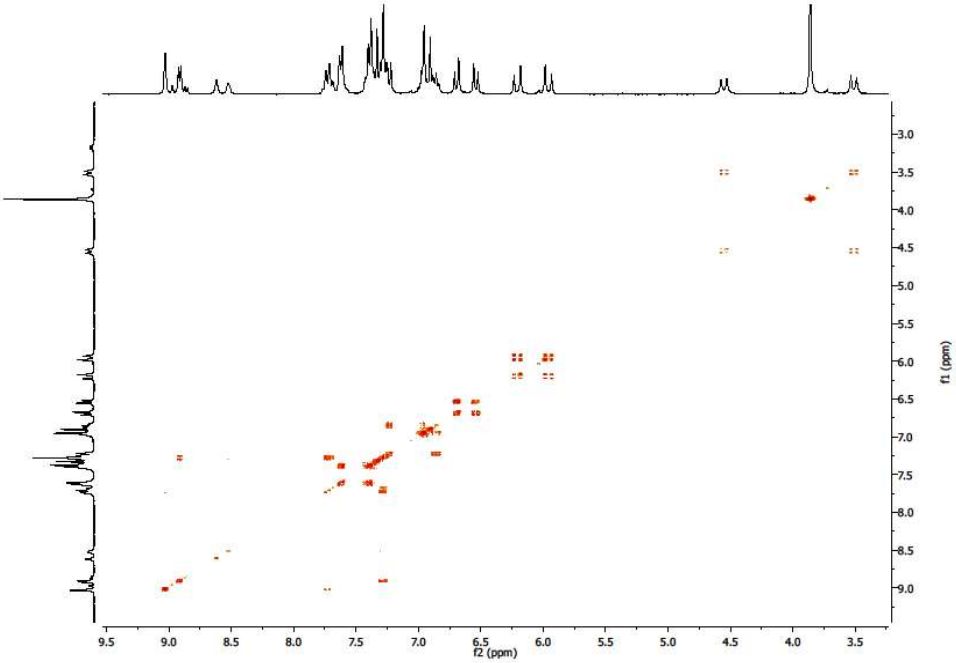

Figure S31. ^{1}H-^{1}H COSY (300 MHz, DMSO-d_6) NMR spectrum of **C2**.

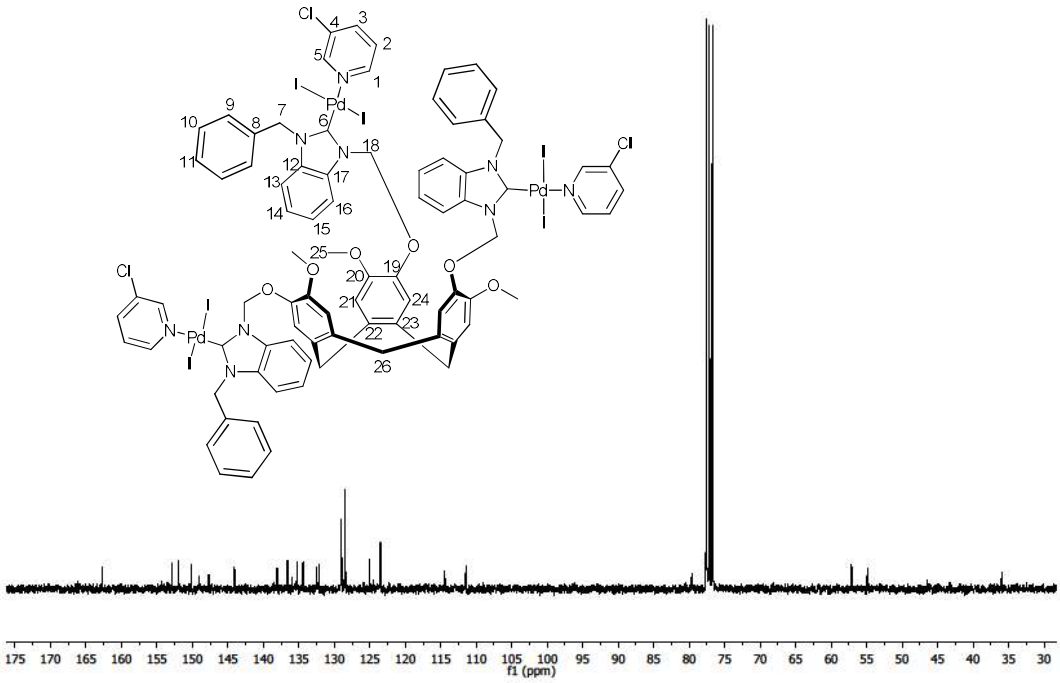

Figure S32. ^{13}C{^{1}H} NMR spectrum (75 MHz, DMSO-d_6) of **H$_3$L1·3I**. δ (ppm) 162.69 (C^{6}), 152.90 (C^{5}), 151.94 (C^{1}), 150.17 (C^{20}), 144.07 (C^{19}), 138.06 (C^{3}), 136.60 (C^{22}), 135.24 (C^{17}), 134.47 (C^{12}), 134.41 (C^{8}), 132.52 (C^{4}), 132.15 (C^{23}), 129.00 (C^{10}, C^{11}), 128.49 (C^{9}), 125.01 (C^{2}), 124.47 (C^{13}), 123.51 (C^{16}, C^{21}), 114.45 (C^{24}), 111.50 (C^{15}), 111.46 (C^{14}), 79.64 (C^{18}), 57.12 (C^{25}), 54.90 (C^{7}), 35.97 (C^{26}).

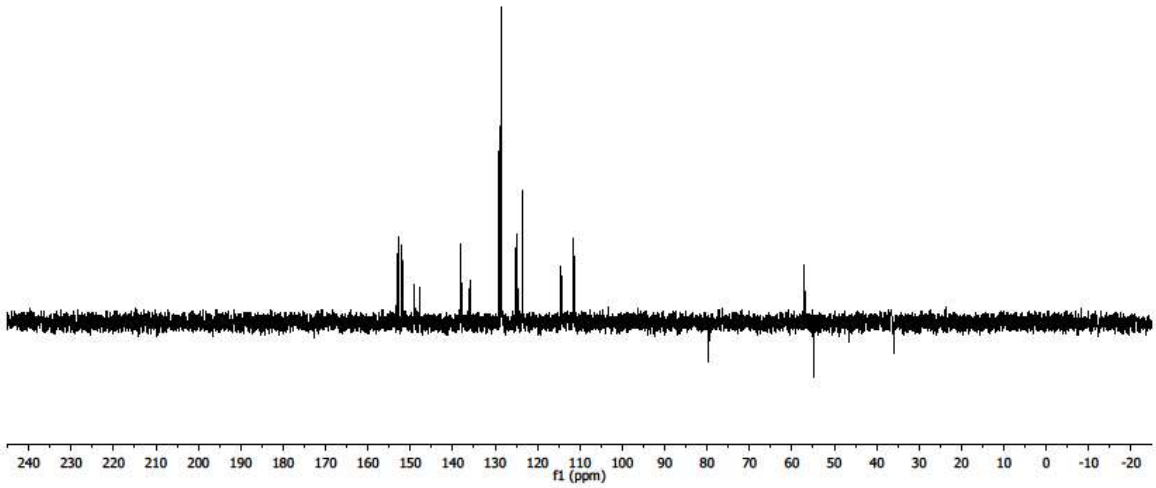

Figure S33. DEPT-135 NMR spectrum of **C2**.

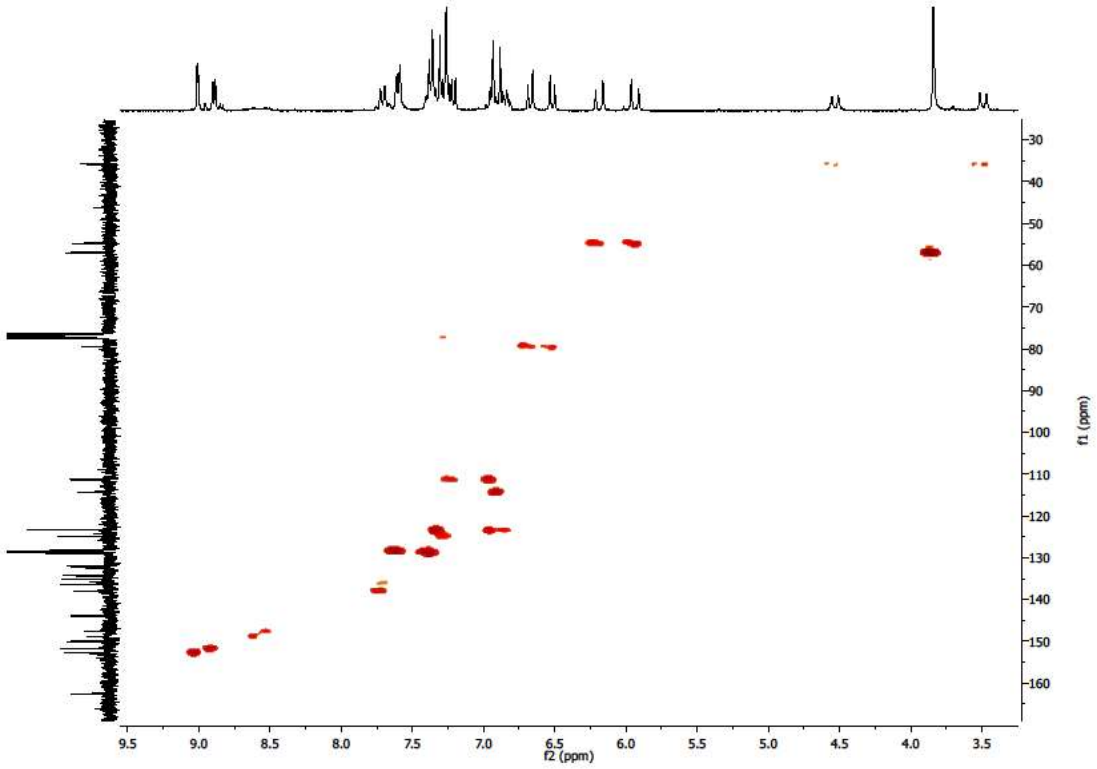

Figure S34. ^{1}H-^{13}C HSQC NMR spectrum of **C2**.

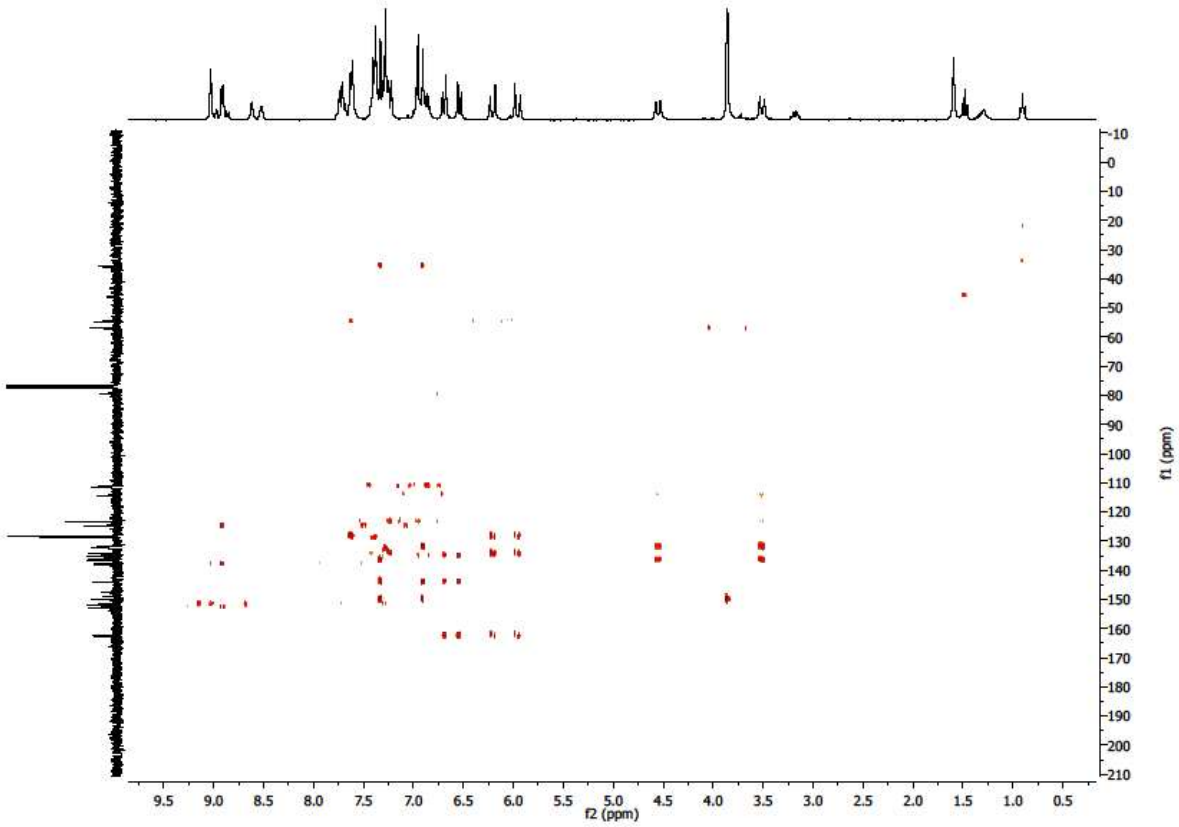

Figure S35. ^{1}H-^{13}C HMBC NMR spectrum of **C2**.

[PdI$_2$(pyCl)(L3)] C3

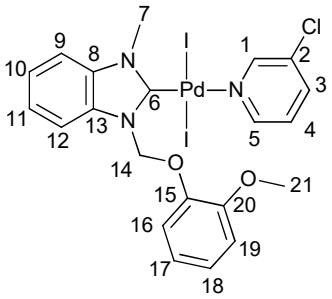

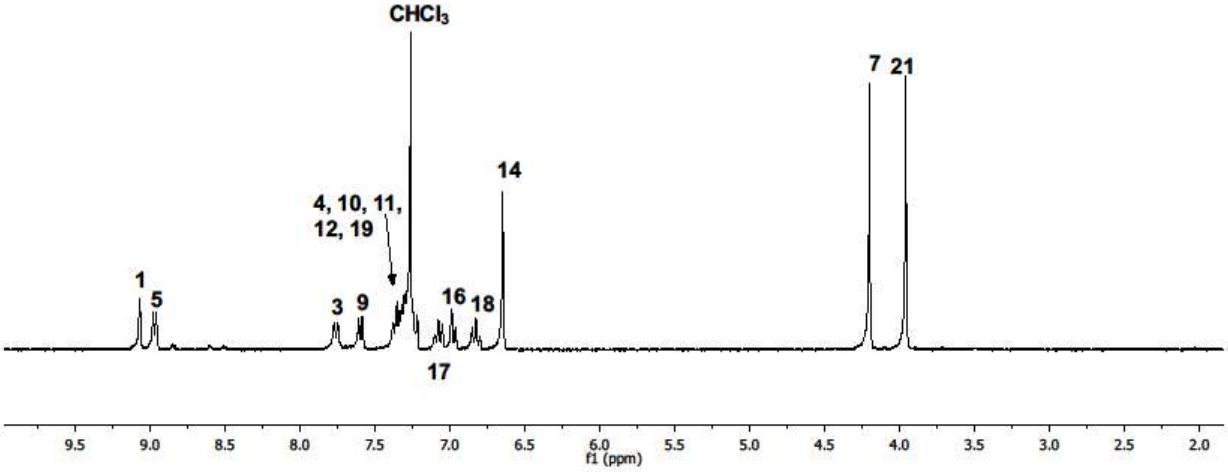

Figure S36: ^{1}H NMR spectrum (300 MHz, DMSO-d_6) of **C3**. δ (ppm) 9.07 (d, 1H, J= 2.3 Hz, H^1), 8.97 (dd, 1H, J= 5.4, 1.4 Hz, H^5), 7.76 (dt, 1H, J= 8.2, 1.8 Hz, H^3), 7.64-7.54 (m, 1H, H^9), 7.41-7.19 (m, 5H, H^4, H^{10}, H^{11}, H^{12}, H^{19}), 7.07 (td, 1H, J= 7.8, 1.7 Hz, H^{17}), 6.97 (dd, 1H, J= 8.2, 1.6 Hz, H^{16}), 6.82 (td, 1H, J= 7.6, 1.6 Hz, H^{18}), 6.65 (s, 2H, H^{14}), 4.20 (s, 3H, H^7), 3.96 (s, 3H, H^{21}).

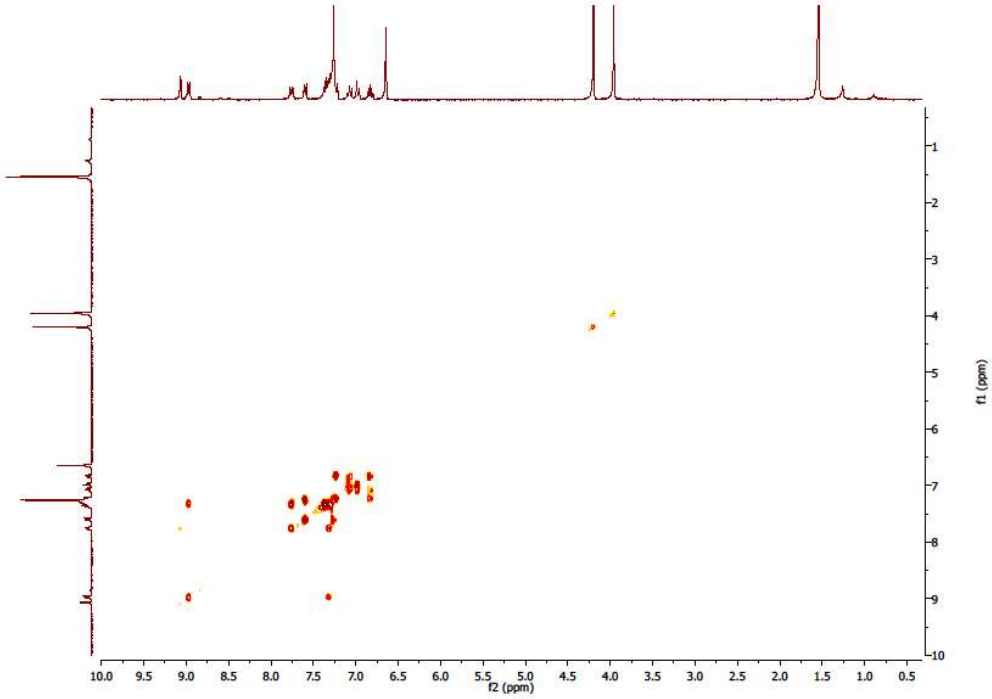

Figure S37. ^{1}H-^{1}H COSY (300 MHz, DMSO-d_6) NMR spectrum of **C3**.

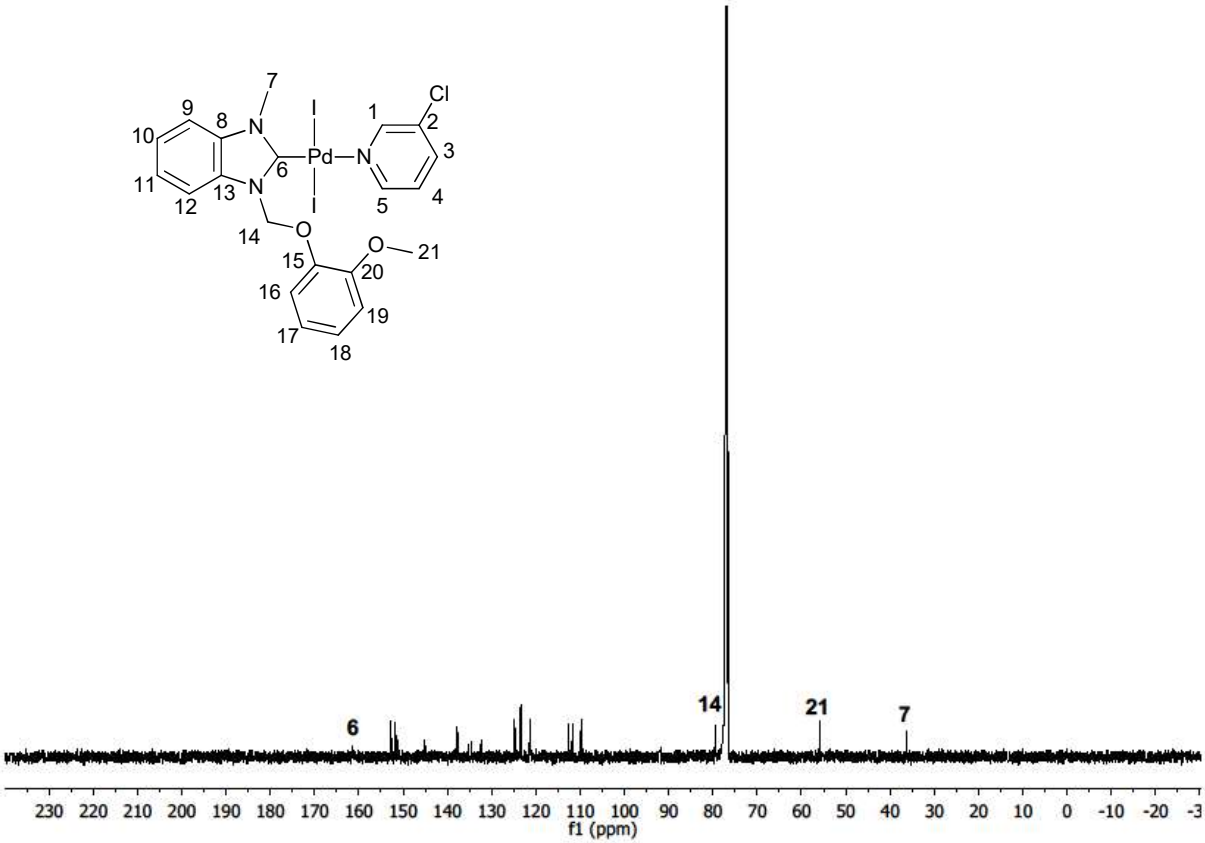

Figure S38. ^{13}C{^{1}H} NMR spectrum (75 MHz, DMSO-d_6) of **C3**. δ (ppm) 161.36 (C^6), 152.72 (C^1), 151.72 (C^5), 151.29 (C^{20}), 145.11 (C^{15}), 137.76 (C^3), 135.28 (C^8), 134.52 (C^{13}), 132.32 (C^2), 124.83

(C^4), 124.77 (C^{17}), 124.69 (C^{11}), 123.43 (C^{10}), 121.40 (C^{19}), 121.18 (C^{18}), 112.69 (C^{16}), 111.70 (C^9), 109.75 (C^{12}), 79.38 (C^{14}), 55.88 (C^{21}), 36.21 (C^7).

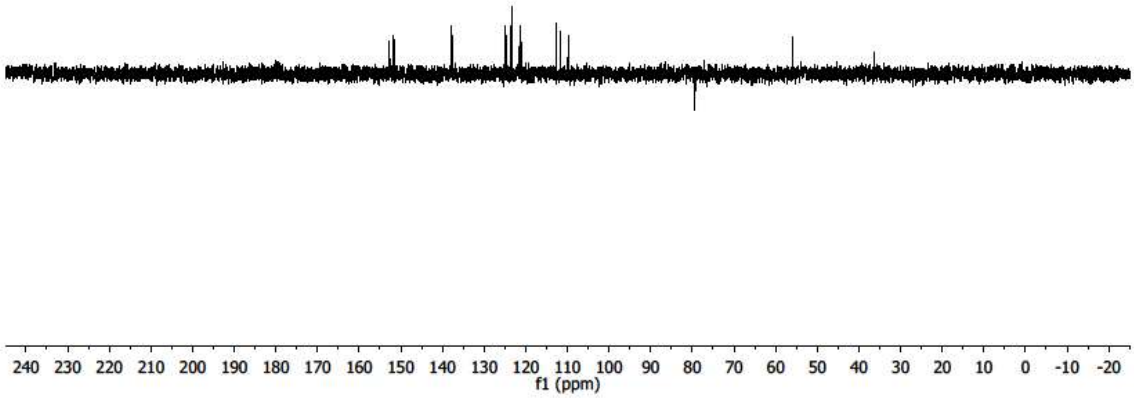

Figure S39. DEPT-135 NMR spectrum of **C3**.

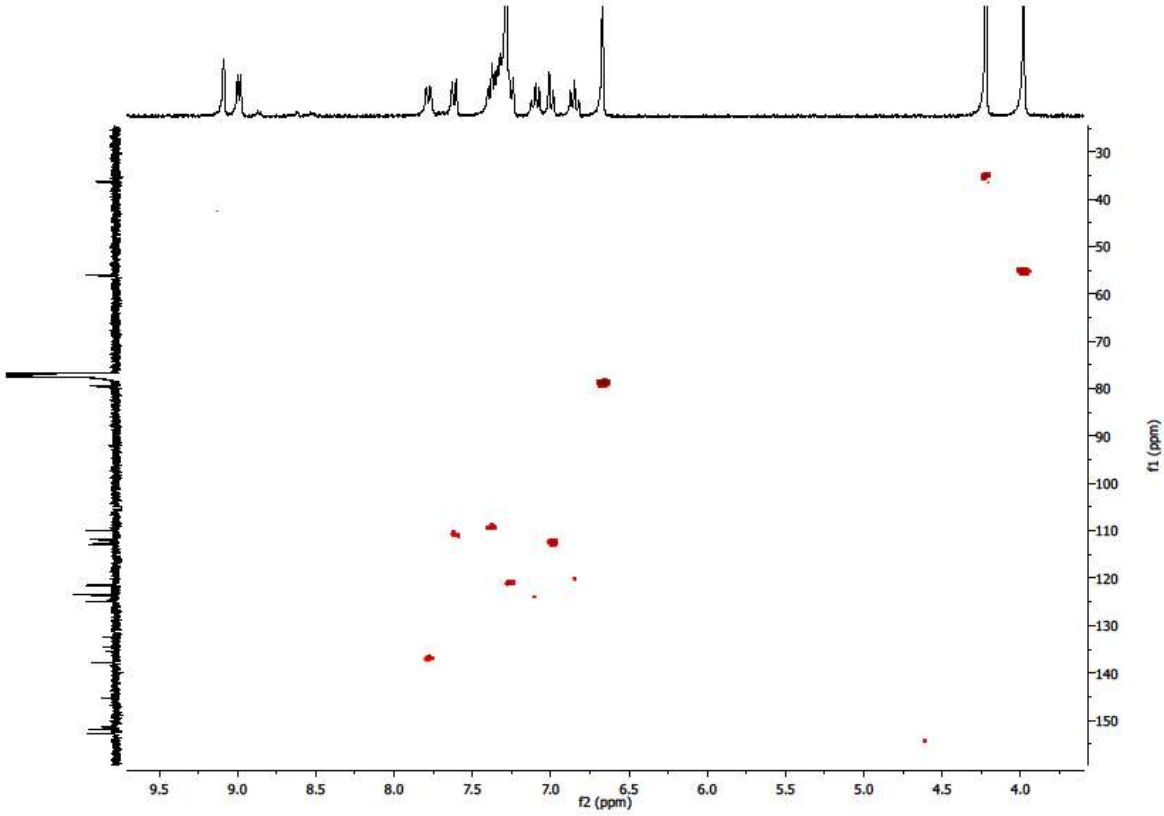

Figure S40. ^{1}H-^{13}C HSQC NMR spectrum of **C3**.

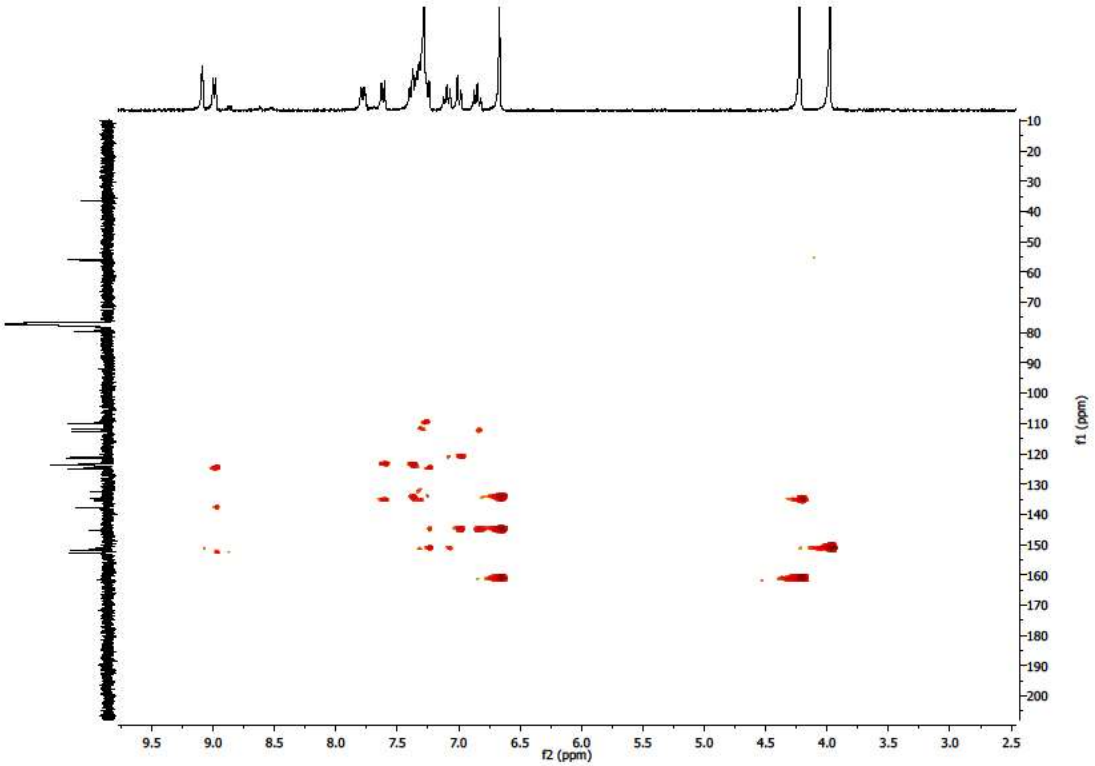

Figure S41. ^{1}H-^{13}C HMBC NMR spectrum of **C3**.

[PdI$_2$(pyCl)(L4)] C4

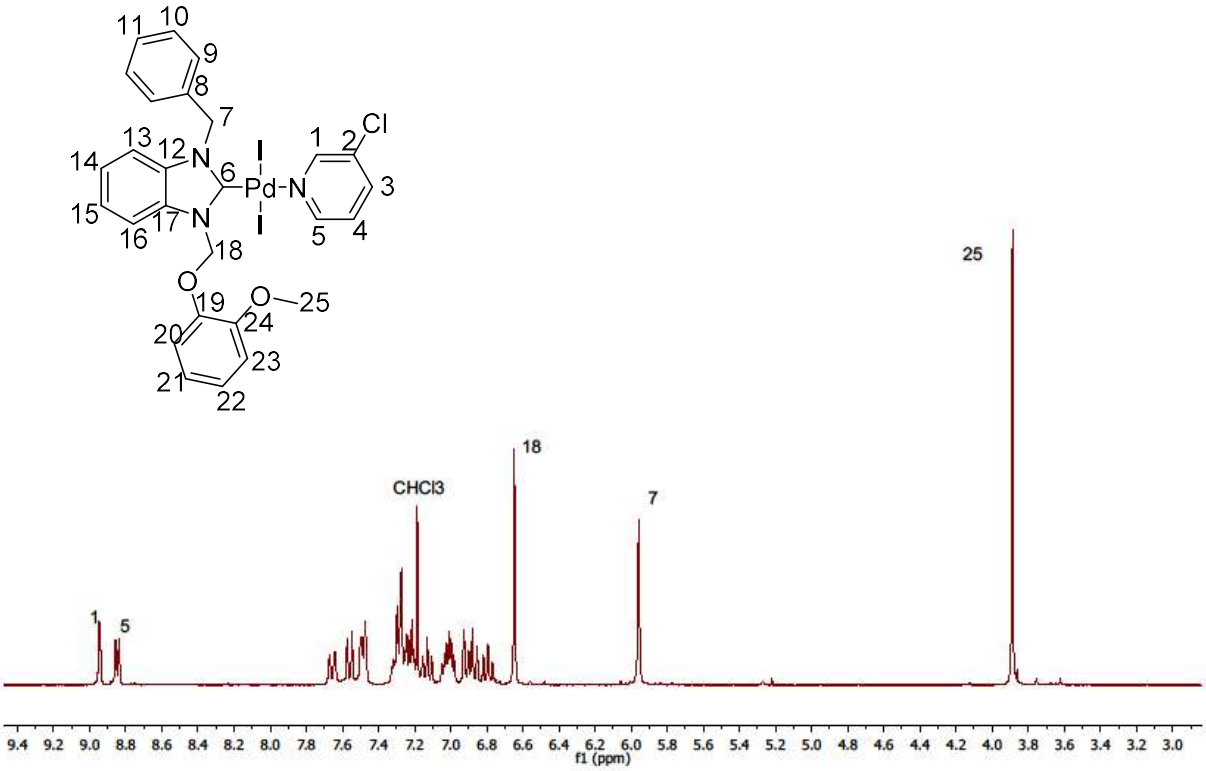

Figure S42: ^{1}H NMR spectrum (300 MHz, DMSO-d_6) of **C4**. δ (ppm) 9.02 (d, 1H, J=2.3 Hz, H^1), 8.92 (dd, 1H, *J*=5.5, 1.3 Hz, H^5), 7.73 (ddd, 1H, *J*= 8.2, 2.4, 1.3 Hz, H^3), 7.63 (d, 1H, *J*= 8.1 Hz, H^{13}), 7.56 (dd, 2H *J*= 7.5, 2.0 Hz, H^{10}), 7.42 – 7.27 (m, 5H, H^4, H^9, H^{11}, H^{23}), 7.20 (td, 1H, *J*= 8.3, 7.8, 1.2 Hz, H^{15}), 7.14 – 7.04 (m, 2H, H^{14}, H^{22}), 6.99 (dd, 1H, *J*= 8.2, 1.6 Hz, H^{20}) 6.94 (d, 1H, *J*= 8.9 Hz, H^{16}), 6.87 (td, 1H, *J*= 7.7, 1.6 Hz, H^{21}), 6.72 (s, 2H, H^{18}), 6.03 (s, 2H, H^7), 3.96 (s, 3H, H^{25})

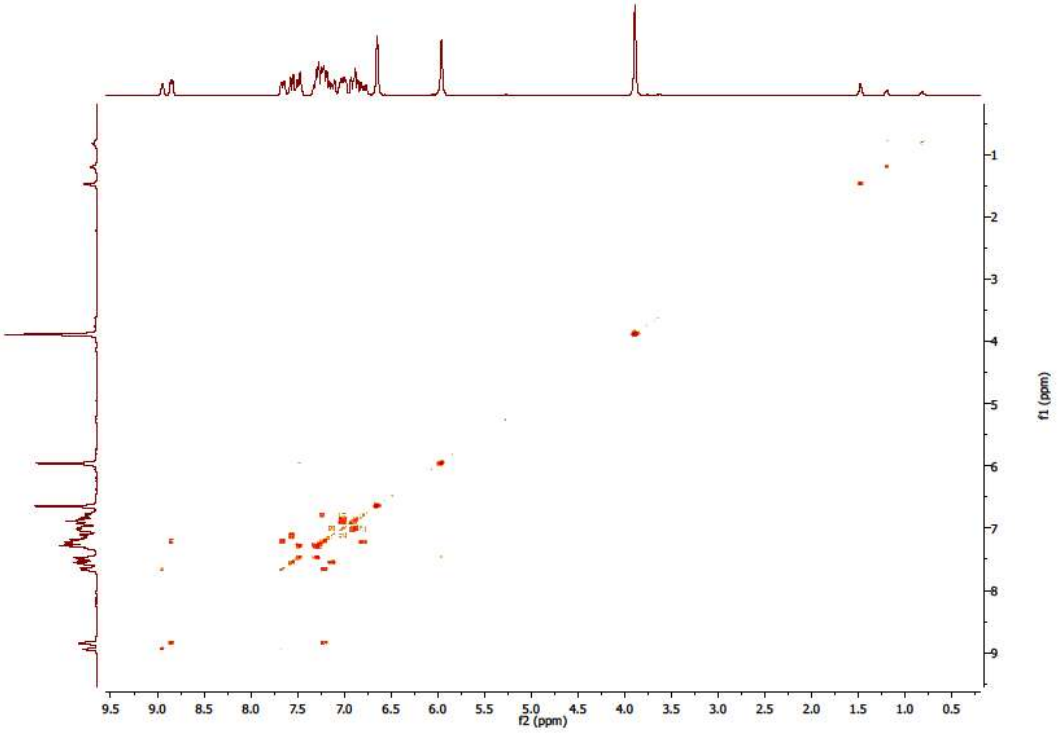

Figure 43. ^{1}H-^{1}H COSY (300 MHz, DMSO-d_6) NMR spectrum of **C4**.

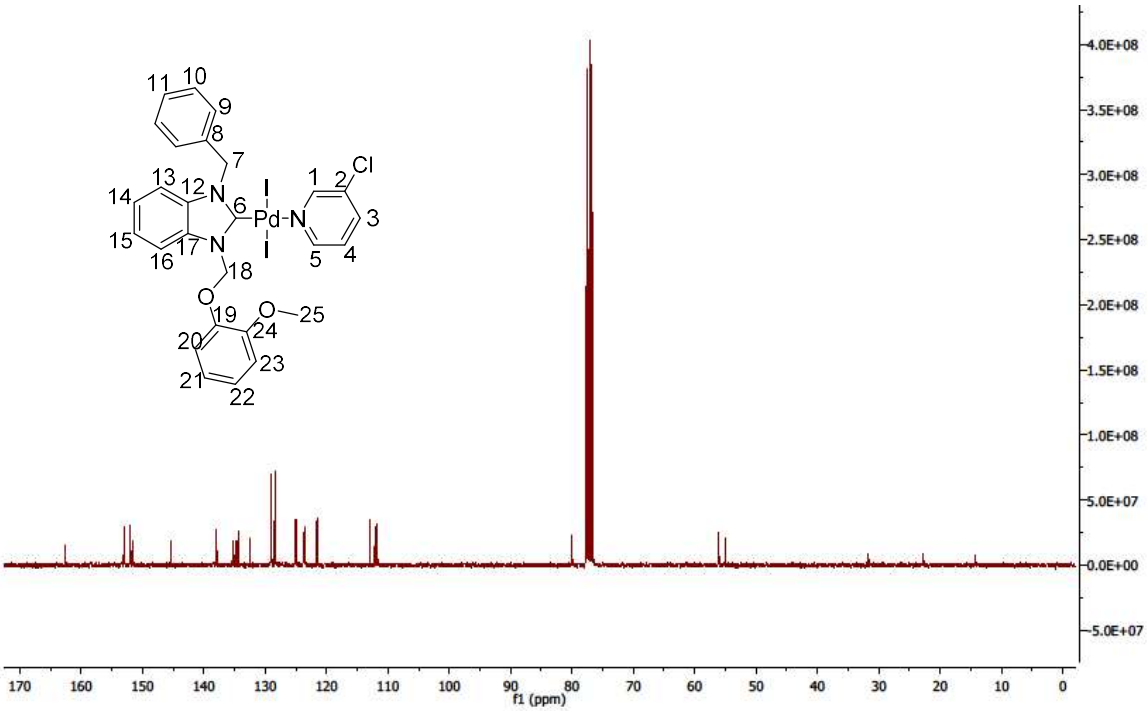

Figure S44. ^{13}C{^{1}H} NMR spectrum (75 MHz, DMSO-d_6) of **H$_3$L1·3I**. δ (ppm) 162.57 (C^{6}), 152.95 (C^{1}), 151.96 (C^{5}), 151.54 (C^{24}), 145.39 (C^{19}), 137.98 (C^{3}), 135.26 (C^{17}), 134.86 (C^{12}), 134.42 (C^{8}), 132.51 (C^{2}), 128.98 (C^{9}), 128.42 (C^{10}), 128.39 (C^{11}), 125.07 (C^{22}), 124.90 (C^{4}), 123.69 (C^{14}), 123.60 (C^{15}), 121.55 (C^{23}), 121.46 (C^{21}), 112.92 (C^{20}), 112.05 (C^{13}), 111.72 (C^{16}), 79.99 (C^{18}), 56.13 (C^{25}), 55.01 (C^{7}).

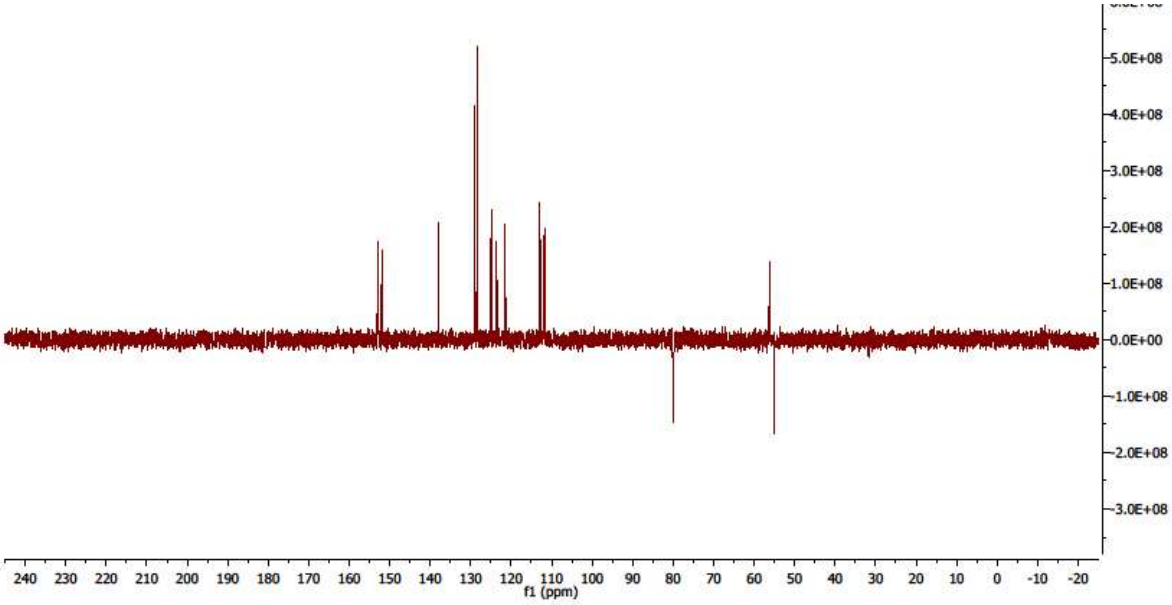

Figure S45. DEPT-135 NMR spectrum of **C4**.

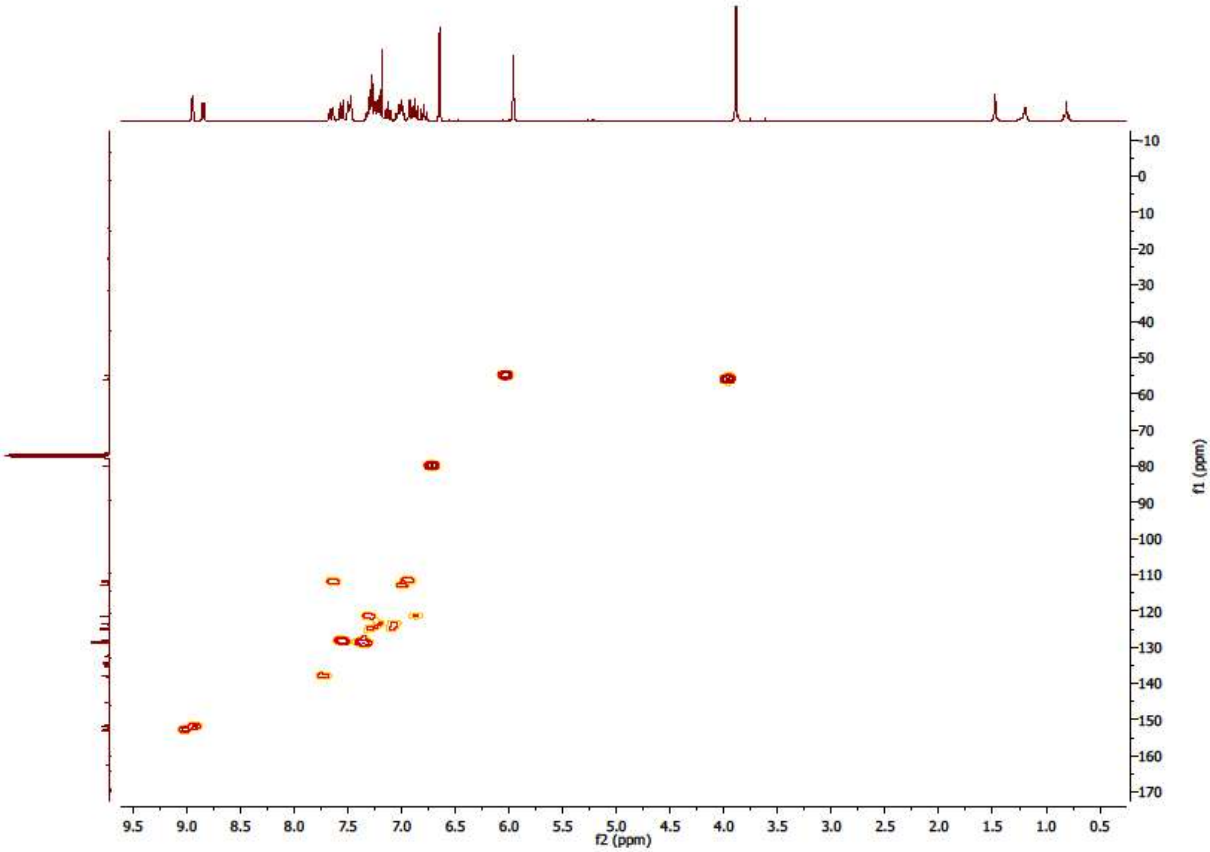

Figure S46. ^{1}H-^{13}C HSQC NMR spectrum of **C4**.

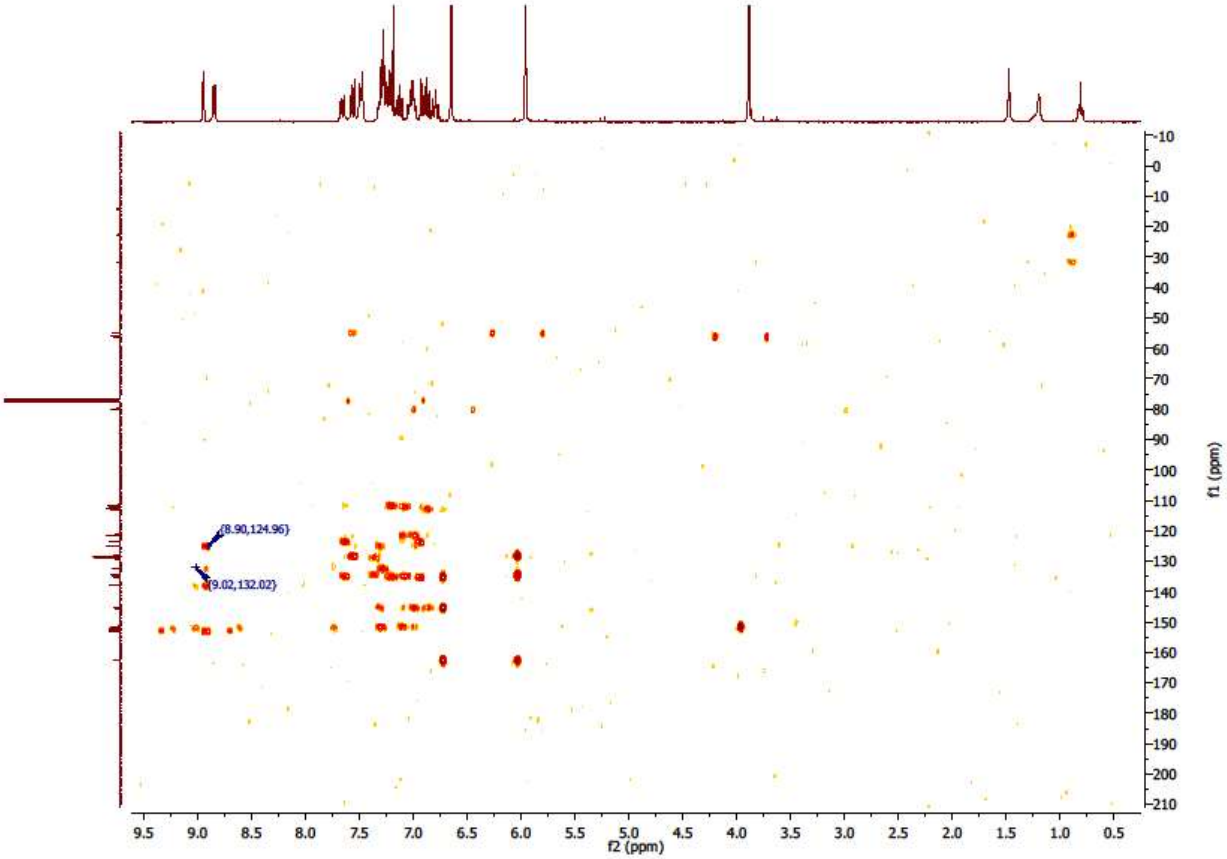

Figure S47. ^{1}H-^{13}C HMBC NMR spectrum of **C4**.

1.2 Mass spectrometry

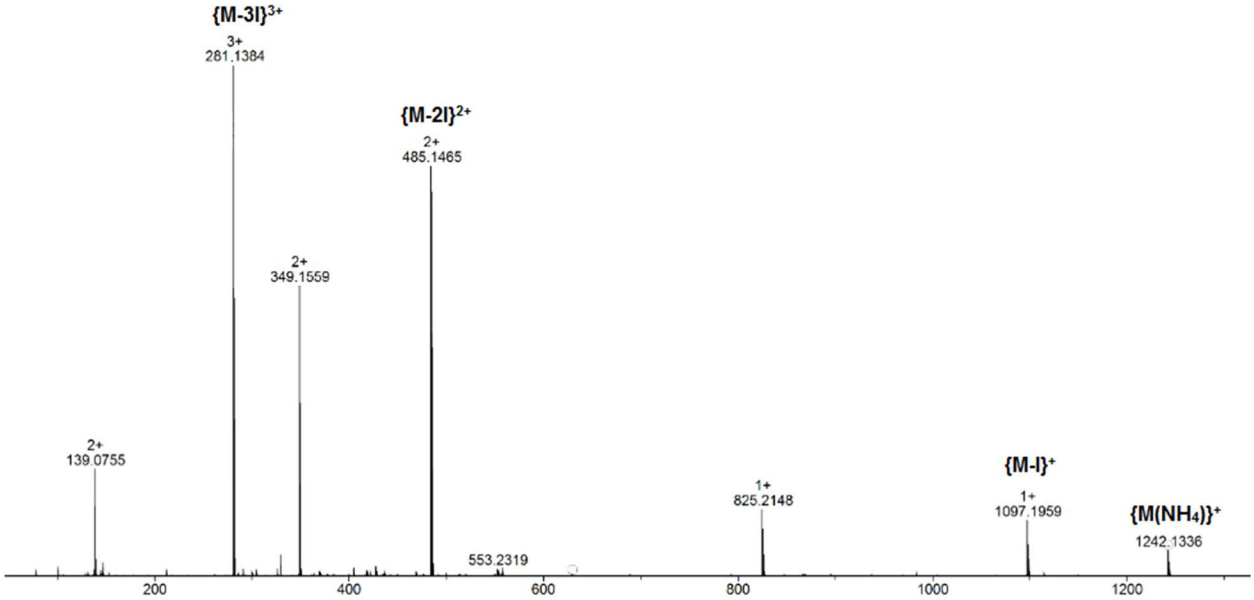

Figure S48. Electrospray mass spectrum of **H_3L1·3I**

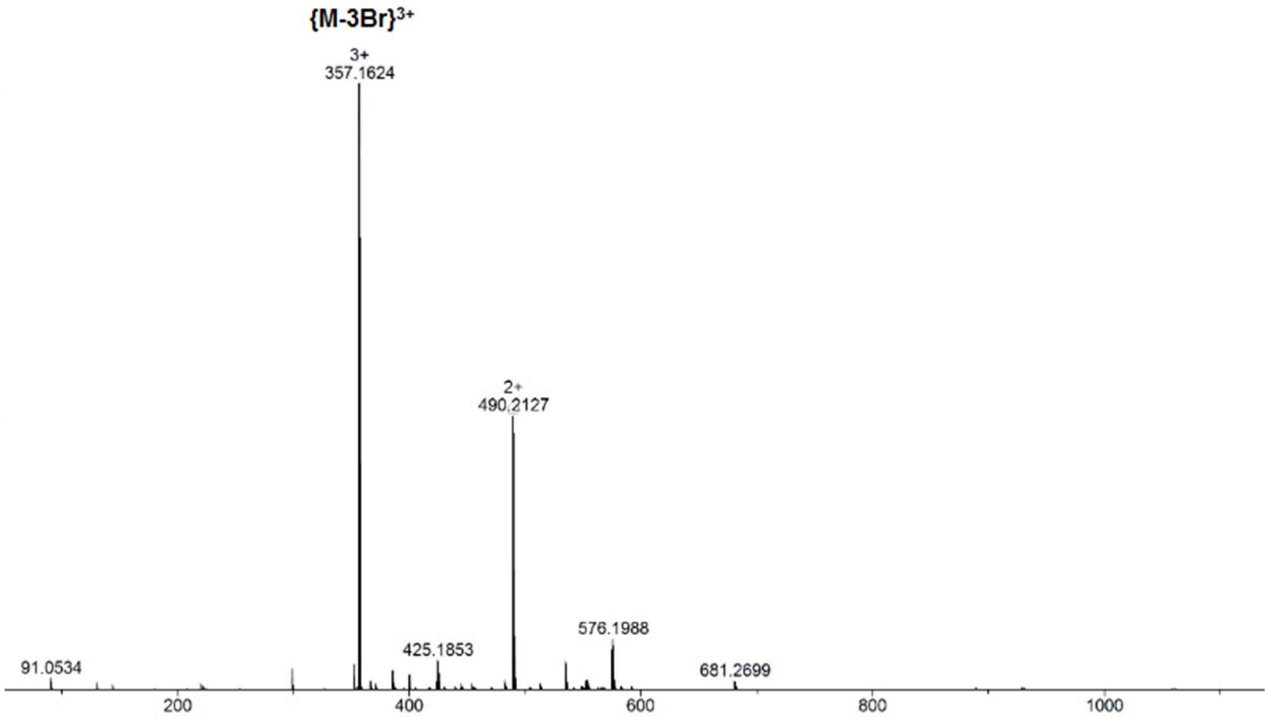

Figure S49. Electrospray mass spectrum of **H_3L2·3Br**

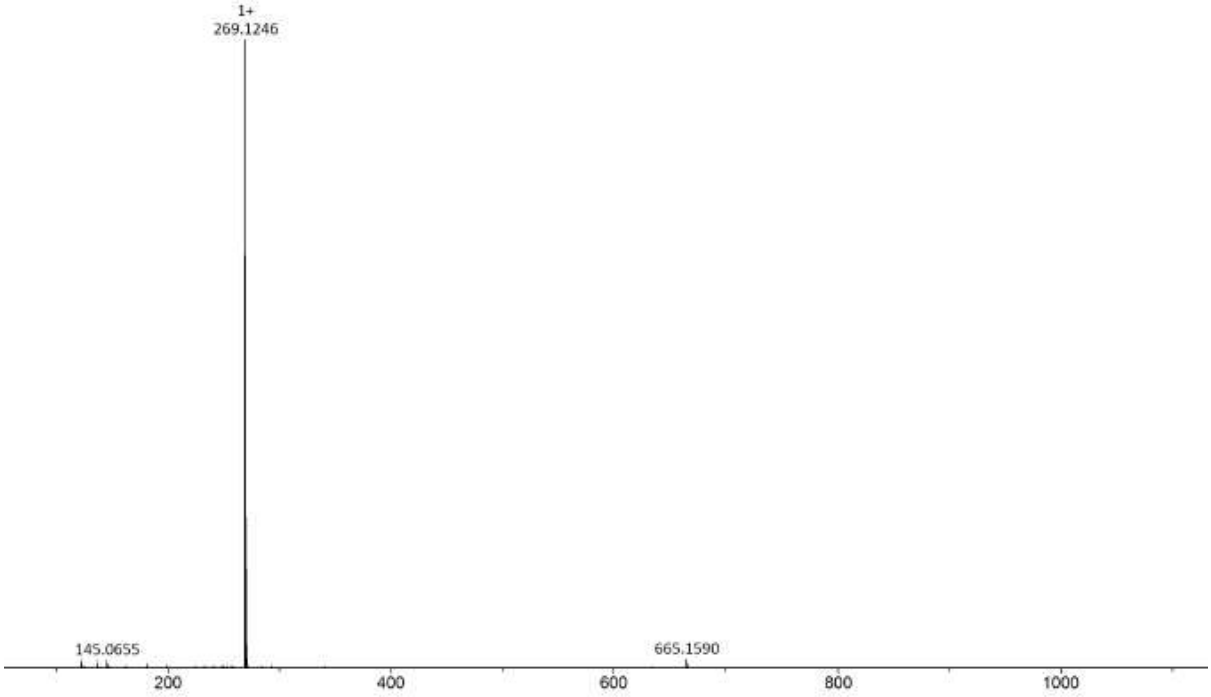

Figure S50. Electrospray mass spectrum of **HL3·I**

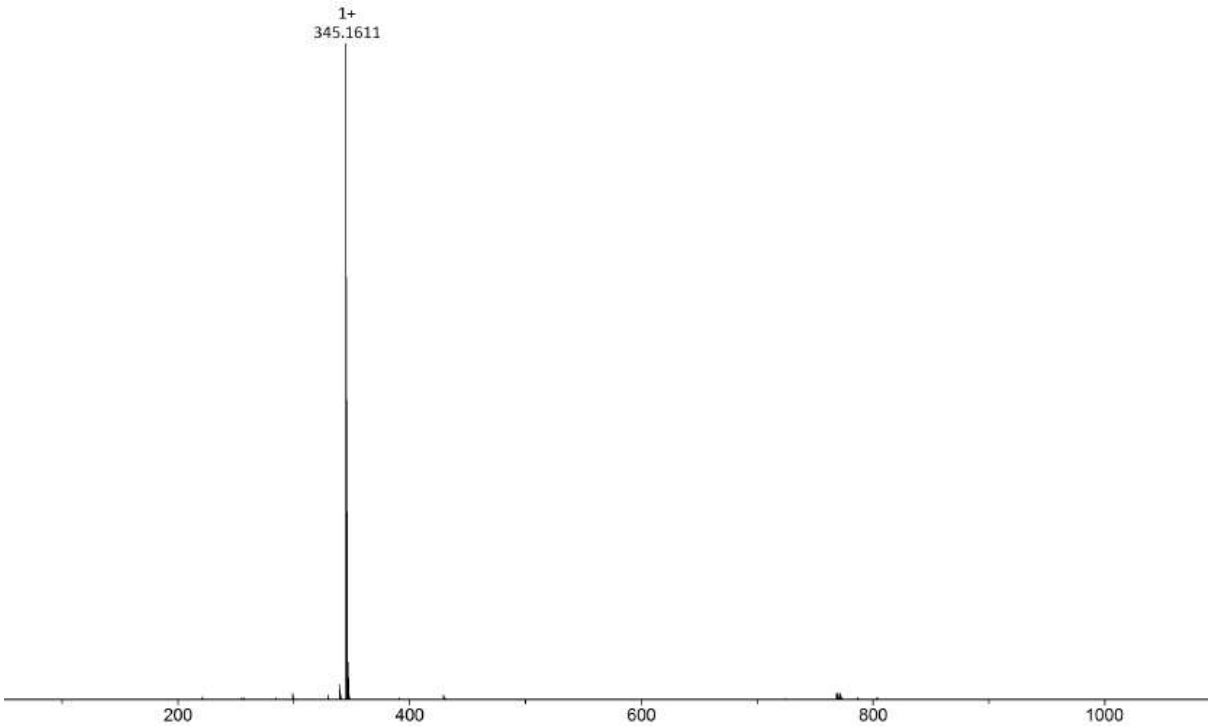

Figure S51. Electrospray mass spectrum of **HL4·Br**

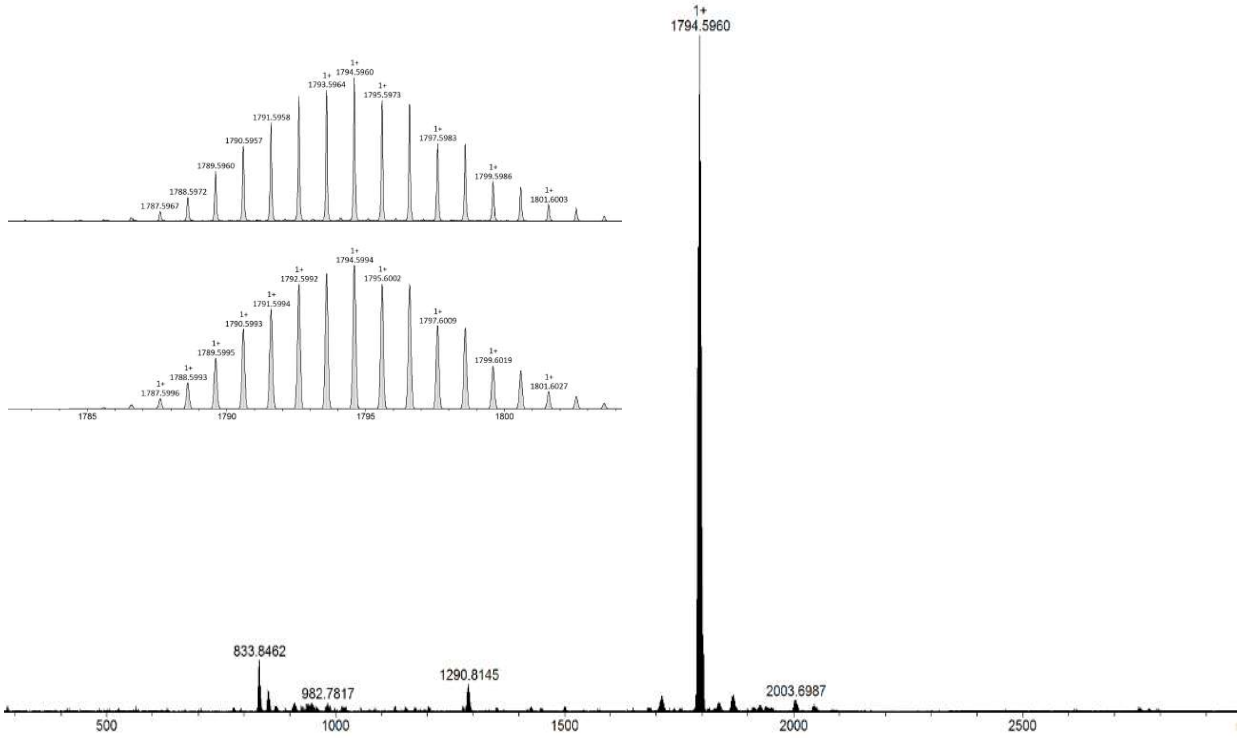

Figure S52. Electrospray mass spectrum of [{PdI_2(pyCl)}$_3$(L1)] **C1** with inset showing observed (top) and calculated peak for species [Pd_3I_5(L1)]+.

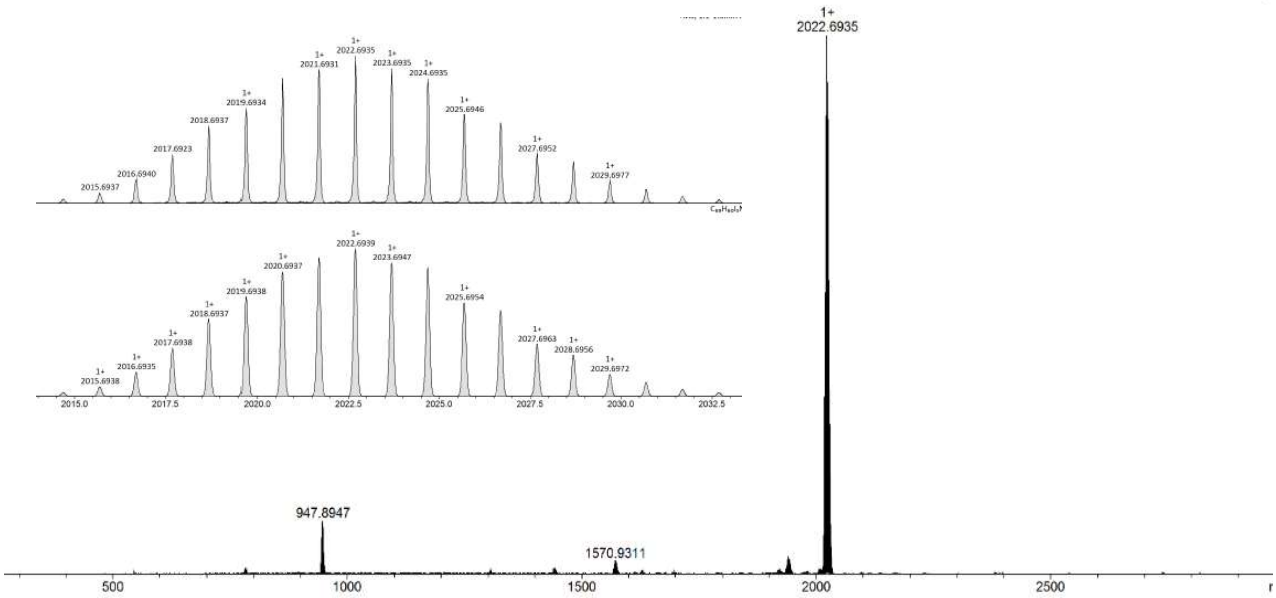

Figure S53. Electrospray mass spectrum of [{PdI_2(pyCl)}$_3$(L2)] **C2** with inset showing observed (top) and calculated peak for species [Pd_3I_5(L2)]+.

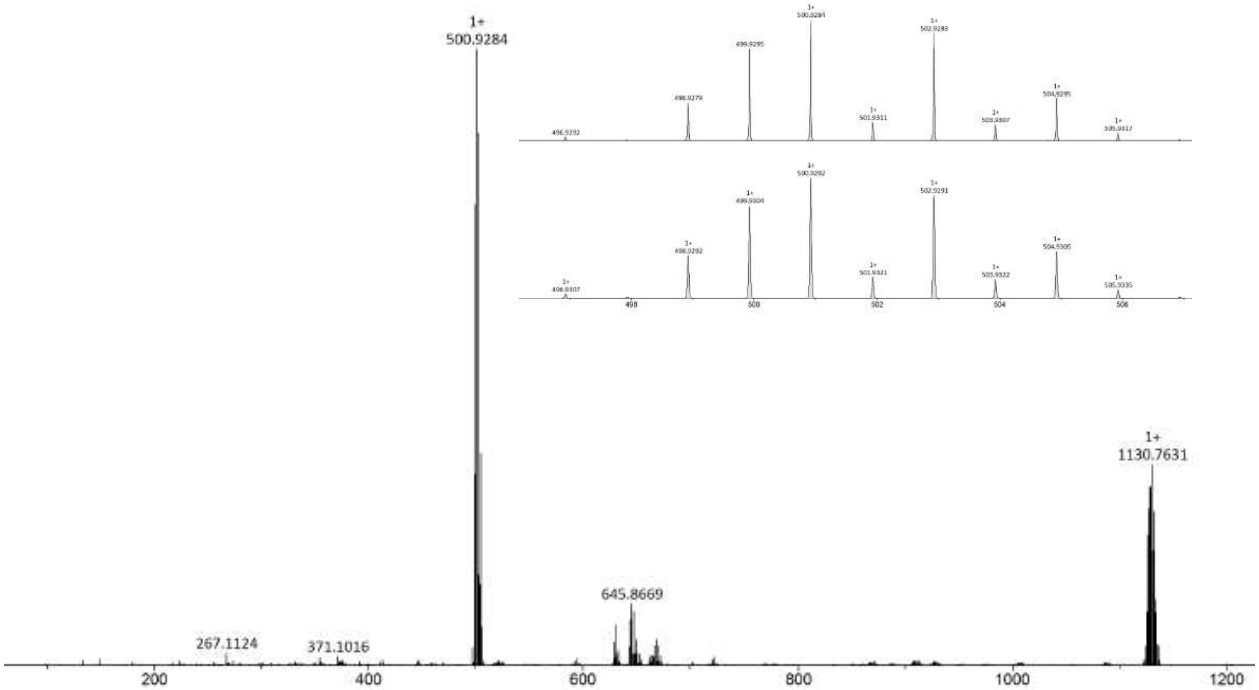

Figure S54. Electrospray mass spectrum of[PdI_2(pyCl)(L3)] **C3** with inset showing observed (top) and calculated peak for species [PdI(L3)]$^+$.

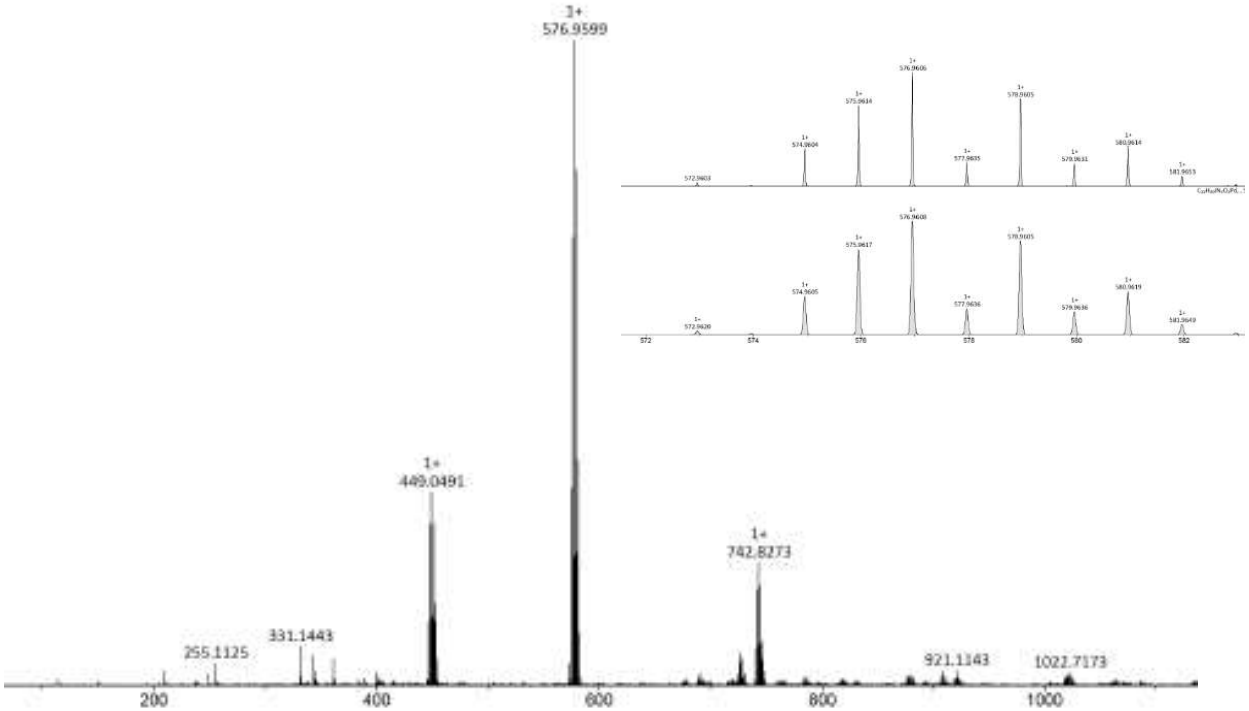

Figure S55. Electrospray mass spectrum of[PdI_2(pyCl)(L4)] **C4** with inset showing observed (top) and calculated peak for species [PdI_2(L4)].K^+.

1.3 Infrared spectroscopy

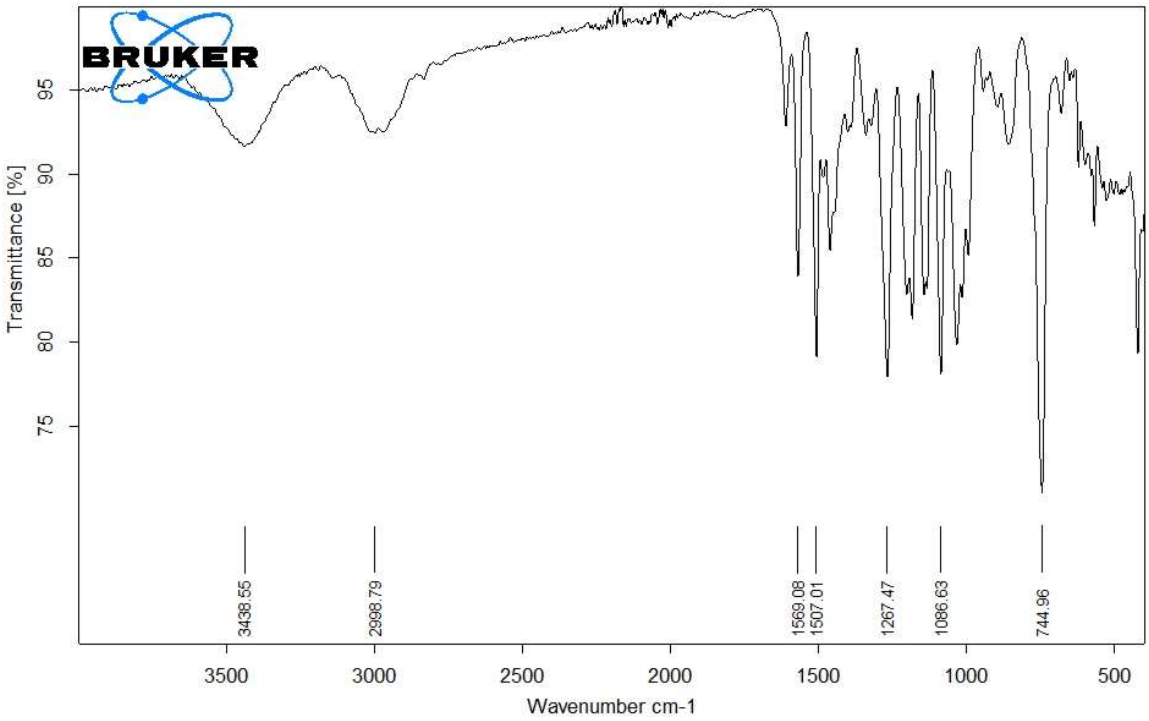

Figure S56. Infrared spectrum of **$H_3L1{\cdot}3I$**

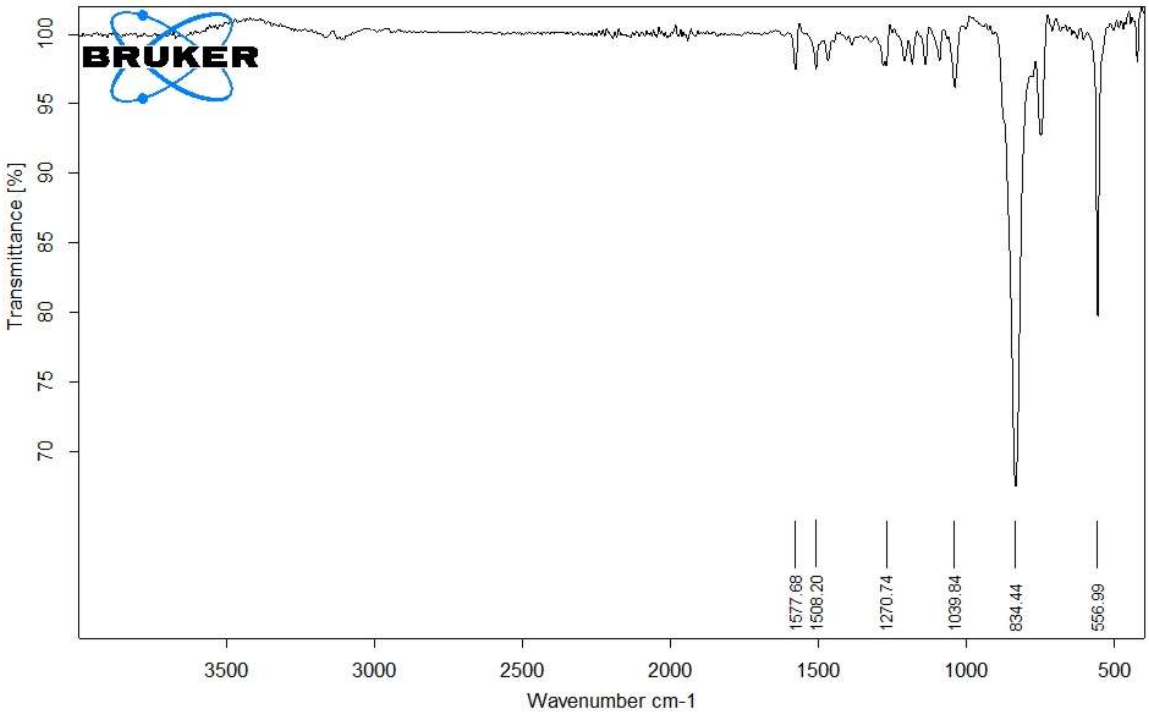

Figure S57. Infrared spectrum of **$H_3L1{\cdot}3(PF_6)$**

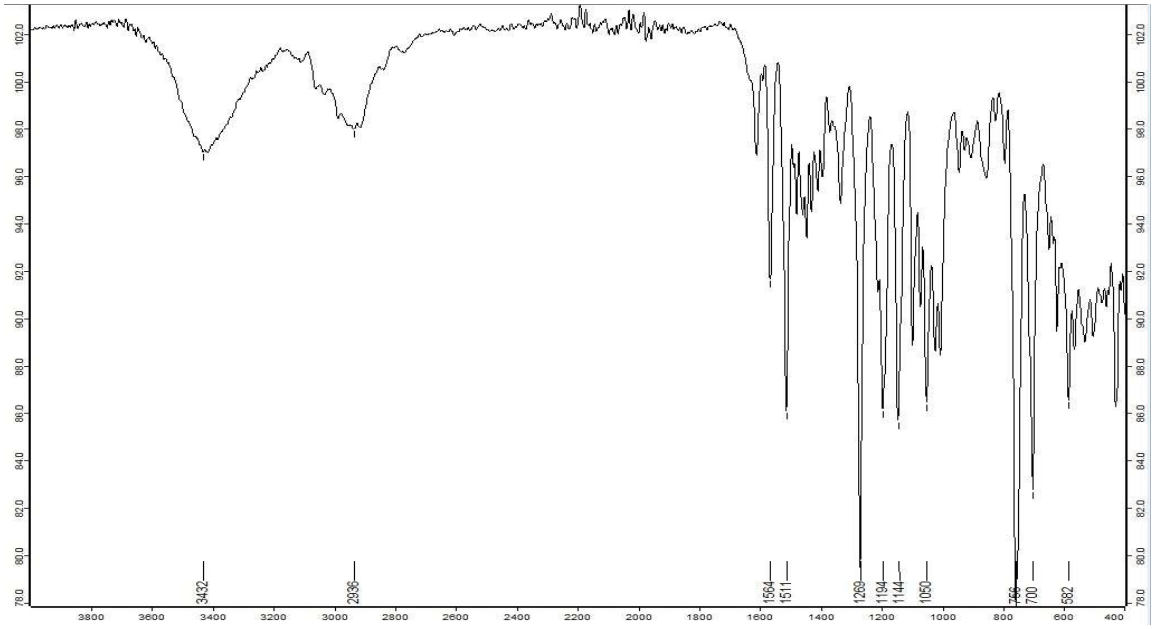

Figure S58. Infrared spectrum of **H_3L2·3Br**

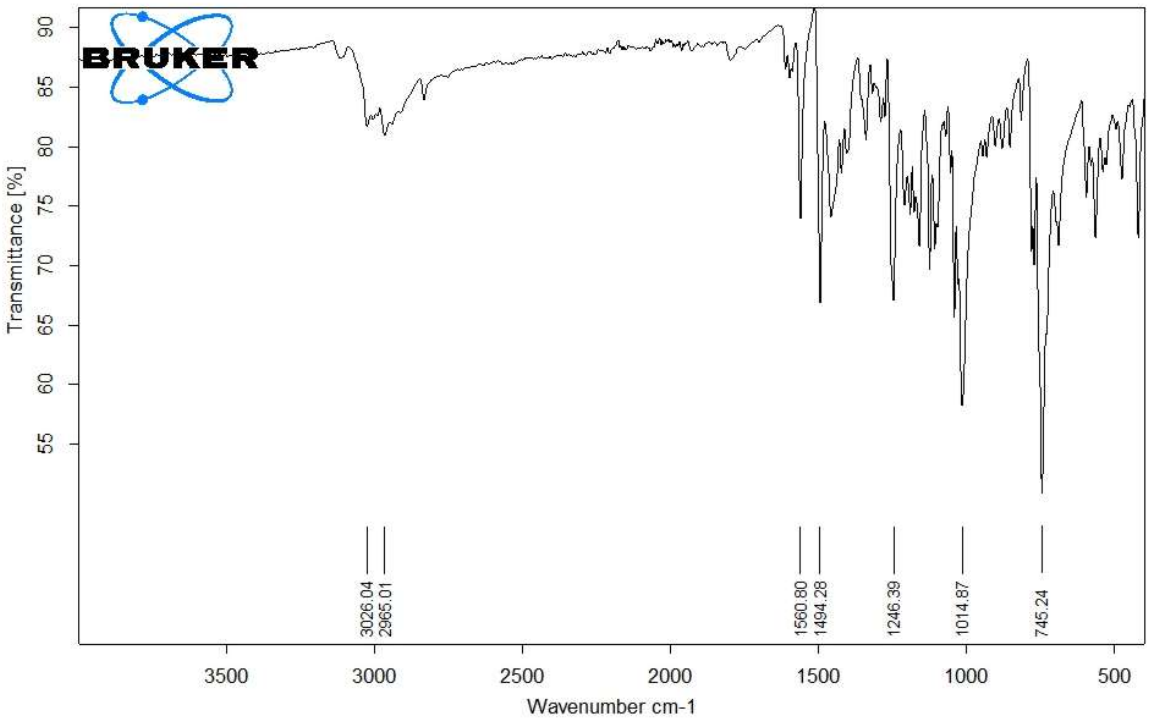

Figure S59. Infrared spectrum of **HL3·I**

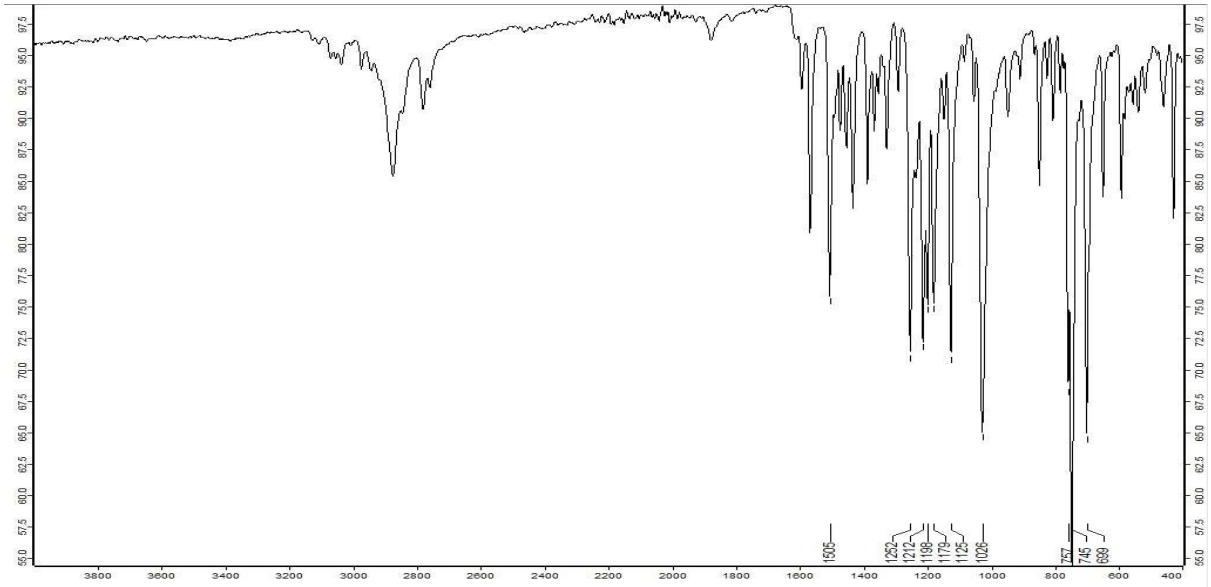

Figure S60. Infrared spectrum of **HL4·Br**

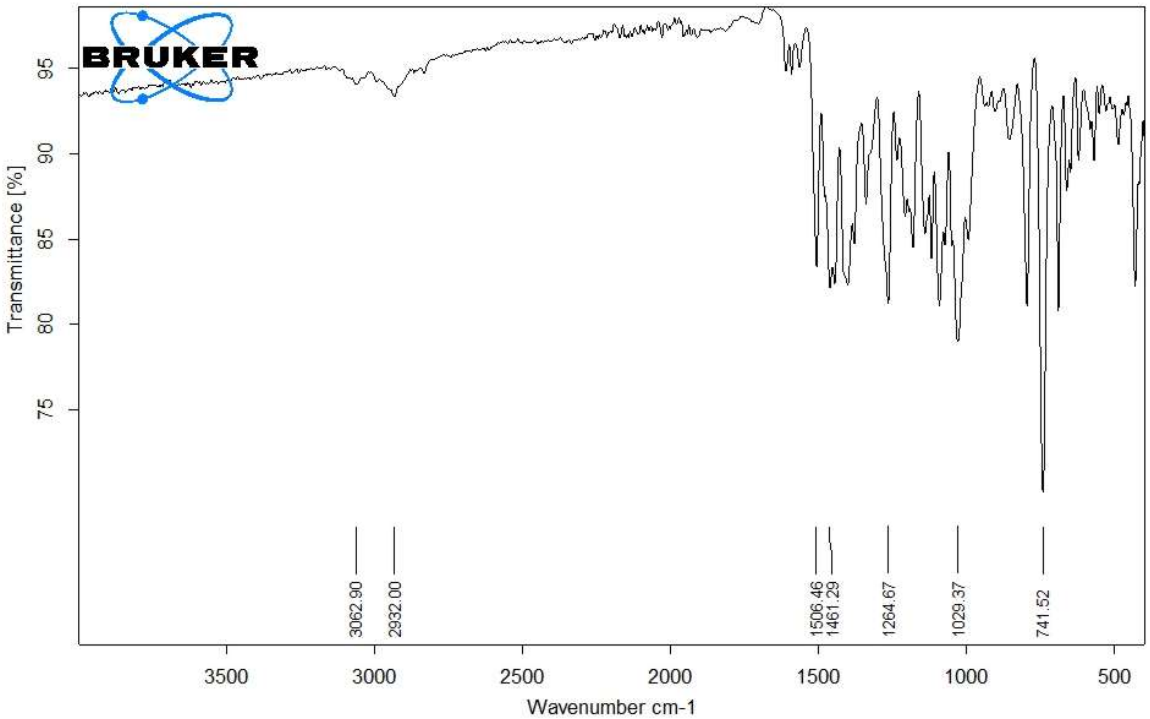

Figure S61. Infrared spectrum of [{PdI_2(pyCl)}$_3$(L1)] **C1**

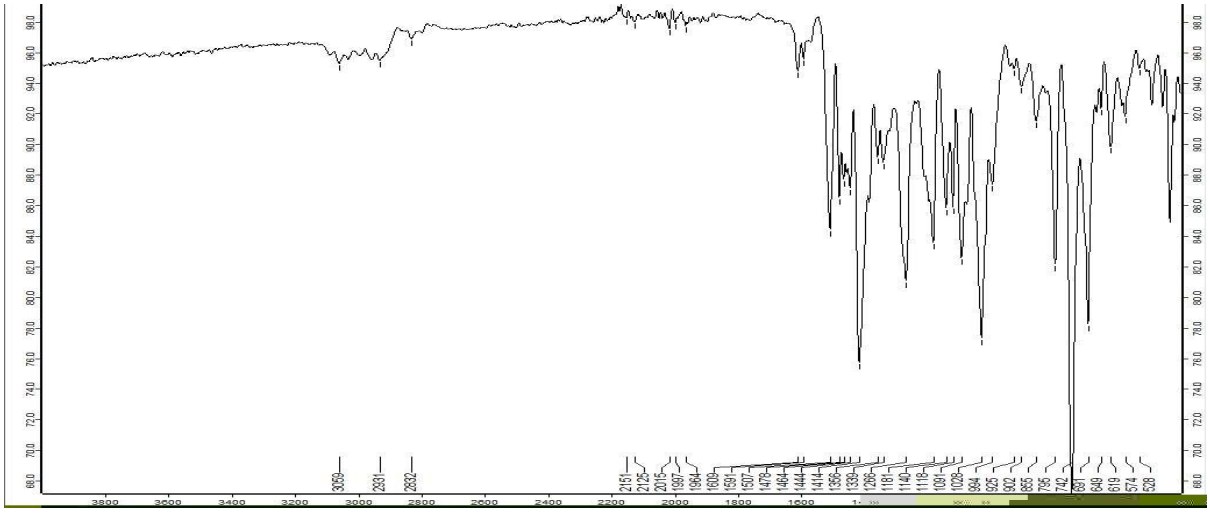

Figure S62. Infrared spectrum of [{PdI_2(pyCl)}$_3$(L2)] **C2**

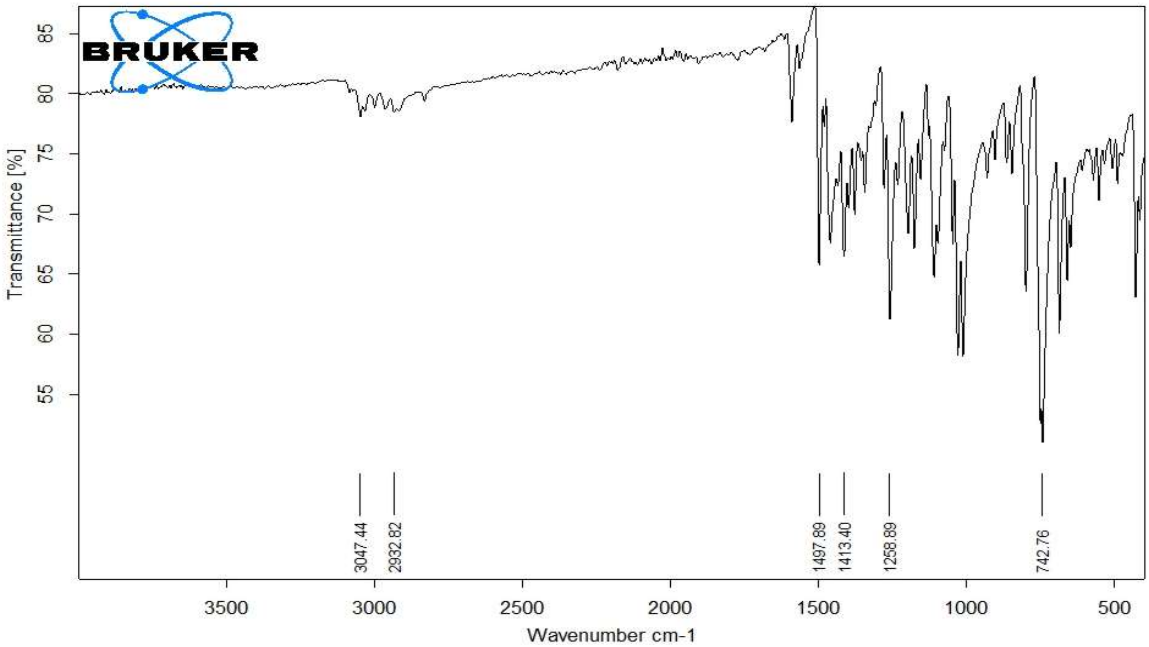

Figure S63. Infrared spectrum of [PdI_2(pyCl)(L3)] **C3**

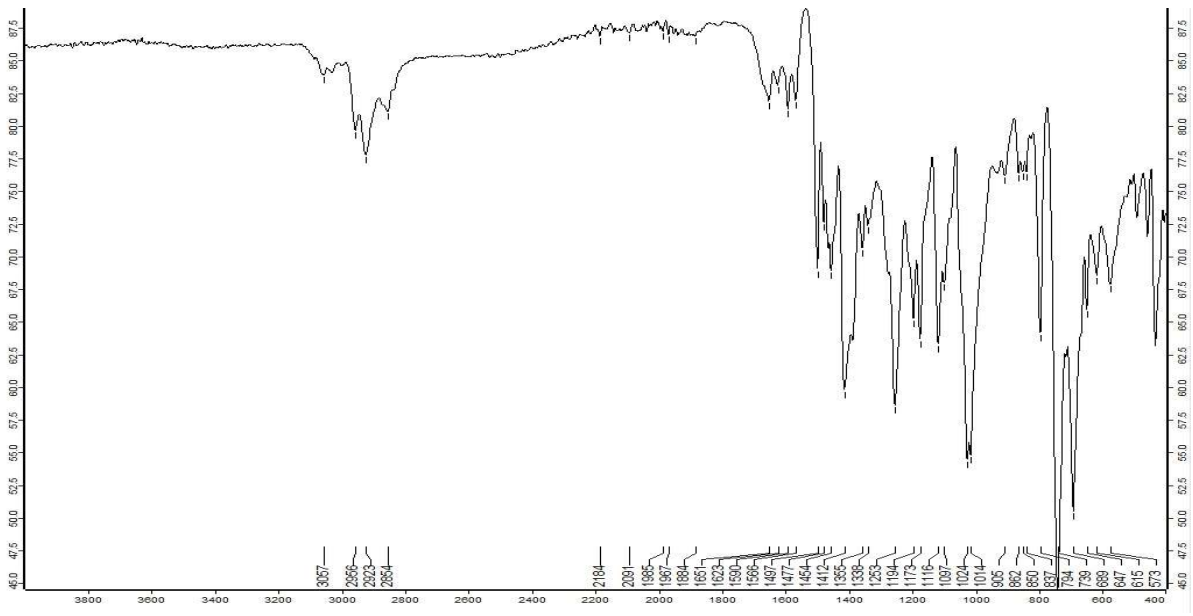

Figure S64. Infrared spectrum of [PdI_2(pyCl)(L4)] **C4**

2. X-ray Crystallography

Crystals were mounted under inert oil on a MiTeGen tip and flash frozen using an Oxford Cryosystems low temperature device. X-ray diffraction data were collected using Cu-K_α radiation (λ= 1.54184 Å) using an Agilent Supernova dual-source diffractometer with Atlas S2 CCD detector and fine-focus sealed tube generator, or using synchrotron radiation (λ = 0.6880 Å) with a 3-circle diffractometer and Dectris Pilatus 2M photon counting pixel detector at station I19 of Diamond Light Source. Data were corrected for Lorenztian and polarization effects and absorption corrections were applied using multi-scan methods. The structures were solved by direct methods using SHELXS-97 and refined by full-matrix on F^2 using SHELXL-97.[3] Unless otherwise specified, all non-hydrogen atoms were refined as anisotropic, and hydrogen positions were included at geometrically estimated positions. Additional details of refinements are given below and in Table S1.

H_3L1·3(PF_6) Crystals were very small and diffracted very weakly even with use of synchrotron radiation, and there was no significant high angle diffraction. Two of the extended arms of the ligand were refined isotropically, with a CH_2-N-CH of one such group modelled as disordered across two positions each at 0.5 occupancy. Attempts at further elucidation of likely disorder in these groups were unsuccessful due to poor data-to-parameter ratio. Two phenyl groups were refined with a rigid body constraint and four other bond lengths were restrained to be chemically reasonable.

[C1]·2(C_5H_{14})·1/2(CH_2Cl_2)·3/2(H_2O) C1_p One 3-chloropyridyl was refined as disordered across two positions at 0.75:0.25 occupancies. A CH_3CH_2 fragment of one pentane was refined across two positions at 0.6:0.4 occupancies, three water sites and the CH_2Cl_2 were refined at 0.5 occupancy. Solvent positions and the low occupancy chloropyridyl site were refined isotropically with the latter restrained to be flat and with its C and N atoms refined with a common U_{iso} value. Some C-C and Cl-C interatomic distances were restrained to be chemically reasonable.

[C1]$_2$·$^{11}/_2$($C_4H_8O_2$) C1_d Four dioxane molecules were refined with 0.5 occupancy, one 3-chloropyridine ligand was refined as disordered across two sites each at 0.5 occupancy, these groups were refined with isotropic displacement parameters. Two such dioxanes were each refined with a group U_{iso} value. Some interatomic distances were restrained to be chemically reasonable.

Table S1. Details of data collections and structure refinements (part 1)

Compound	**H_3L1·3(PF_6)**	**HL3·I**	**[C1]·2(C_5H_{14})·1/2(CH_2Cl_2)·3/2(H_2O) C1_p**
CCDC	1905410	1905413	1905408
Formula	$C_{52}H_{51}F_{18}N_6O_6P_3$	$C_{32}H_{34}I_2N_4O_4$	$C_{76.5}H_{90}Cl_4I_6N_9O_{8.5}Pd_3$
Mr	1278.89	792.43	2493.97
Crystal size (mm)	0.03 x 0.01 x 0.01	0.12 x 0.12 x 0.15	0.06 x 0.08 x 0.11
Crystal system	Triclinic	Triclinic	Triclinic
Space group	$P\bar{1}$	$P\bar{1}$	$P\bar{1}$
a (Å)	7.4847(9)	9.8101(1)	15.6946(6)
b (Å)	16.4088(17)	11.6994(1)	15.8484(8)
c (Å)	22.788(3)	14.6364(1)	21.6110(10)
α (^{0})	75.410(11)	83.317(1)	104.839(4)
β (^{0})	80.946(12)	83.019(1)	111.072(4)
γ (^{0})	78.773(10)	74.051(1)	98.298(3)
V (Å^3)	2639.3(6)	1597.15(3)	4679.2(4)
Z	2	2	2
ρ_{calc} (g.cm^{-3})	1.609	1.648	1.770
λ (Å)	0.68890	0.68890	1.54184
θ range (^{0})	1.71- 20.15	1.761-26.206	3.115-54.242

No. data collected	8730	22265	16060
No. unique data	5085	6966	9748
R_{int}	0.0620	0.0317	0.0356
No. obs. Data ($I > 2\sigma(I)$)	1834	6647	7663
No. parameters	650	383	934
No. restraints	4	0	17
R_1 (obs data)	0.1131	0.0314	0.0533
wR_2 (all data)	0.3380	0.0861	0.1505
S	0.912	1.056	1.019
Max. shift/esd	0.000	0.002	0.003
Largest difference peak and hole/ (e Å^3)	0.827, -0.351	1.770,-0.689	2.016, -1.129

Table S1. Details of data collections and structure refinements (part 2)

Compound	**$[C1]_2 \cdot {}^{11}/_2(C_4H_8O_2)$ C1_d**	**$[PdI_2(pyCl)(L3)]$ C3**	**$[PdI_2(pyCl)(L4)]$ C4**
CCDC	1905411	1905409	1905412
Formula	$C_{154}H_{162}Cl_6I_{12}N_{18}O_{23}Pd_6$	$C_{21}H_{20}ClI_2N_3O_2Pd$	$C_{54}H_{48}Cl_2I_4N_6O_4Pd_2$
Mr	5006.91	742.05	1636.28
Crystal size (mm)	0.07 x 0.06 x 0.05	0.16 x 0.12 x 0.09	0.09 x 0.01 x 0.01
Crystal system	Triclinic	Monoclinic	Monoclinic
Space group	$P\bar{1}$	$P2_1/c$	$P2_1/n$
a (Å)	18.4409(5)	13.61697(5)	11.02430(10)
b (Å)	21.9443(8)	10.99476(3)	14.5623(2)
c (Å)	23.7505(8)	15.82037(5)	35.8034(5)
α (^{0})	99.360(3)	90	90
β (^{0})	97.234(3)	93.4572(3)	98.4410(10)
γ (^{0})	103.156(3)	90	90
V (Å^3)	9100.5(5)	2364.24(9)	5685.58(12)
Z	2	4	4
ρ_{calc} (g.cm^{-3})	1.827	3.335	1.912
λ (Å)	1.54184	0.6889	0.6889
θ range (^{0})	3.116-74.228	1.452-29.998	1.115- 25.502
No. data collected	71312	40488	74794
No. unique data	34313	7553	11597
R_{int}	0.0929	0.0391	0.0869

No. obs. Data ($I > 2\sigma(I)$)	18012	7258	7865
No. parameters	2001	273	651
No. restraints	1812	0	0
R_1 (obs data)	0.0805	0.0181	0.0521
wR_2 (all data)	0.2330	0.0443	0.1574
S	0.997	1.049	1.044
Max. shift/esd	0.001	0.003	0.002
Largest difference peak and hole/ (e Å^3)	2.821, -1.461	0.675, -0.481	1.949, -1.253

Additional Diagrams of Crystal Structures

$H_3L1{\cdot}3(PF_6)$

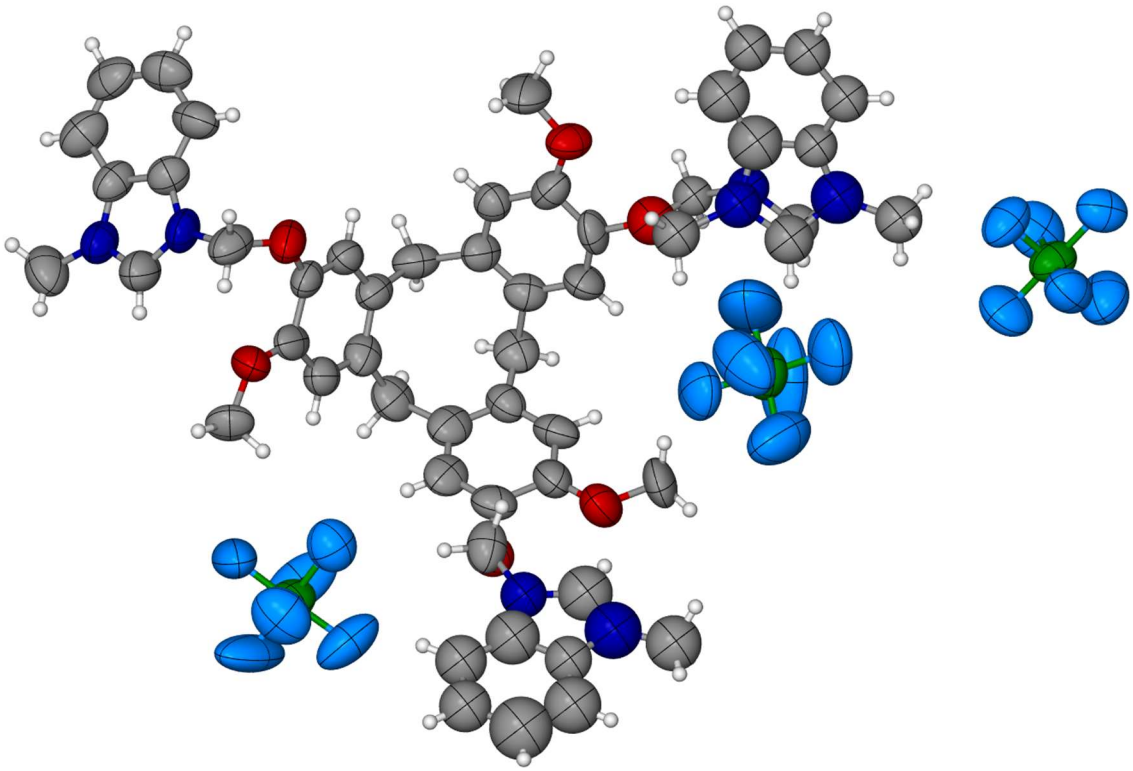

Figure S65: Asymmetric unit of **$H_3L1{\cdot}3(PF_6)$** with ellipsoids shown at 50 % probability levels.

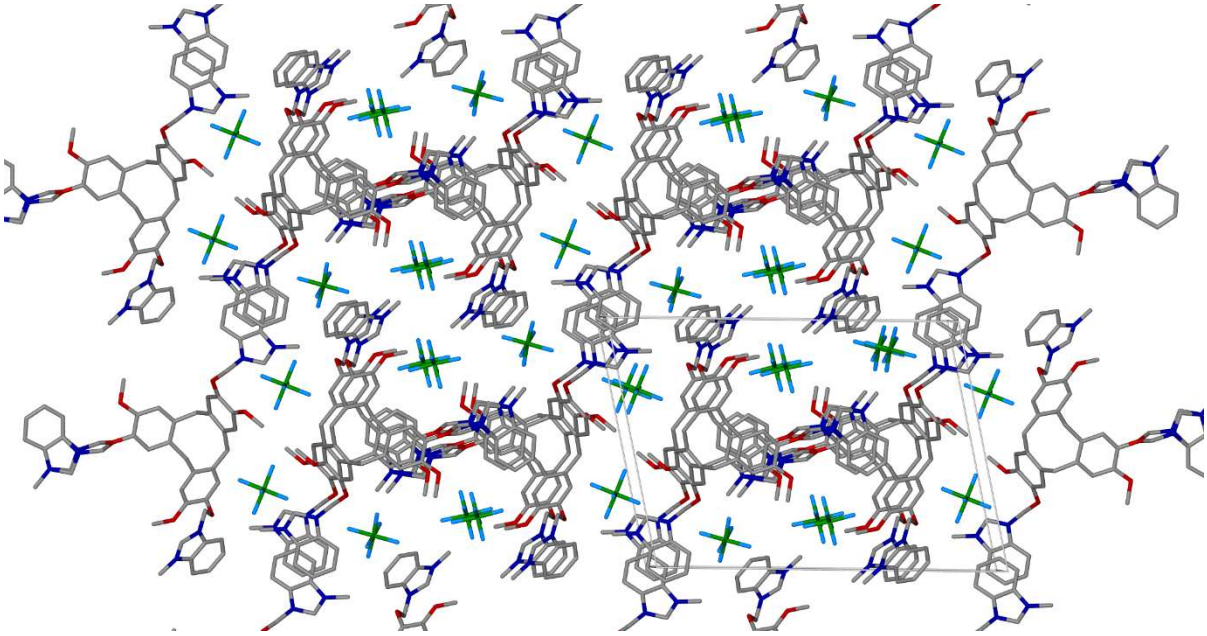

Figure S66: Packing diagram of **H_3L1·3(PF_6)** viewed down the *a* axis.

HL3·I

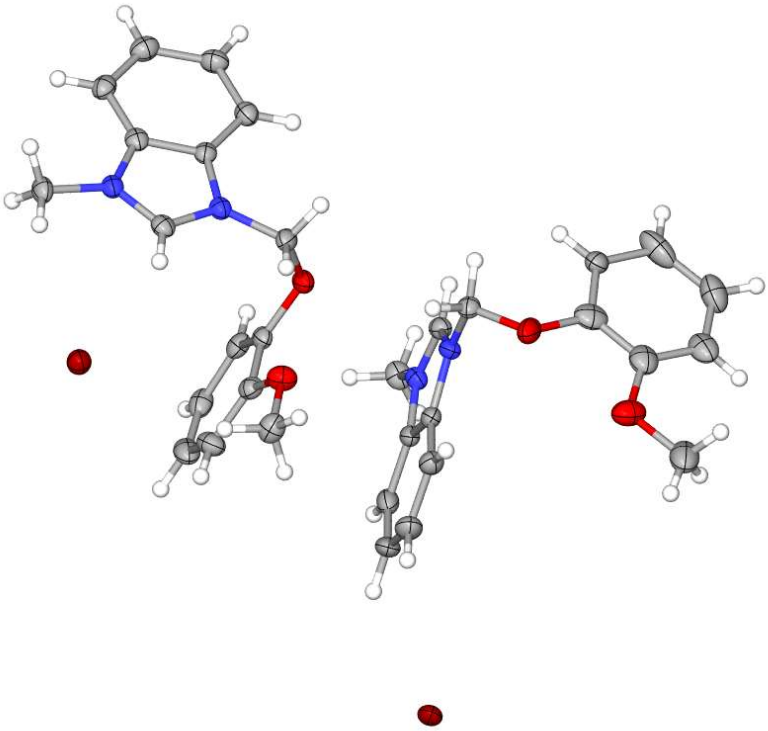

Figure S67. Asymmetric unit of the crystal structure of **HL3·I**. Ellipsoids shown at 50 % probability levels.

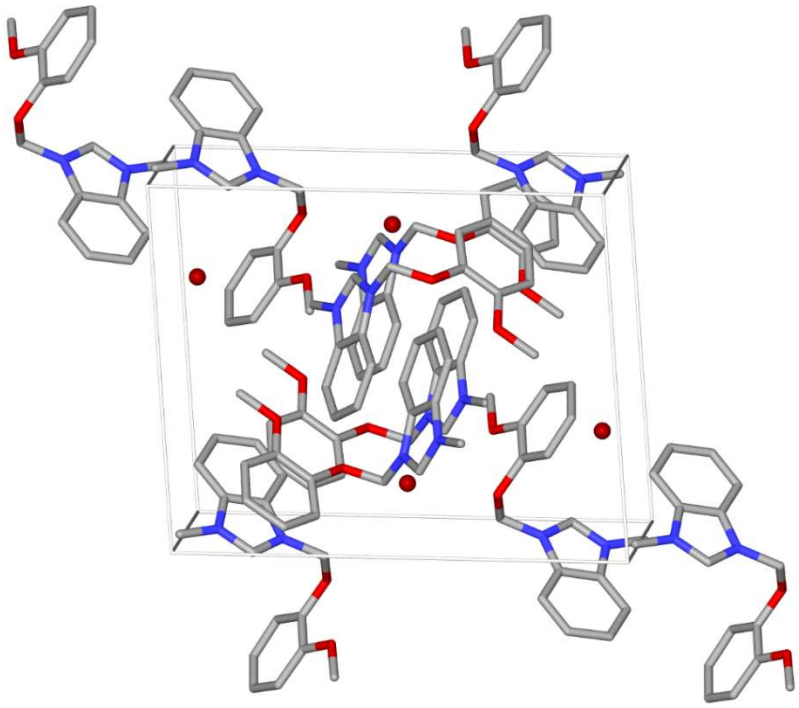

Figure S68. Packing diagram of **HL3·I** viewed displaces from a axis. Hydrogen atoms excluded for clarity.

[C1]·2(C_5H_{14})·1/2(CH_2Cl_2)·3/2(H_2O) C1_p

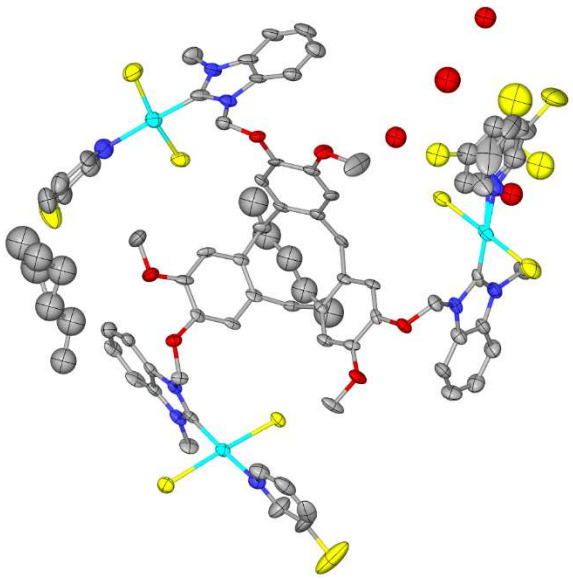

Figure S69. Asymmetric unit of **[C1]·2(C_5H_{14})·1/2(CH_2Cl_2)·3/2(H_2O) C1_p**. Ellipsoids shown at 50 % probability levels.

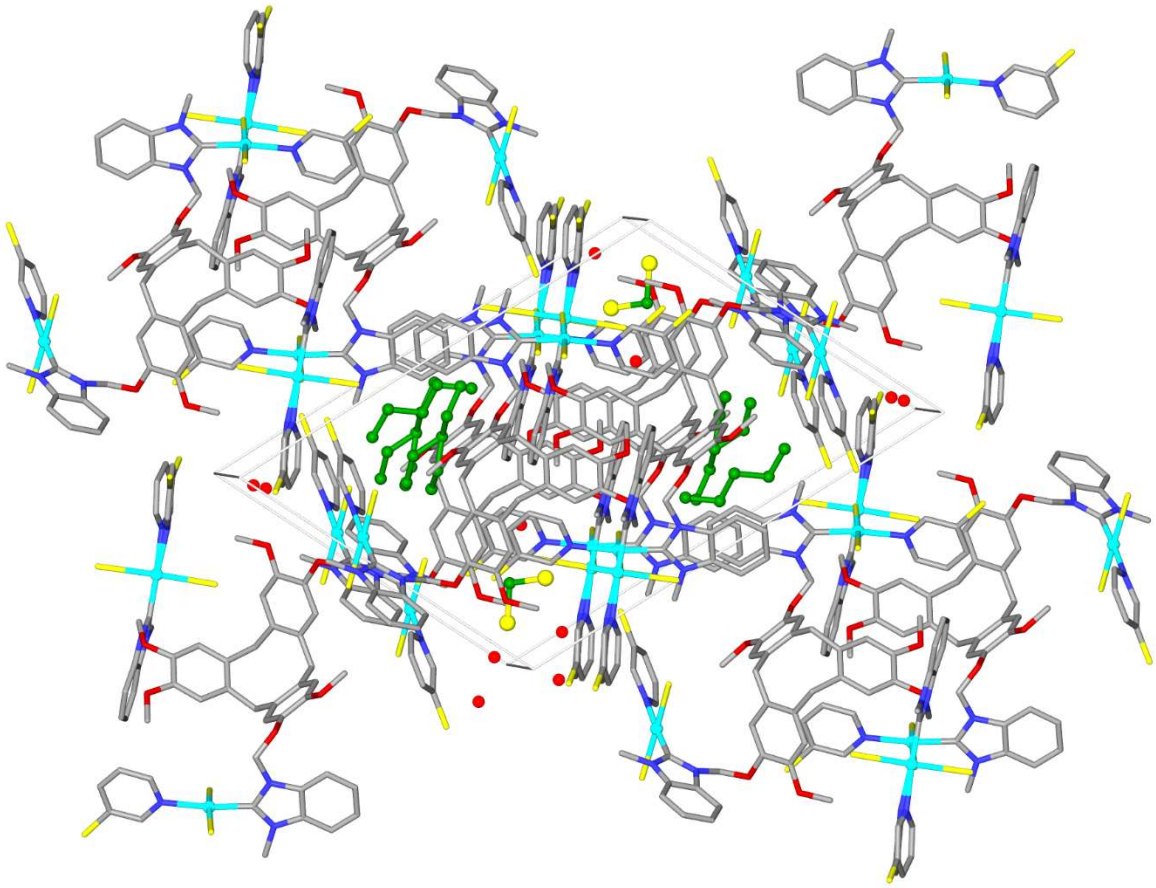

Figure S70. Packing diagram for **[C1]·2(C_5H_{14})·1/2(CH_2Cl_2)·3/2(H_2O) C1_p** viewed down *b***.** Solvent shown in ball-and-stick for clarity

$[C1]_2 \cdot {}^{11}/_2(C_4H_8O_2)$ C1_d

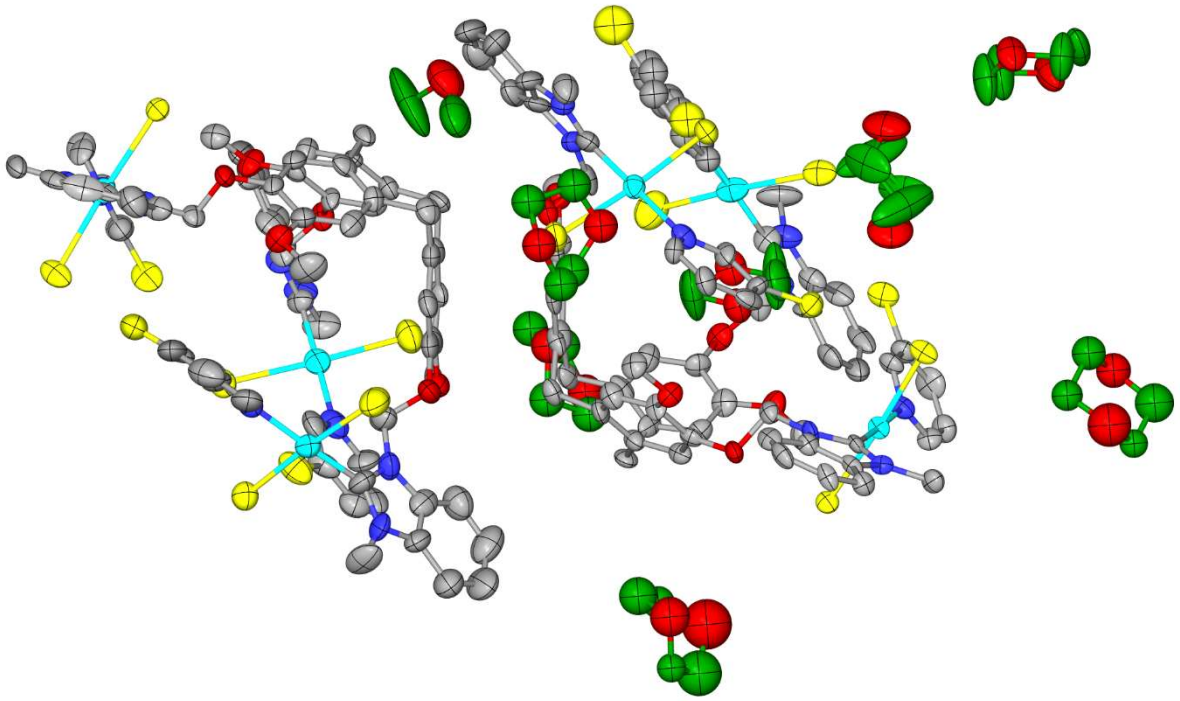

Figure S71. Asymmetric unit of **$[C1]_2 \cdot {}^{11}/_2(C_4H_8O_2)$ C1_d**. Ellipsoids shown at 50 % probability levels and carbon of dioxane shown in green and hydrogen atoms excluded for the sake of clarity.

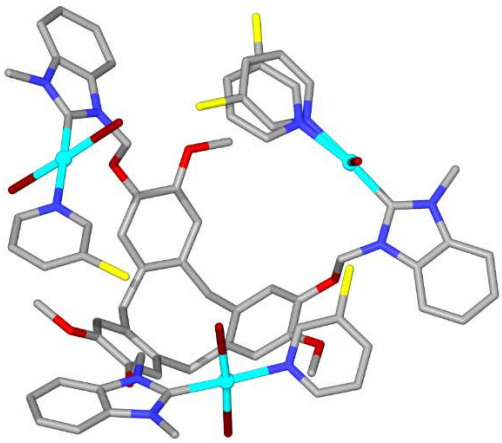

Figure S72. One crystallographically distinct C1 complex of **C1_d** highlighting disorder of pyCl ligand.

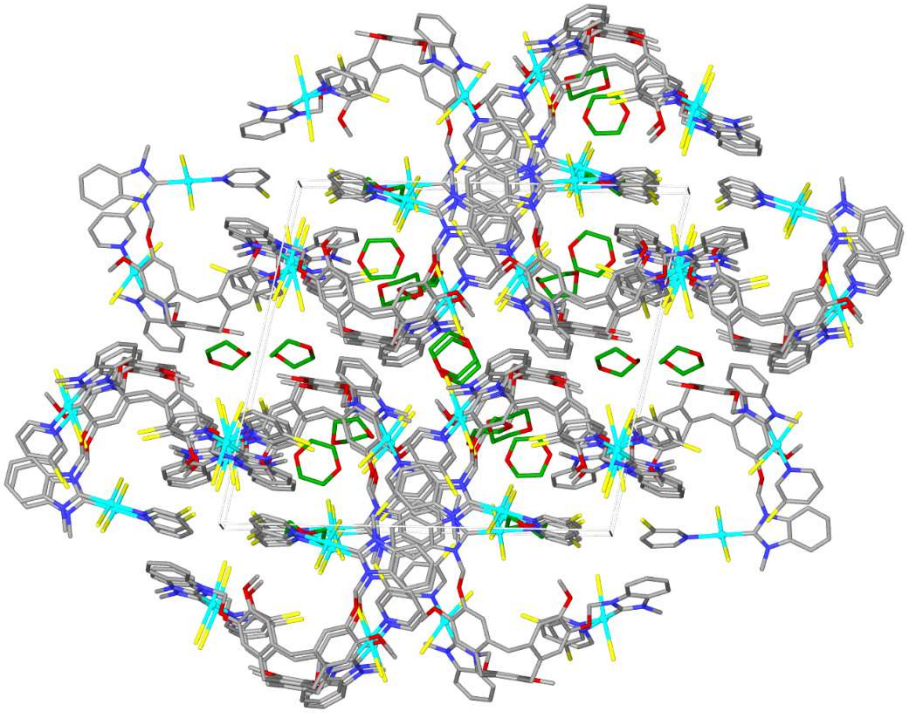

Figure S73. Packing diagram of **[C1]$_2$·$^{11}/_2$($C_4H_8O_2$) C1_d** viewed down a axis. Carbon atoms of dioxane shown in green and hydrogen atoms excluded for the sake of clarity.

[PdI_2(pyCl)(L3)] C3

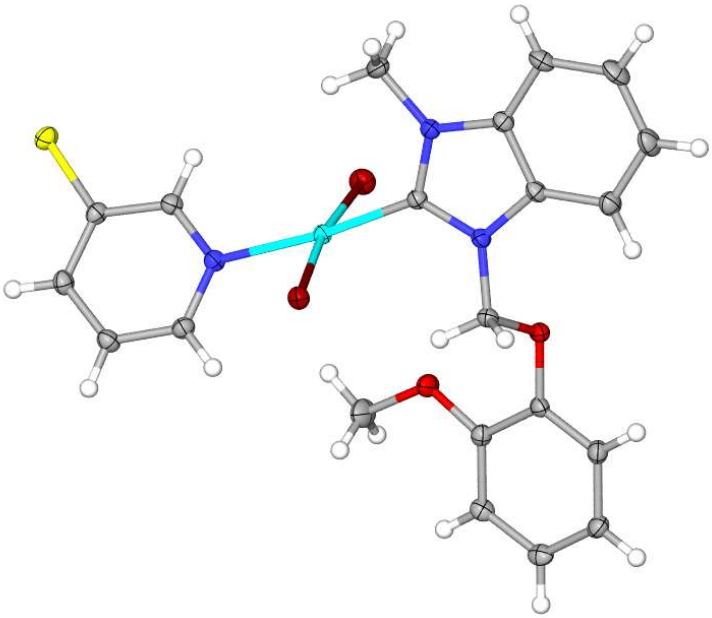

Figure S74. Asymmetric unit of **[PdI_2(pyCl)(L3)] C3**. Ellipsoids shown at 50 % probability levels

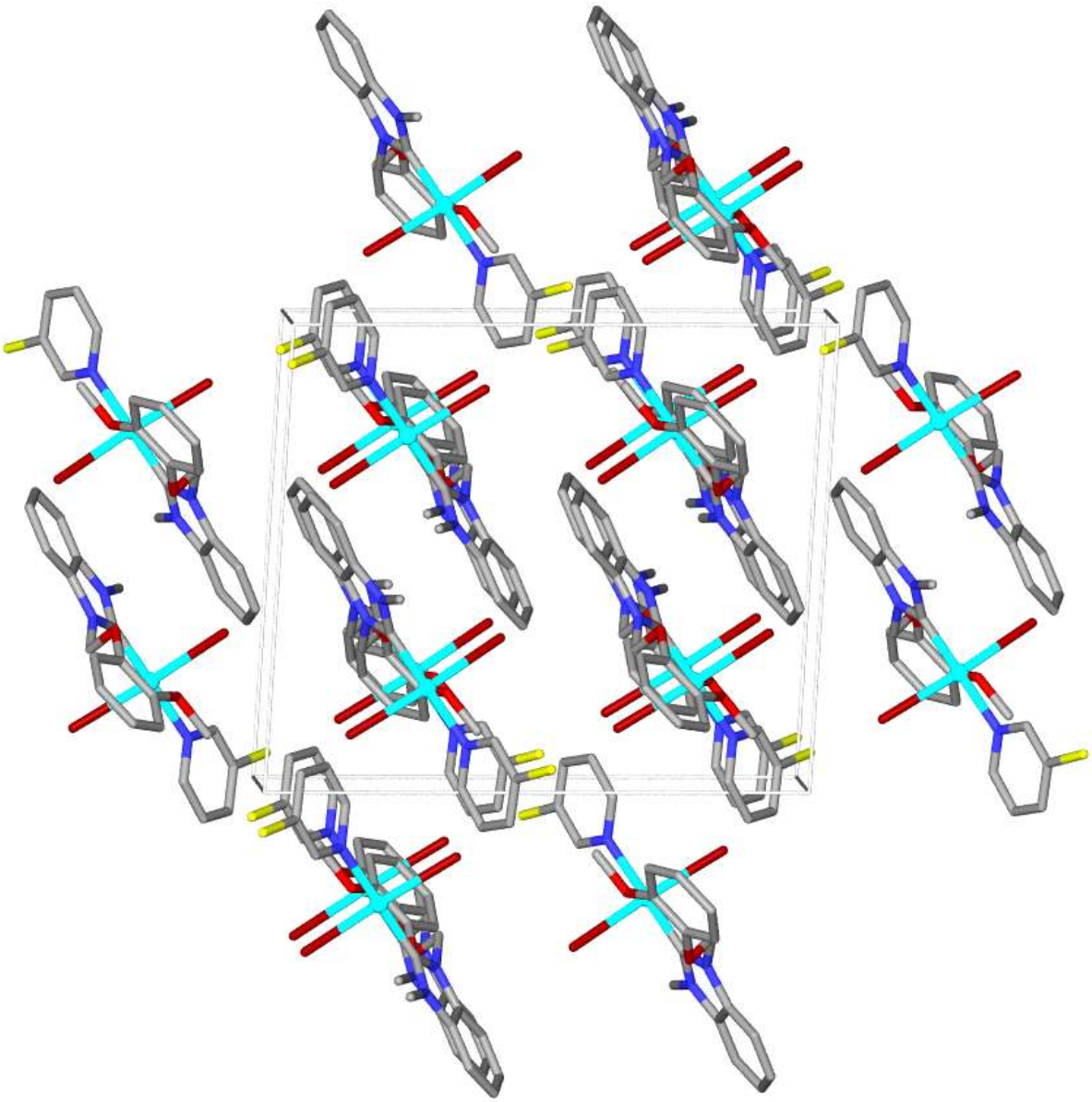

Figure S75. Packing diagram of **[PdI$_2$(pyCl)(L3)] C3** viewed down the *b* axis. Hydrogen atoms excluded for the sake of clarity.

[PdI$_2$(pyCl)(L4)] C4

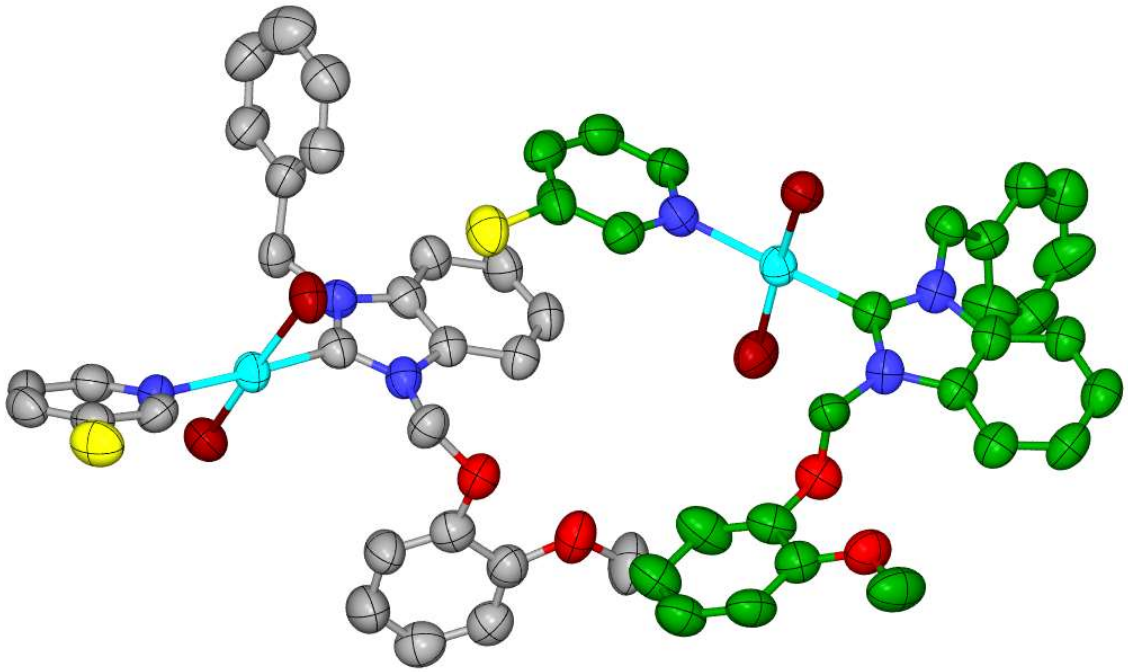

Figure S76. Asymmetric unit of **[PdI$_2$(pyCl)(L4)] C4.** Two different conformations of the complex shown with carbon atoms in different colours. Ellipsoids shown at 50 % probability levels and hydrogen atoms excluded for the sake of clarity.

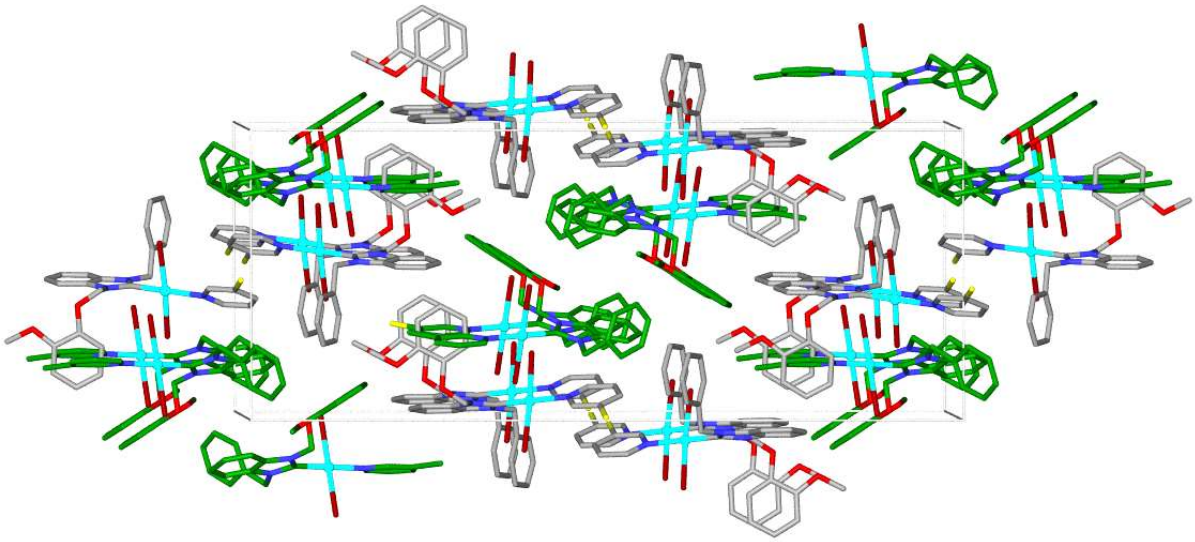

Figure S77. Packing diagram of **[PdI$_2$(pyCl)(L4)] C4** viewed down *a* axis. Two different conformations of the complex shown with carbon atoms in different colours. Hydrogen atoms excluded for the sake of clarity.

3. Additional Catalytic Studies

Table S2. Conversions and product ratios for reaction of 2,5-dibromopyridine and 4-methoxybenzeneboronic acid.

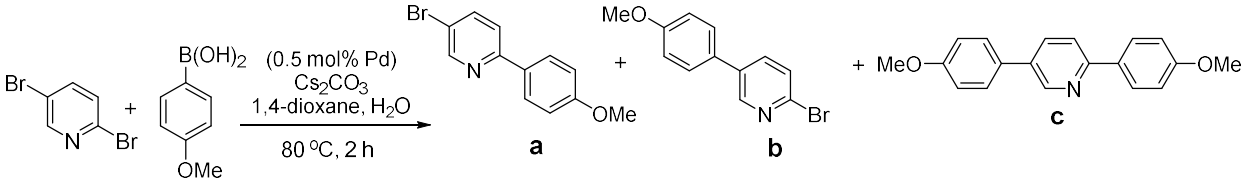

Catalyst	Total conversion (%) ǂ	Ratio **a**:**b** (%)	**c** (%)
1:2 $Pd(OAc)_2$, PPh_3	80	70:5	5
C1	61	31:23	7
C2	51	26:20	5
C3	53	29:18	6
C4	46	24:18	4

ǂ Conversions are an average of two experiments.

Table S3. Conversions and turnover numbers for reaction of 4-bromotoluene and benzeneboronic acid.

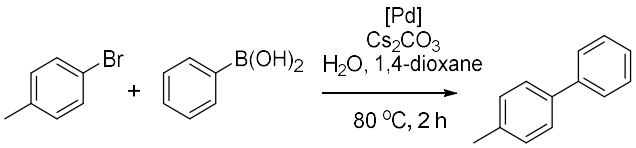

	0.25 mol % Pd		0.5 mol % Pd		1 mol% Pd	
Catalyst	Conversion (%) ǂ	TOF ⊥	Conversion (%) ǂ	TOF ⊥	Conversion (%) ǂ	TOF ⊥
C1	21	42	24	24	20	10
C2	37	74	41	41	22	11
C3	22	44	23	23	42	21
C4	26	52	32	32	55	27.5

ǂ Conversions are an average of two experiments. ⊥ Turnover frequency per Pd per hour.